U.PORTO

FEUP FACULDADE DE ENGENHARIA UNIVERSIDADE DO PORTO

STUDY ON THE APPLICABILITY OF COMBINED PHYSICO-CHEMICAL PROCESSES IN THE BENEFICIATION OF RARE EARTH ELEMENT ORES (REE – RARE EARTH ELEMENTS)

ANOUK SOFIA DAUTO MAGANE

Dissertation submitted in partial fulfilment of the requirements for the degree of

MASTER IN MINING ENGINEERING AND GEO-ENVIRONMENT

Supervisor: Professor Maria Cristina Costa Vila, PhD

Co-supervisor: Professor Maria de Lurdes Proença de Amorim Dinis, PhD

JUNE 2026

CERENA Centro de Recursos Naturais e Ambiente

Reesource

This project has received funding from the European Union's Horizon Europe research and innovation program under grant agreement No 10118460

MASTER'S IN MINING ENGINEERING AND GEO-ENVIRONMENT 2025/2026

DEPARTMENT OF CIVIL AND GEORESOURCES ENGINEERING

Tel. +351-22-508 1901

✉ memg@fe.up.pt

Edited by

FACULTY OF ENGINEERING OF THE UNIVERSITY OF PORTO

Rua Dr. Roberto Frias

4200-465 PORTO

Portugal

Tel. +351-22-508 1400

✉ feup@fe.up.pt

http://www.fe.up.pt

Partial reproduction of this document is authorised provided that the Author is mentioned and reference is made to the *Master's in Mining Engineering and Geo-Environment - 2025/2026 - Department of Civil and Georesources Engineering, Faculty of Engineering of the University of Porto, Porto, Portugal, 2026*.

The opinions and information included in this document represent solely the views of the respective Author, and the Editor cannot accept any legal or other responsibility for any errors or omissions that may exist.

This document was produced from an electronic version provided by the respective Author

Dedicated to my parents

ACKNOWLEDGEMENTS

This work is part of the REESOURCE project and has received funding from the European Union's Horizon Europe framework programme under grant agreement N.º 101138460. This work was developed at R&D Unit CERENA, supported through FCT Project UID/04028/2025 (https://doi.org/10.54499/UID/04028/2025).

ABSTRACT

Rare earth elements are essential raw materials for advanced technologies and the energy transition. However, beneficiation of rare-earth-bearing carbonatite ores is technically challenging because valuable minerals commonly occur in complex associations with carbonate, phosphate, silicate and iron-bearing gangue minerals. The present study evaluated the applicability of physical and physico-chemical processes for the beneficiation of rare-earth-element-bearing materials from the Fen Carbonatite Complex, Norway.

Two ore composites, designated C4 and CG, were investigated through direct froth flotation and combined routes involving hydrogravitic pre-concentration, magnetic pre-concentration, microwave-assisted wet and dry pre-treatment, and sequential flotation. Feed materials and selected products were characterised by particle-size analysis, X-ray fluorescence, inductively coupled plasma mass spectrometry, and scanning electron microscopy with energy-dispersive X-ray spectroscopy. Process performance was evaluated using mass recovery, overflow total rare earth oxide grade, total rare earth oxide recovery, cumulative recovery and enrichment ratio.

Composite CG generally produced higher total rare earth oxide recoveries and overflow grades than composite C4, whereas C4 exhibited stronger relative upgrading under selected combined conditions. For C4, dry microwave pre-treatment followed by flotation produced the principal recovery-oriented response, with 36.71% total rare earth oxide recovery and an enrichment ratio of 1.83. Hydrogravitic pre-concentration followed by dry microwave pre-treatment and flotation produced the strongest C4 upgrading response, with an enrichment ratio of 2.72 and 24.60% recovery. For CG, hydrogravitic pre-concentration followed by flotation achieved the maximum overall recovery of 90.92%, however, the associated mass recovery of 94.14% and enrichment ratio of 0.97 indicated limited selectivity. The strongest selective CG responses were obtained through direct flotation and hydrogravitic pre-concentration followed by dry microwave pre-treatment, producing recoveries of 45.24% and 41.27% and enrichment ratios of 1.92 and 1.91, respectively.

The experimental results demonstrate a pronounced recovery–upgrading trade-off. High total rare earth oxide recovery was frequently accompanied by high mass recovery and limited gangue rejection, whereas stronger enrichment generally occurred at lower recovery. Combined beneficiation improved selected aspects of processing performance, although no route simultaneously maximised recovery, overflow grade and enrichment. Beneficiation-route selection should therefore consider feed characteristics, pre-concentration products and the intended balance between recoveries and concentrate upgrading.

KEYWORDS: Rare Earth Elements, Fen Carbonatite Complex, Mineral Beneficiation, Froth Flotation, Pre-Concentration.

RESUMO

Os elementos de terras raras constituem matérias-primas essenciais para tecnologias avançadas e para a transição energética. No entanto, a beneficiação de minérios carbonatíticos de terras raras apresenta elevada complexidade técnica, uma vez que os minerais de interesse ocorrem frequentemente em associações complexas com minerais de ganga carbonatados, fosfatados, silicatados e portadores de ferro. O presente estudo avaliou a aplicabilidade de processos físicos e físico-químicos na beneficiação de minérios de terras raras provenientes do Complexo Carbonatítico de Fen, na Noruega.

Foram estudados dois compósitos de minério, designados C4 e CG, através de flutuação direta por espumas e de rotas combinadas envolvendo pré-concentração hidrogravítica, pré-concentração magnética, pré-tratamento húmido e seco assistido por micro-ondas e flutuação sequencial. Os materiais de alimentação e produtos selecionados foram caracterizados por análise granulométrica, fluorescência de raios X, espectrometria de massa com plasma acoplado indutivamente e microscopia eletrónica de varrimento acoplada à espectroscopia de raios X por dispersão de energia. O desempenho dos processos foi avaliado com base na recuperação mássica, no teor de óxidos totais de terras raras no produto de overflow, na recuperação de óxidos totais de terras raras, na recuperação cumulativa e na razão de enriquecimento.

O compósito CG apresentou, de modo geral, recuperações de óxidos totais de terras raras e teores no overflow superiores aos obtidos para o compósito C4, enquanto o compósito C4 evidenciou maior enriquecimento relativo em determinadas condições combinadas. Para o C4, o pré-tratamento a seco assistido por micro-ondas seguido de flutuação produziu o melhor desempenho em termos de recuperação, com 36,71% de recuperação de óxidos totais de terras raras e uma razão de enriquecimento de 1,83. A pré-concentração hidrogravítica seguida de pré-tratamento a seco assistido por micro-ondas e flutuação proporcionou a maior resposta de enriquecimento do C4, com uma razão de enriquecimento de 2,72 e uma recuperação de 24,60%. Para o CG, a pré-concentração hidrogravítica seguida de flutuação atingiu a recuperação global máxima de 90,92%. Contudo, a recuperação mássica associada, de 94,14%, e a razão de enriquecimento de 0,97 indicaram seletividade limitada. As respostas mais seletivas do CG foram obtidas por flutuação direta e por pré-concentração hidrogravítica seguida de pré-tratamento a seco assistido por micro-ondas, com recuperações de 45,24% e 41,27% e razões de enriquecimento de 1,92 e 1,91, respetivamente.

Os resultados experimentais demonstraram um compromisso acentuado entre recuperação e enriquecimento. Recuperações elevadas de óxidos totais de terras raras foram frequentemente acompanhadas por recuperações mássicas elevadas e rejeição limitada da ganga, enquanto os maiores enriquecimentos foram geralmente obtidos com recuperações inferiores. As rotas combinadas melhoraram determinados aspetos do desempenho do processamento, embora nenhuma rota tenha maximizado simultaneamente a recuperação, o teor no overflow e o enriquecimento. A seleção da rota de beneficiação deverá considerar as características da alimentação, os produtos de pré-concentração e o equilíbrio pretendido entre a recuperação e o enriquecimento do concentrado.

PALAVRAS-CHAVE: Elementos de Terras Raras, Complexo Carbonatítico de Fen, Processamento Mineral, Flutuação por Espumas, Pré-Concentração.

Table of Contents

LIST OF FIGURES

LIST OF TABLES

Symbols, Acronyms and Abbreviations

C4	Designation assigned to the C4 Fen ore composite
CERENA	Centre for Natural Resources and the Environment
CG	Designation assigned to the CG Fen ore composite
d10	Particle size below which 10% of the cumulative particle-size distribution lies
d50	Median particle size; particle size below which 50% of the cumulative particle-size distribution lies
d90	Particle size below which 90% of the cumulative particle-size distribution lies
EDS	Energy-dispersive X-ray spectroscopy
EDTA	Ethylenediaminetetraacetic acid
Eh	Oxidation–reduction potential or redox potential
ER	Enrichment ratio
EU	European Union
FCT	Fundação para a Ciência e a Tecnologia — Foundation for Science and Technology
FDC	Fe-dolomite carbonatite(s)
FEUP	Faculty of Engineering of the University of Porto
HREE	Heavy rare earth element(s)
HREO	Heavy rare earth oxide(s)
IADs	Ion-adsorption deposits
ICP-MS	Inductively coupled plasma mass spectrometry
IEP	Isoelectric point
LREE	Light rare earth element(s)
LREO	Light rare earth oxide(s)
MIBC	Methyl isobutyl carbinol
N/A	Not available
NdFeB	Neodymium–iron–boron
OHA	Octanohydroxamic acid
ORP	Oxidation–reduction potential
pH	Negative base-10 logarithm of hydrogen-ion activity; measure of acidity or alkalinity

R&D	Research and development
REE	Rare earth element(s)
REE^{3+}	Trivalent rare-earth ion
REE_2O_3	Generic formula for a trivalent rare-earth oxide
REO	Rare earth oxide(s)
rpm	Revolutions per minute
SEM	Scanning electron microscopy
SEM-EDS	Scanning electron microscopy coupled with energy-dispersive X-ray spectroscopy
ΣHREO	Sum of heavy rare earth oxide contents
ΣLREO	Sum of light rare earth oxide contents
TREO	Total rare earth oxides
UP	University of Porto
USA	United States of America
USSR	Union of Soviet Socialist Republics
XRF	X-ray fluorescence spectrometry

1

INTRODUCTION

Rare earth elements (REEs) are essential raw materials for modern technologies, including permanent magnets, batteries, catalysts, electronic devices, specialised alloys and renewable-energy systems. Their strategic relevance has increased with the expansion of electric transportation, wind-energy generation and advanced manufacturing. Neodymium, praseodymium, dysprosium and terbium are particularly important for high-performance permanent magnets used in electric-vehicle motors and wind-turbine generators (Nkiawete and Vander Wal, 2025).

Despite their technological importance, REE mining, processing and refining remain geographically concentrated, creating concerns regarding supply-chain security (Chen et al., 2024). For Europe, the development of domestic resources and processing capacity may contribute to reduce import dependence and greater resilience of critical-raw-material supply chains. However, geological occurrence alone does not ensure technical or economic viability. REEs generally occur within mineral phases that must be concentrated from surrounding gangue before chemical extraction and separation of individual elements can be performed efficiently (Jordens et al., 2013).

Beneficiation of REE-bearing ores is often difficult because valuable minerals may occur as fine grains, intergrowths or composite particles associated with carbonates, phosphates, sulphates, silicates and Fe-bearing minerals (Al-Ali et al., 2020). Separation performance therefore depends on particle-size distribution, mineral associations, liberation degree and differences in physical or surface properties. Gravity separation, magnetic separation and froth flotation may be applied individually or as part of combined beneficiation routes (Shuai et al., 2024).

Froth flotation is particularly relevant for finely disseminated REE-bearing ores because mineral separation can be promoted through controlled differences in surface chemistry. Nevertheless, selective flotation is difficult when REE-bearing minerals and gangue phases respond similarly to collectors and modifiers (Marion et al., 2020). High recovery may consequently be associated with recovery of substantial gangue mass, while stronger upgrading may occur at the expense of overall REE recovery. Evaluation of flotation performance must therefore consider mass recovery, product grade, TREO recovery and enrichment simultaneously.

The present investigation focuses on ore material from the Fen Carbonatite Complex in Telemark, southern Norway. Fen represents an important European REE exploration target containing fluorcarbonate and phosphate REE minerals within carbonate-rich and Fe-bearing assemblages (Dahlgren, 2019). Reported REE-bearing minerals include parisite, synchysite, bastnäsite and monazite, associated with minerals such as Fe-rich dolomite, calcite, barite, apatite, fluorite, magnetite and other

accessory phases (Coint and Dahlgren, 2019). Such mineralogical complexity may limit liberation and reduce the selectivity of physical and physico-chemical separation processes.

Previous investigations have provided geological, geochemical and mineralogical information concerning the Fen Carbonatite Complex (Dahlgren, 2019). Recent studies have also improved understanding of the flotation behaviour of Fen-type material (Akyildiz et al., 2026). However, limited comparative information is available regarding the flotation response of untreated, physically pre-concentrated and microwave-treated Fen materials evaluated within the same experimental programme. Additional investigation is therefore required to determine whether combined beneficiation routes provide measurable advantages relative to direct flotation.

The aim of the present dissertation is to evaluate and compare physical and physico-chemical beneficiation routes for concentrating rare-earth-element-bearing minerals from the Fen Carbonatite Complex.

The specific objectives are:

1. To characterise untreated and pre-concentrated C4 and CG materials through particle-size analysis, X-ray fluorescence, inductively coupled plasma mass spectrometry and scanning electron microscopy with energy-dispersive X-ray spectroscopy.
2. To evaluate the direct flotation response of C4 and CG under different reagent and operating conditions.
3. To assess the influence of hydrogravitic and magnetic pre-concentration on subsequent flotation performance.
4. To evaluate microwave-assisted wet and dry pre-treatment before flotation.
5. To investigate the influence of pH, temperature, collector dosage, depressant selection, chelating agent addition and sequential flotation.
6. To compare the investigated routes using mass recovery, overflow TREO grade, TREO recovery, cumulative TREO recovery and enrichment ratio and to identify recovery-oriented and upgrading-oriented conditions.

The experimental programme was conducted at laboratory scale using two Fen carbonatite composites, designated C4 and CG. Direct flotation was used as a reference for comparison with hydrogravitic pre-concentration, magnetic pre-concentration, microwave-assisted pre-treatment and sequential flotation. Taguchi-based experimental series were also applied to composite CG to evaluate the effects of selected operating and reagent variables.

The investigation focused on mineral beneficiation. The experimental programme was intended to compare route performance and identify promising laboratory-scale conditions rather than establish a definitive industrial flowsheet. Scale-up assessment, complete route recoveries relative to untreated feed, closed-circuit testing and economic evaluation were outside the scope of the work.

The study is divided in five chapters including the introduction. Chapter two presents the State of the Art concerning REE characteristics, criticality, deposits, mineralogy, beneficiation methods, the Fen Carbonatite Complex and froth flotation of REE minerals. Chapter three describes the investigated materials, experimental procedures, analytical methods, metallurgical calculations and limitations during the experimental programme. Chapter four presents and discusses feed characterisation and beneficiation performance for the investigated routes. Chapter five summarises the principal conclusions and recommendations for further work.

1.1 Contribution to sustainable development goals (SDGs)

This dissertation focuses on the processing of a primary ore of Rare Earth Elements, through froth flotation, using reagents with minimal environmental impact and adopting water-saving strategies in the process contributing to the development of more sustainable treatment strategies.

Considering the environmental problems associated with critical raw materials supply, and the need to align processing strategies with the principles of zero pollution and the circular economy, this work contributes to several sustainable development goals (SDGs) defined by the United Nations' 2030 Agenda, of which the main two are highlighted:

SDG 7 – Affordable and clean energy, particularly Target 7.b – "expand infrastructure and upgrade technology for supplying modern and sustainable energy services for all in developing countries…", since the focus of this work helps to expand the supply of rare earth elements that are essential for the production of equipment related to renewable energy;

SDG 9 – Industry, innovation and infrastructure, Target 9.5 – "Enhance scientific research, upgrade the technological capabilities of industrial sectors in all countries…" - The processing of critical raw materials such as REEs is still in the development phase, which requires extensive scientific research. This work was carried out as part of an international project involving several countries, contributing to the advancement of knowledge and its sharing, potentially leading to its scaling up for industrial applications.

2

STATE OF THE ART

2.1. Rare Earth Elements (REEs)

Rare earth elements (REEs) comprise seventeen chemically similar metallic elements, including the fifteen lanthanides, together with yttrium and scandium. In the periodic table, the lanthanides correspond to elements with atomic numbers from 57 to 71, whereas scandium and yttrium belong to the transition metals, with atomic numbers 21 and 39, respectively (Gupta and Krishnamurthy, 2005). REEs are commonly divided into light rare earth elements (LREEs), generally from La to Eu, and heavy rare earth elements (HREEs), generally from Gd to Lu, including yttrium. Although scandium is classified as a rare earth element, it is usually excluded from both LREE and HREE groups due to its distinct geochemical behavior (Jordens et al., 2013).

The designation "rare earth" does not indicate extreme scarcity in the Earth's crust. The term is historically related to the difficulty of isolating and separating individual REEs in pure form, mainly due to their strong chemical similarity and frequent co-occurrence in the same mineral phases (Gupta and Krishnamurthy, 2005). REEs are widely distributed in the Earth's crust, although economically exploitable concentrations are restricted to specific deposits where grade, tonnage, mineralogy and processing feasibility allow potential extraction (Coint and Dahlgren, 2019; Jordens et al., 2013).

REEs do not usually occur as native metals in natural deposits. They are mainly hosted in minerals such as carbonates, phosphates, silicates, oxides and halides (Jordens et al., 2013). Their geochemical behavior is strongly influenced by the predominance of the trivalent oxidation state, represented by REE^{3+}, and by the similarity of ionic radii among adjacent lanthanides. Such characteristics allow different REE ions to substitute for one another within the same mineral structures, explaining their frequent co-occurrence in minerals such as bastnäsite, monazite, xenotime, parisite and synchysite (Gupta and Krishnamurthy, 2005; Jordens et al., 2013).

The gradual decrease in ionic radius across the lanthanide series is known as lanthanide contraction. It results from increasing nuclear charge and limited shielding by 4f electrons, producing small differences between adjacent trivalent lanthanides. Lanthanide contraction contributes to the chemical similarity of REEs and to the difficulty of separating individual rare earth elements during downstream chemical processing (Gupta and Krishnamurthy, 2005). Yttrium is commonly associated with the HREEs because its ionic radius and geochemical behavior are close to heavier lanthanides, while scandium presents a smaller ionic radius and different geochemical behavior (Gupta and Krishnamurthy, 2005; Jordens et al., 2013).

From a beneficiation perspective, REE ores are treated primarily to concentrate REE-bearing minerals rather than to separate individual rare earth elements. The separation of individual REEs usually requires hydrometallurgical or chemical processes after mineral concentration. Therefore, beneficiation performance depends on the mineralogical form of REE occurrence, liberation degree, grain size distribution, mineral associations, density, magnetic response and surface chemistry (Jordens et al., 2013; Al-Ali et al., 2020).

The technological relevance of REEs is associated with their electronic structure, particularly the presence of 4f electrons in the lanthanides. Such electronic configuration contributes to distinctive magnetic, optical and catalytic properties, supporting their use in permanent magnets, catalysts, phosphors, glass additives, polishing compounds, batteries and electronic components (Gupta and Krishnamurthy, 2005; Jordens et al., 2013). Such applications reinforce the strategic importance of efficient beneficiation routes capable of producing REE mineral concentrates suitable for downstream extraction.

2.2. Criticality, Applications and Supply Relevance

Criticality differs from geological scarcity and reflects the combination of economic importance and supply-disruption risk. Within the European Union, rare earth elements are classified as critical raw materials, while light and heavy REEs used in permanent magnets are also considered strategic raw materials because of their importance to green, digital, defence and aerospace technologies and the difficulty of increasing production rapidly (Ragonnaud, 2024).

REEs are used in permanent magnets, catalysts, polishing compounds, metallurgy, batteries, ceramics, glass additives and phosphors. Permanent magnets have particular strategic relevance because neodymium, praseodymium, dysprosium and terbium are required for high-performance NdFeB magnets used in electric-vehicle traction motors, wind-turbine generators and electronic equipment. Growth in electrification and renewable-energy generation has consequently increased demand for magnet-related REEs (Nkiawete & Vander Wal, 2025).

Supply risk is intensified by the geographical concentration of mining and processing capacity. In 2022, China accounted for approximately 70% of global REO mine production and approximately 85% of global processing capacity, despite the wider geographical distribution of REE deposits and the development of new projects outside China (Liu et al., 2023). Furthermore, REE deposits contain individual elements in unequal proportions. Carbonatite deposits are commonly enriched in light REEs, whereas market growth is strongly associated with selected magnet-related elements. An increase in total REE production therefore does not necessarily provide a proportional increase in the supply of every commercially important element (Chen et al., 2024; Shuai et al., 2024).

The European Union remains strongly dependent on imported REEs. Regulation (EU) 2024/1252, designated as the Critical Raw Materials Act, established non-binding benchmarks for 2030 corresponding to 10% of annual strategic raw-material consumption supplied through EU extraction, 40% through EU processing and 25% through recycling. The regulation also aims to limit dependence on any single third country to no more than 65% of annual consumption at a relevant processing stage (Ragonnaud, 2024). Development of European mineral resources, beneficiation technologies and processing capacity is therefore relevant to the diversification and resilience of the REE supply chain.

2.3. Deposits and Mineralogy of Rare Earth Elements

Rare earth elements occur in several geological environments and are hosted by minerals with different chemical compositions, textures and mineral associations. Therefore, the evaluation of REE-bearing ores requires more than the determination of total rare earth oxide content. Mineralogy, grain size, liberation degree and association with gangue minerals are critical parameters because they influence the response of the ore to physical and physico-chemical beneficiation processes. Although REEs are relatively widespread in the Earth's crust, economically significant deposits are geographically restricted and mineralogically variable (Chen et al., 2024; Shuai et al., 2024; Jordens et al., 2013).

2.3.1 Global distribution and production of Rare Earth Resources

Rare earth element resources are distributed worldwide, although reserves and mine production are concentrated in a limited number of regions. China, Vietnam, Russia, Brazil, India, Australia, the United States of America, Greenland, Canada and South Africa are frequently reported as important countries in the global distribution of REE resources. However, geological occurrence does not necessarily imply economic viability, since exploitation depends on grade, tonnage, mineralogy, processing feasibility, environmental constraints and supply-chain conditions (Chen et al., 2024; Shuai et al., 2024).

The contrast between global reserves and mine production is shown in Figure 1. According to Shuai et al. (2024), global REE reserves in 2022 were mainly concentrated in China, Vietnam, Brazil and Russia, whereas mine production was dominated by China, followed by the United States and Australia.

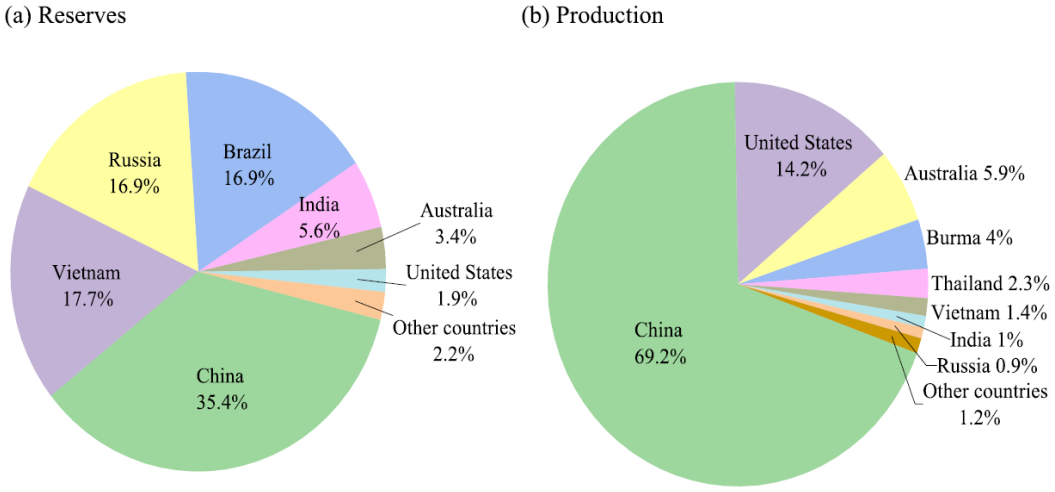

Figure 1: Global rare earth reserves and mine production distribution in 2022. Source: Shuai et al. (2024).

Such distribution indicates a difference between geological resource availability and active production capacity, which is influenced by mining activity, processing infrastructure and supply-chain organisation (Chen et al., 2024; Shuai et al., 2024).

Known REE mines, deposits and occurrences are distributed across several continents, including America, Europe, Africa, Asia and Australia. The global distribution of known REE mines, deposits and occurrences is presented in Figure 2, while the complete numerical identification of the deposit locations represented on the map is provided in Appendix E. In the context of the present study, the Fen Complex in Norway is identified as location 81 in the numerical legend.

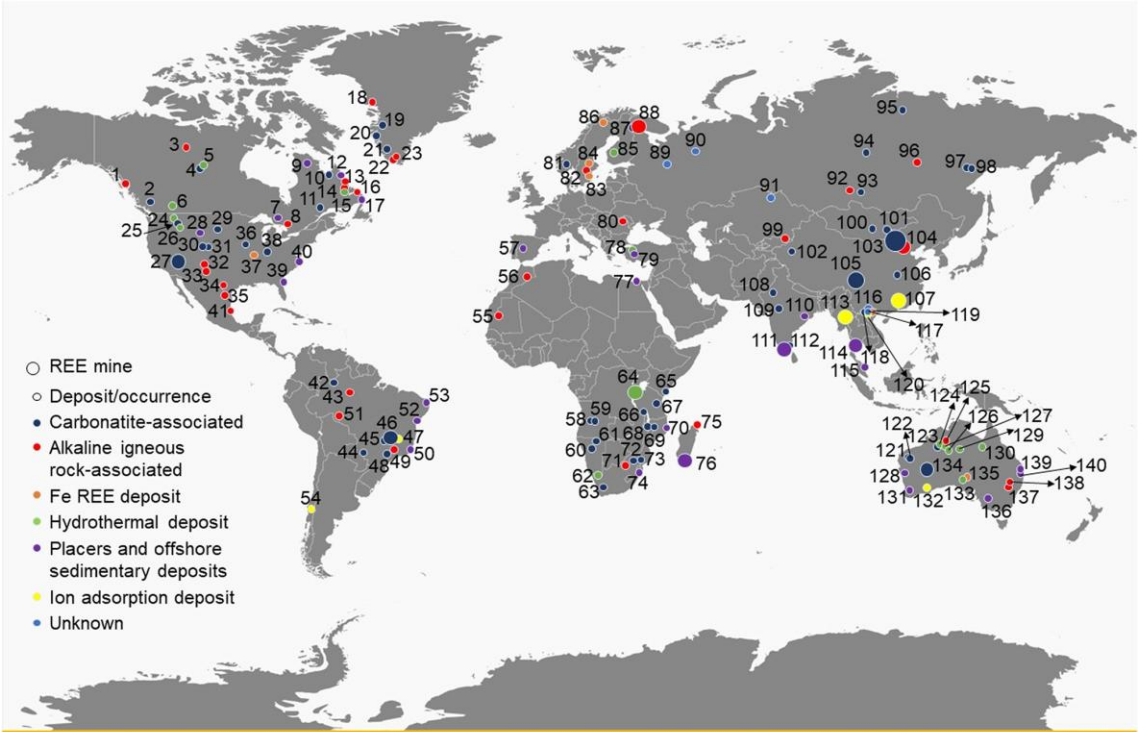

Figure 2: Global distribution of rare earth mines, deposits and occurrences. Adapted from Chen et al. (2024).

2.3.2 Main REE deposit types and REE-bearing minerals

REE deposits may be classified according to geological setting, genetic process, mineralogical association and form of REE occurrence. Chen et al. (2024) distinguish carbonatite-related deposits, deposits associated with alkaline igneous rocks, magmatic-hydrothermal deposits, residual weathering deposits, placer deposits, offshore sedimentary deposits and REEs in coals. Shuai et al. (2024) also classify REE deposits into endogenous and exogenous groups, including carbonatite, alkaline igneous rock, hydrothermal, iron oxide copper–gold, placer and ion-adsorption types. Such classifications show the mineralogical diversity of REE resources and the need to evaluate each deposit according to its mineral hosts and gangue assemblage.

REEs are not found as native metals in natural ores, but occur in minerals such as carbonates, phosphates, silicates, oxides and halides (Jordens et al., 2013). More than 250 REE-bearing minerals have been identified, although only a limited number have commercial relevance. Bastnäsite, monazite and xenotime are generally considered the main economic REE minerals. Bastnäsite is a REE fluorcarbonate mainly associated with light rare earth elements, monazite is a REE phosphate that may contain thorium and uranium, and xenotime is an yttrium phosphate commonly enriched in heavy rare earth elements. Other minerals, including parisite, synchysite, allanite, eudialyte, loparite and REE-bearing apatite, may be important in specific deposits or emerging resources (Chen et al., 2024; Jordens et al., 2013; Dushyantha et al., 2020).

Carbonatite-related deposits are among the most important hard-rock sources of REEs and are commonly enriched in light rare earth elements. They may contain bastnäsite, monazite, parisite, synchysite, ancylite, REE-bearing apatite and, less commonly, xenotime or allanite. These minerals may occur with gangue phases such as calcite, dolomite, ankerite, barite, fluorite, magnetite, hematite, pyrite, silicates and other Fe-bearing minerals (Al-Ali et al., 2020). Deposits associated with alkaline igneous rocks may contain eudialyte, allanite, loparite and other REE-bearing silicates or zirconosilicates, commonly producing more complex mineralogical and metallurgical behaviour (Chen et al., 2024; Shuai et al., 2024).

Placer deposits result from weathering, erosion, transport and concentration of resistant heavy minerals such as monazite and xenotime. In contrast, ion-adsorption clay deposits contain REEs weakly adsorbed onto clay mineral surfaces rather than mainly hosted in discrete crystalline REE minerals. Offshore sediments and REE-bearing coals are also recognised as potential or unconventional REE resources, although exploitation depends strongly on mineral form, grade, environmental constraints and extraction feasibility (Chen et al., 2024; Shuai et al., 2024; Dushyantha et al., 2020).

The mineralogical host of REEs is important because beneficiation separates minerals or mineral-bearing particles rather than individual chemical elements. Mineral-type REE ores, including carbonatite-related, alkaline igneous and placer deposits, may be treated by physical separation and/or froth flotation, depending on liberation, density, magnetic susceptibility, electrical conductivity and surface chemistry. In contrast, ion-adsorption clay deposits are generally treated by leaching because REEs occur mainly as adsorbed ions rather than discrete mineral phases suitable for conventional beneficiation (Jordens et al., 2013; Shuai et al., 2024). The principal REE deposit types, their representative REE-bearing minerals, selected examples and the corresponding mineralogical implications for beneficiation are summarised in Table 1.

Table 1: Main REE deposit types, representative REE-bearing minerals and mineralogical implications for beneficiation, adapted from Chen et al. (2024), Shuai et al. (2024), Jordens et al. (2013)

Deposit type	Representative REE-bearing minerals or occurrence	Relevant examples/regions	Mineralogical implications for beneficiation
Carbonatite-related deposits	Bastnäsite, monazite, parisite, synchysite, REE-bearing apatite	Bayan Obo, Mountain Pass, Mount Weld, Maoniuping, Fen	Major hard-rock REE sources; processing response is influenced by carbonate gangue, fluorcarbonates, phosphates, barite, fluorite and Fe-bearing minerals.
Deposits associated with alkaline igneous rocks	Eudialyte, allanite, loparite, zirconosilicates and REE-bearing silicates	Strange Lake, Kvanefjeld, Norra Kärr, Lovozero	Mineralogically complex; fine intergrowths and refractory silicate or zirconosilicate minerals may affect liberation and downstream treatment.
Magmatic-hydrothermal deposits	Fluorcarbonates, phosphates, oxides and alteration-related REE minerals	Maoniuping, Weishan and other hydrothermal systems	Mineral assemblage and alteration intensity may influence liberation, gangue behavior and flotation selectivity.
Residual weathering deposits	Secondary REE enrichment; residual monazite, bastnäsite, apatite or clay-associated REEs	Weathered carbonatites and alkaline rocks in China, Vietnam, Brazil and Australia	Weathering may enrich REEs but may also generate fine particles and clay-rich material, affecting physical beneficiation and leaching behavior.
Placer deposits	Monazite, xenotime and other resistant heavy minerals	India, Brazil, Australia, South Africa	Dense and resistant minerals may be concentrated using density, magnetic and electrical property differences.
Offshore sedimentary deposits	REE-bearing marine sediments, phosphates, Fe–Mn nodules or sediment-hosted phases	Marine and offshore sedimentary environments	Fine particle size, mineral form and environmental constraints influence potential recovery approaches.
Ion-adsorption clay deposits	REEs weakly adsorbed onto clay mineral surfaces	Southern China, Myanmar and weathered granitic terrains	REEs occur mainly as adsorbed ions rather than discrete minerals; processing is generally leaching-based rather than conventional mineral beneficiation.
REEs in coals and coal by-products	REEs in minerals, organic matter, ash phases or adsorption sites	China, Russia and United States	Potential secondary or unconventional resources; recovery depends on REE mode of occurrence in coal, ash or associated mineral phases.

2.3.3 Fen Carbonatite Complex, Telemark, Norway

The Fen Carbonatite Complex is located in Telemark, southern Norway, and consists of a carbonatite–alkaline intrusive complex with significant REE mineralisation potential. The complex includes Fe-dolomite carbonatites (FDC), also referred to as rauhaugite in previous descriptions, which are reported as the main lithology associated with REE enrichment. REE mineralisation is not uniformly distributed across all lithological units, but is mainly associated with specific Fe-rich dolomite carbonatite facies (Dahlgren, 2019; Coint & Dahlgren, 2019).

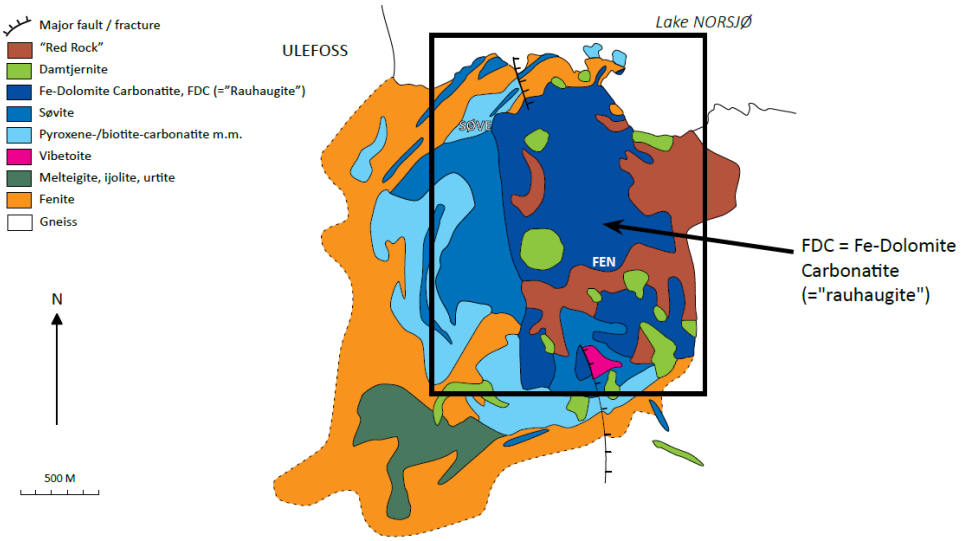

Figure 3 : Simplified geological map of the Fen Carbonatite Complex, highlighting the Fe-dolomite carbonatite area. Source: Dahlgren (2019).

The REE mineralisation reported in the Fen Complex is mainly associated with REE fluorcarbonates, particularly parisite–synchysite intergrowths and bastnäsite, together with monazite as an important REE phosphate phase. Allanite is also reported in minor amounts. According to Dahlgren (2019), parisite commonly occurs syntactically intergrown with synchysite and appears to be among the most widespread REE-bearing phases in several inspected aggregates, whereas bastnäsite may be less common. However, the relative abundance of individual REE minerals remains uncertain because available probe analyses and studied mineralised samples are still limited (Dahlgren, 2019).

Dahlgren (2019) reports theoretical REE_2O_3 contents of approximately 75% for bastnäsite, 51.5–61% for synchysite–parisite mixtures, about 65% for monazite and about 27% for allanite, based on ideal mineral formulas rather than bulk-sample analyses.

From a processing perspective, the Fen Fe-dolomite carbonatites contain several gangue and accessory minerals relevant to beneficiation. Reported associated minerals include Fe-rich dolomite, calcite, quartz, biotite, chlorite, barite, fluorite, magnetite, hematite, pyrite and minor sulphides. Barite is described as a common and widespread phase in most Fe-dolomite carbonatites, while magnetite and hematite are typical Fe-oxide phases. Pyrite is reported as the prevailing sulphide, with pyrrhotite, chalcopyrite, galena and sphalerite occurring in lower amounts (Dahlgren, 2019; Coint & Dahlgren, 2019).

Accessory minerals such as thorite, zircon, rutile, columbite and xenotime may also occur locally or in minor quantities. Thorite is reported as minute crystals closely associated with REE minerals. Dahlgren (2019) also indicates that REE minerals may occur as inclusions in pyrite or magnetite, which is relevant

for beneficiation because such associations may influence sulphide separation, magnetic separation and REE deportment during processing (Dahlgren, 2019; Coint & Dahlgren, 2019).

Mineralogical characteristics provide the basis for selecting beneficiation routes for REE-bearing ores. In carbonatite systems, REE fluorcarbonates and phosphates may occur with carbonates, barite, fluorite, apatite, silicates, oxides and sulphides, causing beneficiation response to depend on mineral identity, grain size, liberation degree and mineral associations. For Fen-type material, such parameters are particularly relevant because different REE-bearing minerals may occur within carbonate-rich and Fe-bearing assemblages (Jordens et al., 2013; Al-Ali et al., 2020; Akyildiz et al., 2026).

2.4. Beneficiation of REE-bearing Ores

2.4.1 General beneficiation approach

After mining, rare earth element ores are processed to separate REE-bearing minerals from gangue minerals and produce an upgraded concentrate. The objective of beneficiation is not the separation of individual rare earth elements, but the concentration of mineral phases containing REEs before downstream extraction. According to Wills and Napier-Munn (2006), mineral processing is based on two fundamental operations: liberation and concentration. Liberation is commonly achieved by crushing and grinding, whereas concentration separates liberated or partially liberated particles according to differences in physical or physico-chemical properties.

In REE-bearing ores, beneficiation is strongly controlled by mineralogical characteristics because REEs occur in discrete mineral phases rather than as native metals. Commercially important REE minerals include bastnäsite, monazite and xenotime, while other minerals such as parisite, synchysite, allanite and REE-bearing apatite may be relevant in specific deposits. Such minerals may be concentrated by gravity separation, magnetic separation, electrostatic separation and froth flotation, depending on liberation, density, magnetic susceptibility, electrical conductivity and surface chemistry (Jordens et al., 2013; Shuai et al., 2024).

Carbonatite-hosted REE ores commonly contain fluorcarbonate, phosphate and accessory REE-bearing minerals associated with carbonates, silicates, apatite, barite, fluorite, magnetite and Fe-bearing carbonates. Such mineral assemblages may create difficulties for selective separation because valuable and gangue minerals can present overlapping physical or surface properties (Al-Ali et al., 2020; Akyildiz et al., 2026).

2.4.2 Comminution and liberation

Comminution is a preliminary stage in rare earth ore beneficiation because valuable minerals must be sufficiently liberated from gangue before pre-concentration or flotation can be effective. Liberation is achieved through crushing and, when required, grinding, until the material contains particles in which valuable and gangue minerals are sufficiently exposed for separation. To produce clean concentrates with limited gangue contamination, the ore must be ground to a particle size compatible with the liberation of associated valuable minerals (Wills and Napier-Munn, 2006).

The required grinding size depends on mineralogical assemblage and ore texture. Ore texture includes mineral grain size, dissemination, association and shape, all of which influence liberation behavior, concentration requirements, achievable concentrate grades and separation difficulties. Therefore, comminution must be defined according to mineralogy rather than as a fixed size-reduction operation (Wills and Napier-Munn, 2006). For Fen-type ore, comminution is therefore considered as preparation

for physical pre-concentration and froth flotation, with the objective of promoting sufficient exposure of REE-bearing minerals while limiting fine-particle generation.

2.4.3 Gravity separation

Gravity separation is a physical concentration method based on density differences between valuable minerals and gangue minerals. Denser particles behave differently from lighter particles under gravity and fluid resistance, allowing separation when adequate density contrast and particle-size control are achieved. The method requires adequate particle-size control because gravity processes become less efficient for very fine particles or poorly classified feeds (Wills and Napier-Munn, 2006).

Many REE minerals present relatively high specific gravities compared with common gangue minerals. Jordens et al. (2013) reported specific gravities of approximately 4–7 for several REE minerals, while Shuai et al. (2024) indicated values of 2,9–7,2 for rare earth minerals and 2,5–3,5 for most gangue minerals. For such reason, gravity separation can be used as a pre-concentration stage to reject light gangue and reduce the mass reporting to later flotation stages.

Gravity methods are particularly relevant in monazite- and xenotime-bearing heavy mineral sands, where high-capacity gravity concentration may be followed by magnetic, electrostatic or additional gravity separation stages, depending on mineralogical composition (Jordens et al., 2013). Shuai et al. (2024) also describe gravity separation equipment such as shaking tables, spiral chutes, jigs and centrifugal separators, and report that gravity separation is commonly used in combined flowsheets, including gravity–magnetic separation and gravity–flotation routes.

The main limitations of gravity separation in complex REE ores are related to fine particle losses, poor liberation and the presence of dense gangue minerals. In carbonatite ores, minerals such as barite, apatite, magnetite and Fe-bearing carbonates may influence separation efficiency because they may occur with REE-bearing minerals or present physical properties that reduce selectivity. For Fen-type carbonatite material, gravity separation may therefore be considered as a possible pre-concentration method, but its applicability depends on mineral associations, liberation degree and grade-specific mineralogical variability (Akyildiz et al., 2026).

2.4.4 Magnetic separation

Magnetic separation is a physical concentration method based on differences in magnetic susceptibility between minerals. Low-intensity magnetic separation is generally applied to strongly ferromagnetic minerals, such as magnetite, whereas high-intensity magnetic separation is used for weakly magnetic minerals. Therefore, the method may be applied either to remove magnetic gangue minerals or to recover valuable minerals with magnetic response before subsequent concentration stages (Wills & Napier-Munn, 2006).

In REE beneficiation, magnetic separation is commonly used to remove Fe-bearing gangue minerals or to concentrate paramagnetic REE-bearing minerals, particularly monazite and xenotime. Jordens et al. (2013) describe monazite and xenotime as paramagnetic minerals and report magnetic separation as one of the main unit operations used in REE mineral beneficiation. Magnetic separation is also relevant in heavy mineral sand processing, where magnetic minerals can be removed before further separation of monazite, xenotime, zircon and rutile-bearing fractions (Jordens et al., 2013).

Recent reviews also describe magnetic separation as an important stage in REE processing flowsheets. Cheng et al. (2024) indicate that RE-bearing ores, except ion-adsorption clays, are commonly beneficiated using flotation, gravity and magnetic separation. In China, magnetic separation is applied

to recover iron-bearing minerals, while REE minerals and fluorite are recovered from magnetic separation tailings through subsequent flotation stages (Cheng et al., 2024; Shuai et al., 2024).

For Fen-type carbonatite material, magnetic separation is mainly relevant as a pre-concentration or gangue-removal stage before flotation. Akyildiz et al. (2026) reported that more than 90% of TREO was recovered in the non-magnetic product across low-, medium- and high-grade Fen samples. However, the medium-grade material showed stronger association between REE minerals and magnetite, indicating possible REE losses during magnetic gangue removal. Therefore, the applicability of magnetic separation depends on mineral liberation, magnetite abundance and the association between REE-bearing minerals and Fe-bearing phases (Akyildiz et al., 2026).

2.4.5 Electrostatic separation

Electrostatic separation is based on differences in electrical conductivity between mineral particles. Conductive minerals dissipate charge rapidly and follow a different trajectory from non-conductive minerals, which retain surface charge and may remain attached to the separator surface. Although electrical separation can be applied to minerals with different conductivity, industrial application is limited by low capacity for fine material and by the requirement for dry feed under controlled humidity conditions (Wills and Napier-Munn, 2006).

In REE beneficiation, electrostatic separation is most relevant in heavy mineral sand processing, commonly after gravity and magnetic separation. The method may assist the separation of monazite and xenotime from associated conductive minerals, especially Ti–Fe minerals such as ilmenite. Shuai et al. (2024) report that electrostatic separation is generally used in heavy placer operations after gravity separation, mainly for impurity removal and comprehensive recovery of concentrates. The same review describes the removal of ilmenite from xenotime-bearing fractions because ilmenite is electrically conductive, whereas xenotime is non-conductive.

For primary carbonatite-hosted REE ores, electrostatic separation has more limited applicability because comminution is commonly performed in wet circuits and drying finely ground material may increase energy consumption. Therefore, for Fen-type carbonatite ore, electrostatic separation is less central than comminution, gravity separation, magnetic separation and froth flotation, which are more directly related to liberation, magnetic response and surface chemistry (Jordens et al., 2013; Akyildiz et al., 2026).

2.4.6 Froth flotation

Froth flotation is a physico-chemical separation technique based on differences in mineral surface properties. Hydrophobic particles attach to air bubbles and report to the froth phase, while hydrophilic particles remain mainly in the pulp. In REE beneficiation, flotation is widely applied because it can treat relatively fine particle sizes and can be adapted to deposit-specific mineralogy through reagent selection and pulp chemistry control (Wills and Napier-Munn, 2006; Jordens et al., 2013; Marion et al., 2020).

REE flotation is particularly important for carbonatite-related ores, where fluorcarbonate and phosphate minerals may occur with carbonate, sulfate, phosphate, silicate and Fe-bearing gangue minerals. Collectors such as hydroxamic acids, carboxylates and phosphoric acid derivatives are commonly reported for REE minerals, while depressants and pH modifiers are used to improve selectivity against gangue minerals (Jordens et al., 2013; Marion et al., 2020; Shuai et al., 2024). The principles, surface chemistry and reagent systems of REE flotation are discussed in detail in Section 2.5.

2.4.7 Combined beneficiation flowsheets

The beneficiation of rare earth element ores commonly involves more than one separation technique because REE minerals may occur with gangue phases such as carbonates, silicates, fluorite, barite, apatite and Fe-bearing minerals. The selection of each stage depends on mineral properties such as density, magnetic susceptibility, electrical conductivity and surface chemistry. Cheng et al. (2024) reported that most REE beneficiation routes use combinations of gravity separation, magnetic separation and froth flotation, while electrostatic separation is more limited due to the requirement for dry feed.

Bayan Obo, located in Inner Mongolia, China, is a major example of combined REE beneficiation. The deposit is a complex Fe–REE–Nb polymetallic ore containing more than 170 minerals, with bastnäsite and monazite as the main REE-bearing minerals. Several routes have been tested or applied, including magnetisation roasting–low-intensity magnetic separation–reverse flotation, low-intensity magnetic separation–flotation–high-intensity magnetic separation, and low-intensity magnetic separation–semi-preferential semi-bulk flotation–gravity separation–flotation. The route developed in 1990, based on low-intensity magnetic separation, high-intensity magnetic separation and flotation, is described as the most successful industrial process for Bayan Obo due to its adaptability to the complex ore properties (Shuai et al., 2024). Cheng et al. (2024) also reported that Bayan Obo processing uses magnetic separation to recover magnetite and hematite, while REE minerals and fluorite are recovered from magnetic separation tailings by sequential flotation.

Mountain Pass, located in California, United States, is a bastnäsite-dominated deposit in which beneficiation is mainly based on flotation after crushing and grinding. The ore contains bastnäsite with gangue minerals such as calcite, barite and quartz. According to Shuai et al. (2024), the raw ore is crushed and ground to 80% passing 0,15 mm before flotation. Sodium carbonate, sodium fluosilicate and ammonium lignosulfonate are used as regulators, while tall oil is used as collector. A closed-circuit flotation process with one roughing stage and four cleaning stages at pH 8,8 can produce a rare earth concentrate with 60–63% REO and 65–70% recovery (Shuai et al., 2024). Gupta and Krishnamurthy (2005) described the Mountain Pass route as hot froth flotation after crushing, blending and grinding, followed by rougher flotation and four cleaning stages. Bulatovic (2010) also described thermal conditioning with soda ash, sodium fluorosilicate, lignin sulfonate and tall oil fatty acid, with plant results producing a bastnäsite concentrate of approximately 64% REO.

Maoniuping, located in Sichuan Province, China, is another bastnäsite-dominated REE deposit. The main minerals include bastnäsite, barite, fluorite, quartz and feldspar. Processing is affected by weathering, slime generation and similar surface behaviour among bastnäsite, barite and fluorite. Shuai et al. (2024) reported several beneficiation routes used over time, including single gravity separation, gravity–magnetic separation, magnetic–gravity separation and gravity–flotation. Current local plants commonly apply gravity separation followed by flotation. In the reported route, the ore is ground to 92% passing 200 mesh, and shaking tables are used for slime removal and preliminary bastnäsite enrichment by rejecting light gangue minerals such as quartz, feldspar and mica. Flotation is then performed using sodium carbonate as regulator, water glass as depressant and mixed collectors such as phthalic acid with H205 or H316, producing a concentrate with 66,91% REO and 72,19% recovery (Shuai et al., 2024).

Weishan, located in Shandong Province, China, is reported as an industrial REE flotation operation. The deposit contains bastnäsite, parisite, britholite and minor monazite, associated with calcite, barite, fluorite and quartz. According to Shuai et al. (2024), bastnäsite dissemination is relatively coarse and the REE minerals are more easily liberated than in more complex ores. When grinding fineness reaches 75% passing 0,074 mm, the liberation degree of REE minerals can reach 89,41%. Cheng et al. (2024)

identified Weishan Lake as an industrial-scale REE flotation example together with Bayan Obo and Mountain Pass.

Heavy mineral sand operations provide a further example of combined beneficiation, mainly for monazite and xenotime. Gravity separation is commonly used to produce a heavy-mineral pre-concentrate, followed by magnetic, electrostatic and additional gravity separation according to mineralogical composition. Jordens et al. (2013) described monazite beneficiation from beach sands as a route involving wet gravity concentration to remove low-density gangue, low-intensity magnetic separation to remove ferromagnetic minerals and further gravity, magnetic and electrostatic stages for separation of monazite, zircon and rutile fractions.

2.5. Froth Flotation of REE Minerals

2.5.1 Principles of froth flotation

Froth flotation is a physico-chemical separation process based on differences in surface properties between valuable minerals and gangue minerals. In a system containing solid particles, water and air bubbles, hydrophobic particles attach to bubbles and are transported to the froth phase, while hydrophilic particles remain mainly in the pulp (Wills and Napier-Munn, 2006).

Mineral recovery during flotation may occur through selective attachment to air bubbles, entrainment in water reporting to the froth and physical entrapment between particles attached to bubbles. Selective attachment, or true flotation, is the main chemically selective mechanism, whereas entrainment and entrapment are mainly mechanical and may recover both valuable minerals and gangue minerals (Wills and Napier-Munn, 2006).

In direct flotation, the valuable mineral reports to the froth product, while in reverse flotation the gangue minerals are floated. Flotation performance is influenced by particle size, since very fine particles may increase entrainment and coarse particles may detach from bubbles. Reagents are also essential: collectors increase mineral hydrophobicity, frothers stabilise the froth phase, depressants reduce mineral floatability and pH modifiers control pulp chemistry (Wills and Napier-Munn, 2006).

Froth flotation is widely applied in REE beneficiation because many REE-bearing minerals occur within particle-size ranges suitable for flotation, and reagent conditions can be adapted to deposit mineralogy. According to Jordens et al. (2013) and Marion et al. (2020), flotation is the most commonly used beneficiation method for rare earth minerals, except for ion-adsorption clay deposits. Common REE minerals treated by flotation include bastnäsite, monazite and xenotime.

2.5.2 Surface chemistry, IEP and zeta potential

Surface chemistry influences the interaction between mineral particles, water and flotation reagents. In flotation, mineral surface charge affects reagent adsorption and, consequently, flotation behaviour (Jordens et al., 2013; Marion et al., 2020).

Zeta potential is commonly used to describe the apparent surface charge of mineral particles in water, while the isoelectric point (IEP) corresponds to the pH at which surface charge is neutral. Depending on pulp pH, mineral surfaces may become positively or negatively charged, influencing interaction with collectors, depressants and dissolved ions (Jordens et al., 2013).

In REE flotation, surface-chemical studies have mainly focused on bastnäsite and monazite. Reported IEP values for these minerals vary in the literature due to differences in mineral composition, dissolved species, sample origin and experimental conditions (Jordens et al., 2013). The presence of semi-soluble

gangue minerals, including carbonates, fluorite, barite and apatite, may also modify surface charge and reagent adsorption through the release of dissolved ions into the pulp (Marion et al., 2020).

Zeta potential and IEP are therefore mainly used in the literature to interpret reagent adsorption and flotation behaviour under different pH conditions in REE flotation systems (Jordens et al., 2013; Marion et al., 2020).

2.5.3 Collector chemistry

Collectors are flotation reagents used to increase mineral surface hydrophobicity and promote attachment to air bubbles. In REE flotation, collector chemistry is important because REE minerals commonly occur with gangue minerals presenting similar surface properties, such as calcite, dolomite, fluorite and barite (Jordens et al., 2013; Marion et al., 2020).

The main collector groups reported for REE flotation are carboxylic acids, hydroxamic acids and phosphoric acid derivatives. Such reagents contain oxygen- or nitrogen-bearing functional groups capable of interacting with REE surface cations and promoting adsorption (Shuai et al., 2024). Fatty acids, including oleic acid, sodium oleate and tall oil, were among the earliest collectors used for REE flotation. They provide strong collecting ability but may show limited selectivity because they can also adsorb onto calcium- and barium-bearing gangue minerals (Jordens et al., 2013; Marion et al., 2020).

Hydroxamic acids are among the most studied collectors for REE minerals. Their selectivity is commonly related to the formation of stable chelates with rare earth cations on mineral surfaces. Compared with fatty acids, hydroxamic acids are generally reported as more selective for REE minerals. Collectors such as octanohydroxamic acid, benzohydroxamic acid and commercial hydroxamate mixtures have been applied in bastnäsite and carbonatite-related REE flotation systems (Shuai et al., 2024; Akyildiz et al., 2026).

Phosphoric and phosphonic acid collectors have also been investigated, although they often require acidic conditions, which may be difficult to maintain in carbonate-rich ores due to acid consumption by carbonate minerals (Jordens et al., 2013). Collector dosage is also relevant, because low dosages may reduce recovery, while excessive dosages may increase adsorption onto gangue minerals and decrease selectivity (Marion et al., 2020; Akyildiz et al., 2026).

2.5.4 Depressants, modifiers and pH control

Depressants and modifiers are used to control selectivity between REE minerals and gangue minerals. In complex REE ores, collectors alone may be insufficient because calcite, dolomite, fluorite, barite, apatite and silicates can also interact with collector systems. Depressants are therefore used to reduce gangue floatability or modify pulp chemistry (Jordens et al., 2013; Marion et al., 2020; Shuai et al., 2024).

Sodium silicate, also known as water glass, is one of the most reported depressants in REE flotation. It has been used to depress silicate gangue, fluorite, barite, calcite, dolomite and Fe-bearing minerals. Its action is commonly associated with adsorption of silicate species on gangue surfaces, formation of hydrophilic surface films and removal of calcium or magnesium ions from solution, which may otherwise consume collector (Marion et al., 2020; Shuai et al., 2024).

Ethylenediaminetetraacetic acid (EDTA) is a chelating modifier reported for the control of calcium-bearing gangue minerals. Marion et al. (2020) reported EDTA use for removing calcium ions from monazite surfaces and as a possible fluorite depressant during bastnäsite flotation. Its action is associated with soluble calcium–EDTA complex formation and removal of adsorbed hydroxamate from calcium-

rich gangue minerals. Shuai et al. (2024) also described EDTA as a depressant for calcium-containing gangue minerals, especially fluorite and calcite, under alkaline conditions.

Other depressants and modifiers reported in REE flotation include sodium fluorosilicate, lignin sulfonate, sodium hexametaphosphate, citric acid, oxalic acid, starch and carboxymethyl cellulose. Sodium fluorosilicate and lignin sulfonate have been used in bastnäsite flotation systems, including Mountain Pass, to depress gangue minerals such as fluorite, barite and calcite (Jordens et al., 2013; Marion et al., 2020; Shuai et al., 2024).

Pulp pH controls mineral surface charge, collector speciation, depressant behavior and dissolved ion chemistry. In bastnäsite flotation, sodium carbonate is frequently used as a pH regulator and carbonate-ion source. Sodium hydroxide may also be used for pH adjustment, depending on the reagent system. In carbonate-rich REE ores, pH control and depressant dosage are closely linked to the behavior of semi-soluble gangue minerals and dissolved ions such as Ca^{2+}, Mg^{2+} and Ba^{2+} (Marion et al., 2020; Akyildiz et al., 2026).

2.5.5 Flotation of Fen-relevant REE minerals

Bastnäsite is one of the most studied REE minerals in flotation due to its occurrence in several carbonatite deposits. It is a REE fluorcarbonate mainly enriched in light rare earth elements. Reported collector systems include fatty acids, hydroxamic acids and phosphoric acid derivatives, with hydroxamates frequently associated with improved selectivity toward REE minerals. Bastnäsite flotation is affected by carbonate and sulfate gangue minerals, such as calcite and barite, which may interact with the same collectors (Jordens et al., 2013; Marion et al., 2020; Shuai et al., 2024).

Monazite is a REE phosphate mineral commonly containing Ce, La and Nd, and may also incorporate thorium. Its flotation behaviour differs from REE fluorcarbonates because of its phosphate surface chemistry and its association with phosphate-bearing gangue minerals. Studies reported by Marion et al. (2020) describe the use of oleate and hydroxamate collectors for monazite flotation, with flotation performance affected by dissolved ions, reagent conditioning and pulp chemistry. In carbonatite systems, monazite may occur with apatite and carbonate minerals, which can reduce flotation selectivity (Marion et al., 2020; Akyildiz et al., 2026).

Parisite and synchysite are calcium-bearing REE fluorcarbonates reported in several carbonatite systems, although fewer flotation studies are available for these minerals compared with bastnäsite and monazite. In the Fen carbonatite material studied by Akyildiz et al. (2026), parisite, monazite, bastnäsite and synchysite were identified as the main REE-bearing minerals. The flotation tests used benzohydroxamic acid and Aero® 6493 as collectors, together with sodium silicate, sodium carbonate, Brij 58, citric acid and sodium hydroxide under weakly alkaline conditions (Akyildiz et al., 2026).

In the same Fen study, the flotation circuit consisted of one rougher stage followed by two cleaner stages after grinding below 150 µm. The second cleaner concentrate reached mineral recoveries of 72% for parisite, 75% for bastnäsite, 70% for monazite and 69% for synchysite. Akyildiz et al. (2026) also reported differences in liberation and mineral associations: parisite and bastnäsite were among the better recovered REE minerals, monazite was associated with apatite, barite and carbonate gangue, and synchysite showed stronger association with other REE minerals.

2.5.6 Effect of pH and temperature

Pulp pH is one of the main variables controlling REE mineral flotation because it affects mineral surface charge, collector ionisation, dissolved species and depressant action. In REE flotation systems, pH is

commonly adjusted with sodium carbonate or sodium hydroxide, depending on collector type and gangue mineralogy. Sodium carbonate is frequently reported in bastnäsite flotation because it acts as a pH regulator and may influence carbonate species in solution (Jordens et al., 2013; Marion et al., 2020).

Hydroxamic acid collectors are commonly applied under weakly alkaline to alkaline conditions, whereas some phosphoric or phosphonic acid collectors require more acidic conditions. In carbonate-rich ores, acidic conditions may be difficult to maintain due to carbonate dissolution and acid consumption, which explains the frequent use of hydroxamate-based systems in REE flotation studies involving carbonatite ores (Jordens et al., 2013; Marion et al., 2020).

Temperature has also been reported as an important variable in REE flotation. At Mountain Pass, elevated temperature was used during bastnäsite flotation with fatty acid collectors. The literature reports that heating the pulp with collector can improve bastnäsite flotation selectivity through changes in collector adsorption on bastnäsite relative to calcite and barite, although excessive temperature may reduce concentrate grade when gangue minerals adsorb more collector (Pradip, 1981, *apud* Jordens et al., 2013; Bulatovic, 2010).

In the Fen carbonatite flotation study, Akyildiz et al. (2026) maintained pulp temperature at 50 °C to promote mineral dissolution and reagent activation. The tests used hydroxamate based collectors, sodium silicate, sodium carbonate, citric acid and sodium hydroxide, with pH adjusted to weakly alkaline conditions after depressant addition. The authors reported flotation of parisite, monazite, bastnäsite and synchysite from Fen material under such conditions (Akyildiz et al., 2026).

2.5.7 Flotation challenges in carbonatite ores

Carbonatite-hosted REE ores commonly contain several REE-bearing minerals associated with carbonate, sulfate, phosphate, silicate and Fe-bearing gangue phases. Flotation selectivity is difficult because REE fluorcarbonates and gangue minerals such as calcite, dolomite, fluorite, barite and apatite may show similar surface behaviour and interact with the same collectors. Semi-soluble gangue minerals may also release Ca^{2+}, Mg^{2+} and Ba^{2+} into the pulp, modifying mineral surfaces and affecting collector adsorption (Jordens et al., 2013; Marion et al., 2020; Al-Ali et al., 2020).

For Fen-type carbonatite ore, mineralogical variability is also relevant. Akyildiz et al. (2026) reported that parisite, monazite, bastnäsite and synchysite occur with different liberation degrees and mineral associations. Synchysite was more strongly associated with other REE minerals, while monazite showed associations with apatite, barite and carbonates. The Fen flotation study also used hydroxamate collectors, sodium silicate, sodium carbonate, citric acid and sodium hydroxide under weakly alkaline conditions and at 50 °C, reflecting the reagent control required in carbonate-rich REE flotation systems (Marion et al., 2020; Akyildiz et al., 2026).

2.6 Process Mineralogy and Research Gap

Process mineralogy provides the link between ore characterisation and beneficiation route selection. For REE-bearing carbonatite ores, relevant parameters include the identity and abundance of REE minerals, gangue mineralogy, grain size distribution, liberation degree, mineral associations and elemental deportment (Al-Ali et al., 2020; Akyildiz et al., 2026).

In the Fen Carbonatite Complex, previous studies have described REE mineralisation mainly in Fe-dolomite carbonatites, with REE fluorcarbonates such as bastnäsite, parisite and synchysite, together with subordinate monazite (Dahlgren, 2019; Coint & Dahlgren, 2019). Reported gangue and accessory phases include carbonates, barite, fluorite, apatite, silicates, Fe-oxides and sulphides, all of which may

influence separation behaviour during beneficiation (Dahlgren, 2019; Coint & Dahlgren, 2019; Al-Ali et al., 2020).

Recent work on Fen-type material has related beneficiation response to mineralogical variability. Akyildiz et al. (2026) reported that monazite-, apatite-, barite- and Fe-carbonate-rich intervals may respond differently during magnetic separation and flotation, depending on mineral associations and liberation characteristics. The same study also showed that parisite, bastnäsite, monazite and synchysite can be recovered by hydroxamate-based flotation under controlled reagent, pH and temperature conditions (Akyildiz et al., 2026).

Compared with major REE deposits such as Bayan Obo, Mountain Pass and Maoniuping, fewer beneficiation studies are available for Fen material, particularly regarding combined physical pre-concentration and froth flotation under controlled reagent conditions. Therefore, the available literature identifies mineralogical variability, liberation, gangue association and flotation response as key aspects for evaluating the beneficiation of Fen carbonatite ore (Dahlgren, 2019; Coint & Dahlgren, 2019; Akyildiz et al., 2026).

3

MATERIALS AND METHODS

Chapter 3 describes the materials, experimental procedures, analytical methods and performance calculations applied to evaluate the beneficiation of rare earth element-bearing ore from the Fen Carbonatite Complex. The experimental programme was based on laboratory-scale froth flotation of two ore composites, designated C4 and CG, under different feed preparation, pre-concentration, reagent and operating conditions.

The methodology was organised according to the sequence followed during laboratory work. Section 3.1 presents the research design and experimental strategy. Section 3.2 describes the ore samples and composite preparation. Section 3.3 presents the beneficiation routes investigated. Section 3.4 describes the flotation reagents and operating variables. Section 3.5 presents the flotation equipment and procedure. Section 3.6 describes product handling and sample preparation. Section 3.7 presents the analytical methods, while Section 3.8 defines the metallurgical calculations used for interpretation of the experimental results. Section 3.9 identifies the main methodological limitations of the experimental programme.

3.1. Research design and experimental strategy

The experimental work was designed to assess the response of rare earth element-bearing Fen carbonatite ore to froth flotation and combined pre-concentration routes. The study focused on two representative ore composites that were selected for beneficiation testing. Composite C4 was evaluated through direct flotation, staged flotation and flotation after pre-concentration. Composite CG was evaluated through direct flotation, hydrogravitic pre-concentration followed by flotation, magnetic pre-concentration followed by flotation and Taguchi-based flotation series with staged flotation.

The experimental programme included four main methodological routes: direct froth flotation of untreated material; hydrogravitic pre-concentration followed by froth flotation; microwave-assisted digestion prior to froth flotation; magnetic separation as a pre-concentration and parameter-based flotation testing using Taguchi experimental design for composite CG, as two stage flotation. Route selection followed laboratory work developed during research fellowship.

A summary of the flotation tests performed during the experimental programme is presented in Table 2. The table includes the experimental routes, tests designations, feed conditions, product codes and number of tests. Complete experimental records and operating conditions, are provided in chapter 4 and in Appendix A.

Table 2: Summary of flotation tests performed during the experimental programme.

Composite	Experimental route	Flotation test designation	Feed or pre-treatment condition	Final products generated	Number of tests
C4	Preliminary direct flotation tests	C4_F1; C4_F1a; C4_F1a2; C4_F2–C4_F12B	C4 composite, including first- and second-stage flotation products	Overflow (_O) and underflow (_U) products from each test	16
C4	Hydrogravitic pre-concentration followed by flotation	C4_ST_R4_C_F13; C4_ST_R4_M_F14	C4 hydrogravitic pre-concentrated fractions	C4_ST_R4_C_ F13_O/U; C4_ST_R4_M_ F14_O/U	2
CG	Hydrogravitic pre-concentration followed by flotation	CG_ST_M_F15; CG_ST_C_F16; CG_ST_M_F17; CG_ST(3)_M_F20; CG_ST(3)_C_F21; CG_ST(3)_M_F23; CG_ST(3)_C_F24	CG hydrogravitic pre-concentrated fractions (concentrate and middlings)	Overflow (_O) and underflow (_U) products from each test	7
CG	Preliminary direct flotation tests	CG_F18; CG_F19	CG composite	CG_F18_O/U; CG_F19_O/U	2
CG	First stage CG_F22A Taguchi series	CG_F22_1–CG_F22_8; CG_F22_1R	CG composite	Overflow (_O) and underflow (_U) products from each test	9
CG	Magnetic pre-concentration followed by flotation	CG_NMAG_F25	CG nonmagnetic fraction	CG_MAG_F25_ O/U	1
CG	Sequential flotation tests	CG_F26A; CG_F26B	CG composite	CG_F26A_O/U; CG_F26B_O/U	2
CG	Second stage CG_F22B Taguchi series	CG_F22_1B–CG_F22_6B	CG_F22A overflow	Overflow (_O) and underflow (_U) products from each test	6
CG	First stage CG_F27A Taguchi series	CG_F27_1A_T; CG_F27_1A–CG_F27_8A; CG_F27_2AR; CG_F27_8AR	CG composite	Overflow (_O) and underflow (_U) products from each test	11

CG	Second stage CG_F27B Taguchi series	CG_F27_1B–CG_F27_8B	CG_F27A overflow	Overflow (_O) and underflow (_U) products from each test	8
Total	—	—	—	—	**64**

Note: Product suffix "_O" identifies overflow material, corresponding to floated concentrate recovered during froth flotation. Product suffix "_U" identifies underflow material, corresponding to non-floated material remaining inside flotation cell. Letter "R" identifies replicate testing. Letter "M" corresponds to the middlings hydrogravitic fraction and "C" identifies the concentrate hydrogravitic fraction. Test series identified by letter "A" correspond to the 1st stage of flotation and "B" to the second stage of flotation.

3.2. Ore samples and composite preparation

The two Fen carbonatite ore composites, C4 and CG served as feed materials for laboratory-scale beneficiation tests described in Section 3.1. The samples where sent already prepared. The subsequent sample preparation aimed to obtain suitable feed materials for froth flotation, chemical analysis and mineralogical observation. Preparation included representative material handling, particle size control, milling when required and systematic sample labelling. Feed materials comprised untreated composites, hydrogravitic and nonmagnetic pre-concentrated products and pre-treated materials generated during experimental routes (first stage flotation overflow). The pre-concentration materials where performed by another college in the project.

For direct flotation routes, untreated C4 and CG composites were used as flotation feed. For physical pre-concentration routes, hydrogravitic separation generated concentrate, middlings and tailings fractions. Concentrate and middlings fractions were retained for subsequent flotation testing. Sample codes identified composite, pre-concentration stage, fraction type and flotation test number. For C4, hydrogravitic products included codes such as C4_ST_R4_C and C4_ST_R4_M. For CG, equivalent products included codes such as CG_ST_C, CG_ST_M, CG_ST(3)_C and CG_ST(3)_M. For the magnetic separation, only the nonmagnetic fraction was used as a feed material, designated as CG_NMAG_F25.

Particle-size control was applied before analytical characterisation. Material retained on a calibrated 74 µm screen was milled to achieve target particle-size specification below 75 µm for chemical analysis. Materials subjected to milling included raw ore feeds without previous pre-concentration and hydrogravitic pre-concentration products, including concentrate and middlings fractions. Milling was performed at FEUP, Porto, Portugal.

Prepared materials were submitted to analytical characterisation as described in Section 3.7. Particle size distribution was measured for feed materials prior to flotation. X-ray fluorescence, inductively coupled plasma mass spectrometry and were applied to feed materials and final flotation products. Scanning electron microscopy with Energy-Dispersive X-Ray Spectroscopy was used for mineralogical observation of selected feed.

3.3. Beneficiation routes investigated

Beneficiation routes were selected to evaluate flotation response of Fen carbonatite ore under different feed preparation and pre-treatment conditions. Experimental design included direct froth flotation, hydrogravitic pre-concentration followed by froth flotation, microwave-assisted digestion prior to froth flotation and Taguchi-based direct flotation testing for composite CG. Figure 4 describes the routes applied for the composites C4 and CG. In chapter 4, only the most relevant tests where discussed.

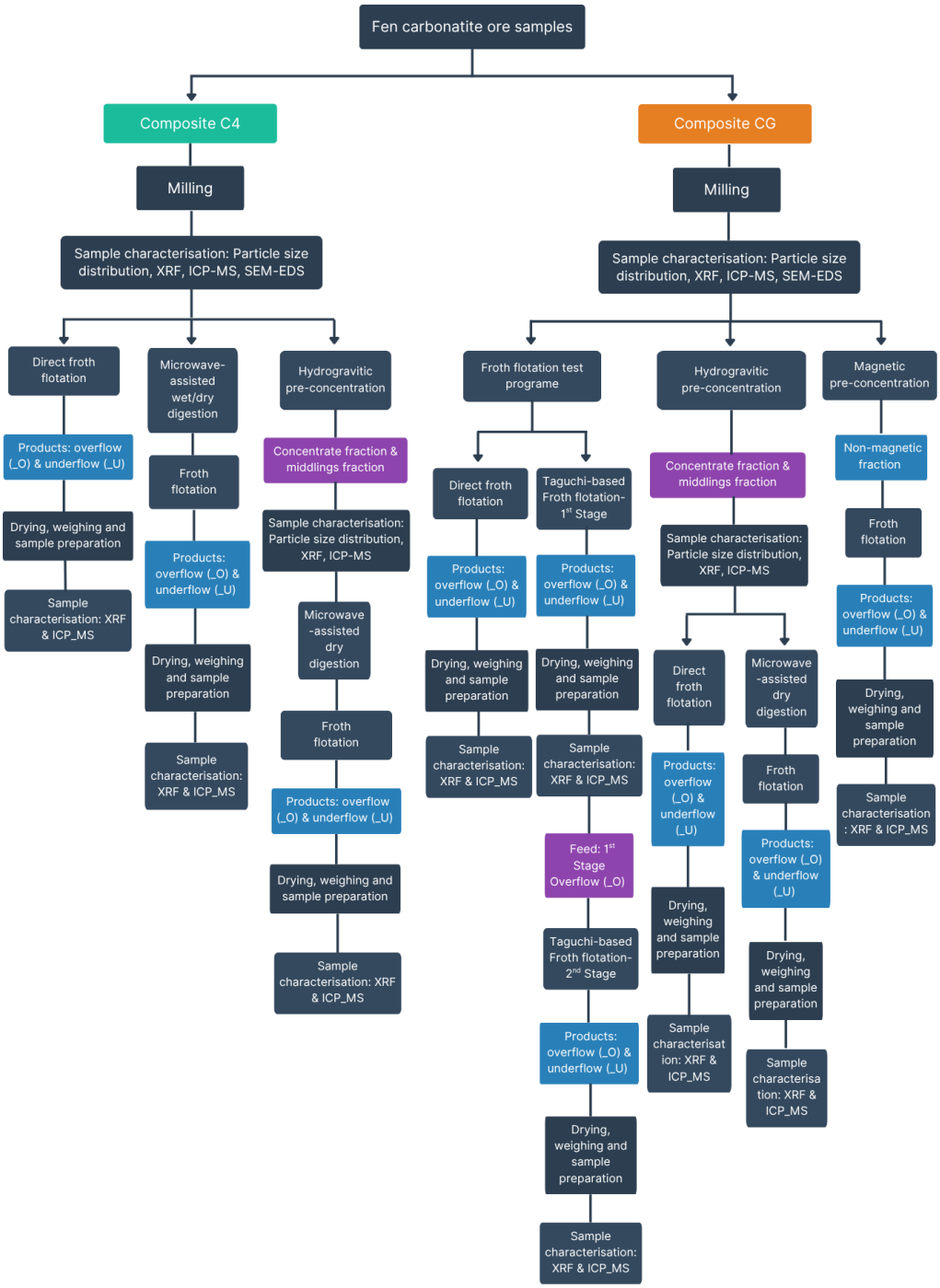

Figure 4: Experimental programme applied to the C4 and CG composites.

3.3.1. Direct froth flotation

Direct froth flotation was applied to untreated C4 and CG composites. In such route, raw material was used as flotation feed without previous hydrogravitic separation, microwave-assisted digestion or magnetic pre-treatment. The feed were milled first to particle size control before flotation.

For composite C4, direct flotation included preliminary and staged tests identified from C4_F1 to C4_F12B. Some test went to a digestion step (microwave-assisted) and others were performed as sequential stages, where flotation products from a previous stage were used for subsequent flotation. For composite CG, direct flotation included preliminary tests identified as CG_F18 and CG_F19, as well as additional direct flotation series associated with CG_F22, CG_F26 and CG_F27 experimental groups.

3.3.2. Hydrogravitic pre-concentration followed by flotation

Hydrogravitic pre-concentration was applied before flotation to generate density-based separated fractions from raw ore. Laboratory procedure produced concentrate, middlings and tailings fractions. Concentrate and middlings fractions were retained for subsequent flotation testing, whereas tailings were not used as main flotation feed in any of the routes applied. For a particle size control, the feed materials were also milled before flotation.

For composite C4, hydrogravitic pre-concentration route included products identified as C4_ST_R4_C and C4_ST_R4_M. Concentrate and middlings fractions were subsequently subjected to microwave-assisted dry digestion before froth flotation, according to route developed during laboratory work.

For composite CG, hydrogravitic pre-concentration routes included products identified as CG_ST_C, CG_ST_M, CG_ST(3)_C and CG_ST(3)_M. Such fractions were processed by froth flotation either directly after hydrogravitic separation or after additional dry digestion, depending on route.

3.3.3. Microwave-assisted digestion followed by flotation

Microwave-assisted digestion was applied as pre-treatment before flotation in selected routes. Laboratory work included wet digestion and dry digestion conditions. Wet digestion involved aqueous medium before flotation, while dry digestion involved microwave-assisted treatment without aqueous digestion medium prior to flotation, only the dried ore sample.

For composite C4, microwave-assisted digestion was applied directly to raw ore in wet digestion and dry digestion routes. Hydrogravitic concentrate and middlings from C4 were also subjected to dry digestion before subsequent flotation.

For composite CG, dry digestion was only applied after hydrogravitic pre-concentration in selected routes. Concentrate and middlings fractions obtained through hydrogravitic separation were submitted to microwave-assisted dry digestion before froth flotation.

3.3.4. Magnetic pre-concentration followed by flotation

Magnetic pre-concentration was applied to composite CG before flotation in one experimental route. The flotation feed corresponded to the non-magnetic fraction obtained after magnetic separation. The test was identified as CG_NMAG_F25.

3.3.5. Taguchi experimental design for composite CG

Taguchi-based flotation testing was applied to composite CG to organise selected flotation variables into structured experimental series. Two main Taguchi groups were performed, considering two level of variables and producing eight experimental conditions or tests for both as shown in table 3 and 4.

Such route was used to evaluate controlled variation of selected operating parameters while reducing number of required experimental runs.

First Taguchi group was associated with CG_F22 series. Experimental variables included collector dosage, temperature and pH. It was also added sodium silicate (Na_2SiO_3) as a depressor with a fixed dosage of 1 750 mg/kg for all tests of the first and second stages. Tests were identified as CG_F22_1A to CG_F22_8B. The second stage was identified as CG_F22_1B to CG_F22_6B. The two last flotation tests, CG_F22_7B and CG_F22_8B were not performed due to laboratory constraints.

Table 3: Factor levels for the first Taguchi series, including the 1st and 2nd stage.

Taguchi Experimental plan			
First and second stage			
Factors	**Collector dosage**	**Temperature**	**pH**
Level I	500	50	8
Level II	1500	80	9,5

Second Taguchi group was associated with CG_F27 series. First stage included, CG_F27_1A to CG_F27_8A, and replicate tests CG_F27_2AR and CG_F27_8AR. Second stage included CG_F27_1B to CG_F27_8B. Variables considered in CG_F27 series included collector dosage, two different depressant and EDTA addition, with pH and temperature maintained the same throughout the experimental tests.

Table 4: Factor levels for the second Taguchi series, including the 1st and 2nd stage.

Taguchi Experimental plan						
	First stage			**Second stage**		
Factors	**Collector dosage (mg/kg)**	**Na_2SiO_3 dosage (mg/kg)**	**Quinic acid dosage (mg/kg)**	**Collector dosage (mg/kg)**	**Na_2SiO_3 dosage (mg/kg)**	**Quinic acid dosage (mg/kg)**
Level I	500	0	0	500	0	0
Level II	200	500	500	200	250	250

3.4. Flotation reagents and operating variables

Flotation reagents and operating variables were selected according to experimental routes described in Section 3.3. Reagent scheme included collectors, depressants, pH modifiers, chelating agent and frother. Operating variables included pH, temperature, collector dosage, depressant dosage, agitation speed, air flow, conditioning time and flotation time. Such variables were controlled or varied according to each flotation route, composite type and experimental series.

Reagent selection followed laboratory work developed during research fellowship and was consistent with flotation chemistry reported for rare earth element-bearing carbonatite ores.

Table 5 presents reagents used during flotation tests and corresponding functions in experimental work.

Table 5: Reagents used during froth flotation tests.

Reagent	Chemical formula	Function in flotation tests
Octanohydroxamic acid (OHA)	$C_8H_{17}NO_2$	Collector
Castor oil	—	Collector
Phytic acid	$C_6H_{18}O_{24}P_6$	Depressant
Quinic acid	$C_7H_{12}O_6$	Depressant
Sodium silicate	Na_2SiO_3	Depressant
Barium chloride	$BaCl_2 \cdot 2H_2O$	Depressant
Ethylenediaminetetraacetic acid (EDTA)	$C_{10}H_{16}N_2O_8$	Chelating agent / modifier
Methyl isobutyl carbinol (MIBC)	$C_6H_{14}O$	Frother
Sodium carbonate	Na_2CO_3	pH modifier
Sodium hydroxide	NaOH	pH modifier
Hydrochloric acid	HCl	pH modifier

Pulp pH was adjusted using sodium hydroxide or hydrochloric acid according to target value defined for each test. Sodium carbonate was also used as pH modifier in selected experiments. Temperature was controlled by thermostatic bath, according to target operating range for each composite and test group.

Table 6: Operating ranges applied during C4 and CG flotation tests.

Parameter	C4	CG
Feed mass (g)	138,5 - 167	87,16 - 181,9
Solids percentage (%)	19 - 24,31	15,10 - 25
Temperature (°C)	50–80	50–80
pH	8,0–10,0	8,0–9,5
Air flow (L/min)	4,797–5,33	5,33
Agitation speed (rpm)	400–450	350–400
Conditioning time (min)	6–12	6–12
Flotation time (min)	Not fixed for all tests	6

For composite C4, the exact values and conditions for the first and second stage of the Taguchi experimental plan are summarized in table 7.

Table 7: CG_F22 series experimental plan.

First and second stage			
Experiments	**Collector (mg/kg)**	**T (ºC)**	**pH**
CG_F22_1A-B	500	50	8
CG_F22_2A-B	500	50	9,5
CG_F22_3A-B	500	80	8
CG_F22_4A-B	500	80	9,5
CG_F22_5A-B	1500	50	8
CG_F22_6A-B	1500	50	9,5
CG_F22_7A-B	1500	80	8
CG_F22_8A-B	1500	80	9,5

For composite CG, the Taguchi-based series CG_F27A and CG_F27B the exact values and conditions are summarized in table 8.

Table 8: CG_F27 series experimental plan.

First stage					
Experiment	**Collector dosage (mg/kg)**	**EDTA dosage (mg/kg)**	**Depressant dosage (mg/kg)**	**pH**	**Temperature (°C)**
CG_F27_1A	500	0	500 sodium silicate; 2 drop	8	50
CG_F27_2A	500	500	500 sodium silicate; 2 drop	8	50
CG_F27_3A	500	0	500 quinic acid	8	50
CG_F27_4A	500	500	500 quinic acid	8	50
CG_F27_5A	200	0	500 sodium silicate; 2 drop	8	50
CG_F27_6A	200	200	500 sodium silicate; 2 drop	8	50
CG_F27_7A	200	0	500 quinic acid	8	50
CG_F27_8A	200	200	500 quinic acid	8	50
Second stage					
Experiment	**Collector dosage (mg/kg)**	**EDTA dosage (mg/kg)**	**Depressant dosage (mg/kg)**	**pH**	**Temperature (°C)**
CG_F27_1B	500	0	250 sodium silicate; 1 drop	8	50
CG_F27_2B	500	500	250 sodium silicate; 1 drop	8	50
CG_F27_3B	500	0	250 quinic acid	8	50
CG_F27_4B	500	500	250 quinic acid	8	50
CG_F27_5B	200	0	250 sodium silicate; 1 drop	8	50
CG_F27_6B	200	200	250 sodium silicate; 1 drop	8	50
CG_F27_7B	200	0	250 quinic acid	8	50
CG_F27_8B	200	200	250 quinic acid	8	50

Reagent addition followed conditioning sequence described in Section 3.5. Depressant or pH modifier was introduced before collector addition, according to defined test condition. Frother addition occurred after conditioning, before air introduction and froth collection.

3.5. Froth flotation equipment and procedure

Froth flotation tests were performed using a laboratory-scale flotation setup assembled for pulp conditioning, temperature control, pulp chemistry monitoring, air introduction and froth collection. Setup configuration allowed control of operational variables described in Section 3.4, including pH, temperature, agitation speed, air flow, conditioning time and flotation time.

Laboratory setup included a thermostatic bath, mechanical agitator, flotation vessel, pH meter, oxidation–reduction potential meter, conductivity meter, thermometer, aluminium collection plate and drying oven. All the equipment components and respective functions are presented in Table 9. A photograph or schematic representation of flotation setup should be inserted as Figure 5.

Table 9: Laboratory equipment used during froth flotation tests.

Equipment	Model / manufacturer	Function during flotation tests
Microwave	LABTRON	Microwave-assisted digestion for sample pre-conditioning prior to flotation.
Thermostatic bath	Precisterm, Selecta	Temperature control during pulp conditioning and flotation
Mechanical agitator	Heidolph	Pulp suspension, mixing and reagent dispersion
Flotation vessel	skyLab	Pulp containment during conditioning and flotation
pH meter	inoLab	pH monitoring and adjustment
ORP meter	inoLab	Oxidation–reduction potential monitoring
Conductivity meter	inoLab	Conductivity monitoring during pulp preparation and flotation
Thermometer	—	Temperature verification
Aluminium plate	Custom-made	Froth concentrate collection
Oven	Binder	Drying of flotation products
Scale (balance)	KERN PFB and Chyo (JL-180)	Accurate weighing of solid samples and reagents.

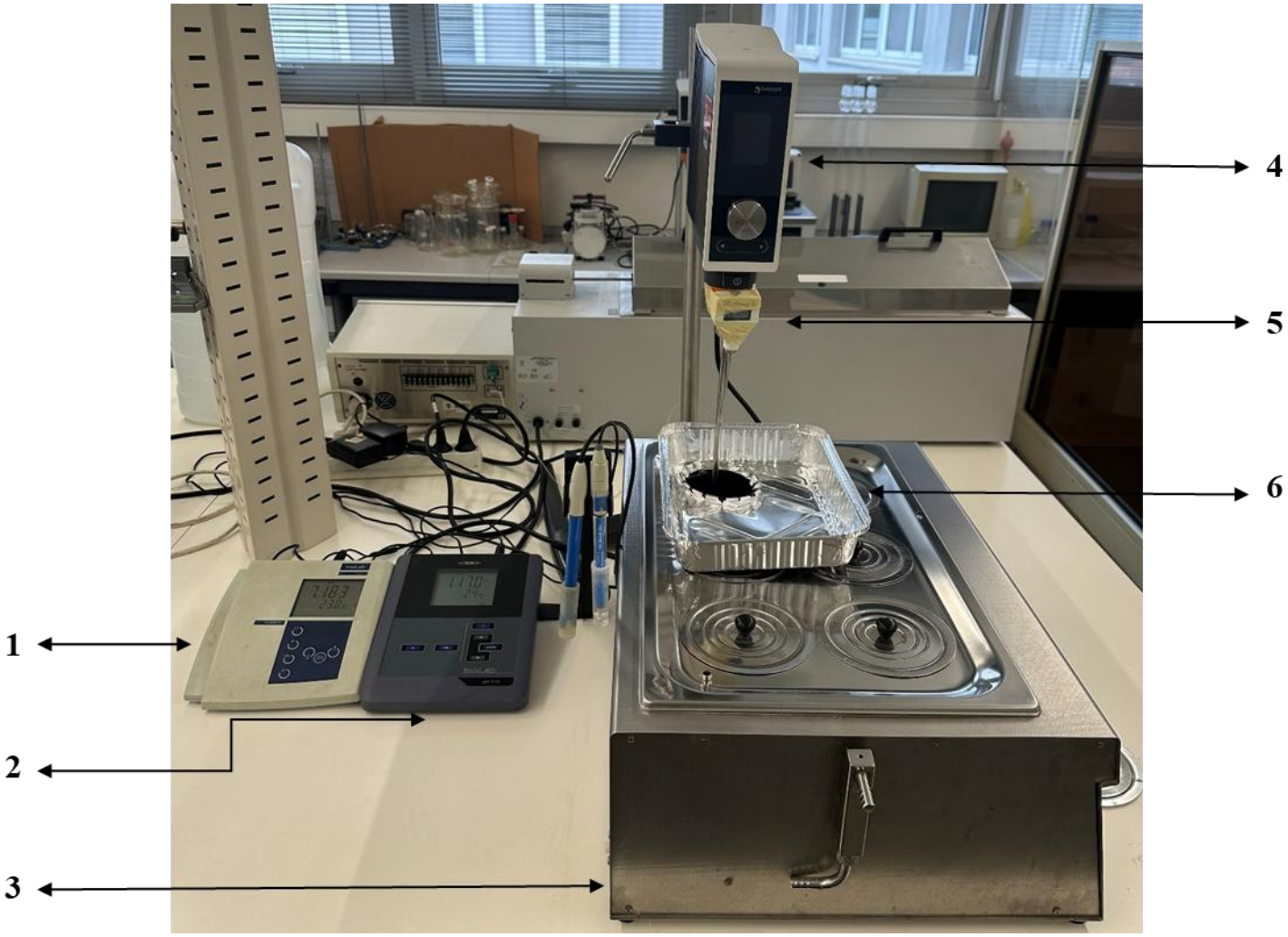

Figure 5: Laboratory froth flotation setup used during experimental tests.

Legend:

1- pH meter
2- ORP meter
3- Thermostatic bath
4- Mechanical agitator
5- Thermometer
6- Aluminum plate

Each flotation test began with the preparation of the pulp in the flotation vessel. A weighed mass of feed material was mixed with distilled water to obtain the target solids percentage for the respective test. The feed mass, solids percentage and principal operating conditions were within the ranges summarised in Table 6, while the specific conditions applied in each experiment are presented in Appendix A. The pulp was homogenised at the prescribed agitation speed before reagent addition. The initial pH, oxidation–reduction potential (ORP) and temperature were measured before the conditioning stages.

Conditioning was performed in sequential stages according to the experimental plan established for each test. The pulp pH was adjusted when required using the specified pH modifier. A depressant, collector or combination of both was subsequently added according to the reagent scheme applied in each experiment. When both reagent types were used, the depressant was added before the collector. The frother was added after the conditioning sequence and dispersed for three minutes before air introduction.

During conditioning, the pulp pH was monitored and adjusted when required using sodium hydroxide or hydrochloric acid. The temperature was maintained using a thermostatic bath according to the target value established for each test group. The agitation speed remained within the range reported in Table 6, ensuring suspension of the solid particles and adequate dispersion of the reagents.

After conditioning, air was introduced at the specified flow rate to initiate bubble generation and froth formation. The froth product was collected manually using an aluminium plate during the flotation period defined for each test. The collected froth constituted the overflow product, whereas the material remaining in the flotation vessel constituted the underflow product. The general operating sequence is summarised in Table 10.

Table 10: Summary of the froth flotation operating sequence.

Step	Procedure
1	Feed material was weighed according to required solids percentage.
2	Distilled water was added to flotation vessel.
3	Pulp was homogenised under prescribed agitation speed.
4	Initial pH, ORP and temperature were measured.
5	pH was adjusted, when required, using NaOH, HCl or Na_2CO_3.
6	Depressant was added according to experimental plan.
7	Collector was added according to experimental plan.
8	Pulp conditioning was performed under controlled agitation and temperature.
9	Frother was added after conditioning sequence.
10	Air was introduced at defined flow rate.
11	Froth was collected manually using aluminium plate.
12	Overflow and underflow products were recovered for subsequent handling.

3.6. Product handling

After each flotation test, overflow and underflow streams were recovered separately to preserve product identity and enable subsequent analytical characterisation. Product codes followed nomenclature defined in Section 3.1, with suffix "_O" assigned to overflow and suffix "_U" assigned to underflow.

Overflow material was transferred from collection plate to suitable container and dried in oven. The underflow pulp remaining in the flotation vessel was recovered and subjected to solid–liquid separation by filtration. The liquid phase was collected separately as filtrate and classified as wastewater, while the

retained solid phase formed the filter cake. After drying under the same conditions applied to the overflow material, the filter cake was considered the final underflow product.

Both overflow and underflow solids were oven-dried at 65 °C for 24 h. After drying, products were weighed, labelled and stored in plastic containers. Product mass was recorded for subsequent mass balance and metallurgical calculations described in Section 3.8. Product labels included composite code, flotation test designation and stream suffix.

3.7. Analytical methods

Analytical characterisation was performed on feed materials and flotation products generated during experimental programme. Analytical characterisation included particle-size analysis, X-ray fluorescence, inductively coupled plasma mass spectrometry and scanning electron microscopy with energy-dispersive X-ray spectroscopy. The principal equipment used for sample preparation, particle-size analysis, XRF analysis and sample weighing is summarised in Table 11. ICP-MS and SEM-EDS analyses were performed by external collaborating entities.

3.7.1. Particle size analysis

Particle-size analysis was performed on flotation feed materials to characterise granulometry before beneficiation tests. Analysed materials included untreated composites and selected products from hydrogravitic pre-concentration. The analysis was performed at UP/FEUP using a laser granulometer. Particle-size distribution was expressed through characteristic diameters d10, d50 and d90, corresponding to particle sizes below which 10%, 50% and 90% of cumulative material fraction were contained.

3.7.2 X-Ray Fluorescence Spectrometry (XRF)

X-ray fluorescence was used to determine bulk elemental composition of feed materials and flotation products. Analyses were performed at UP/FEUP. Prepared samples were analysed after drying, milling and size control when required, following sample preparation described in Section 3.6. XRF data were used to describe major and trace element composition of feed materials and products.

3.7.3 Inductively Coupled Plasma Mass Spectrometry (ICP-MS)

Inductively coupled plasma mass spectrometry was used to quantify rare earth elements in feed materials and flotation products. Analyses were performed by a collaborating laboratory in Romania. Samples and final products were transferred for analysis, and datasets were returned to UP/FEUP. ICP-MS results included individual rare earth element concentrations and corresponding rare earth oxide values.

3.7.4 Scanning Electron Microscopy with Energy-Dispersive X-Ray Spectroscopy (SEM-EDS)

Scanning electron microscopy was applied to selected feed materials and flotation products for mineralogical observation. SEM images were used to identify mineral phases, textural relationships and associations between rare earth minerals and gangue phases within analysed areas. Observations supported mineralogical description of C4 and CG feed materials and selected overflow products.

Table 11: Equipment used for sample preparation and analytical procedures.

Equipment	Model / Manufacturer	Primary Function
Ring mill	Siebtechnik	Comminution of ore samples to target particle size distribution.
Shaking screens	Retsch	Classification of particles by size.
Laser granulometer	Malvern	Determination of particle size distribution.
XRF	OXFORD Instruments, X-MET 7500	Chemical composition analysis
Scale (balance)	KERN PFB and Chyo (JL-180)	Accurate weighing of solid samples and reagents.

3.8.Metallurgical calculations

Flotation performance was evaluated using mass recovery, total rare earth oxide (TREO) grade, TREO recovery, cumulative TREO recovery and enrichment ratio. Calculations were based on the dry masses of the overflow and underflow products and on the rare earth oxide concentrations determined by inductively coupled plasma mass spectrometry (ICP-MS).

For the calculations applied in the present work, the flotation feed mass was reconstructed from the sum of the dry overflow and underflow product masses, as well as the feed grade. Therefore, the mass and the feed grade used as the feed basis was calculated according to Equation 1 and Equation 2:

$$m_{F,rec} = m_O + m_U \tag{1}$$

$$G_{TREO,F,rec} = \frac{(m_o \times G_{TREO,O}) + (m_u \times G_{TREO,U})}{m_{F,rec}} \tag{2}$$

Where:

- $m_{F,rec}$ is the reconstructed feed mass (g);
- m_O is the overflow mass (g);
- m_U is the underflow mass (g);
- $G_{TREO,F,rec}$ is the reconstructed feed TREO grade (%);
- $G_{TREO,O}$ is the overflow TREO grade (%);
- $G_{TREO,U}$ is the underflow TREO grade (%).

The reconstructed feed mass was used because the mass balance calculations were based on the final dried products generated during each flotation test. Consequently, potential material losses occurring during pulp conditioning, froth collection, filtration, drying or sample handling were not included in the reconstructed feed mass.

For direct flotation tests, the flotation feed corresponded to the untreated C4 or CG composite. For tests performed after hydrogravitic or magnetic pre-concentration, the feed corresponded to the respective pre-concentrated product. For two-stage flotation tests, the overflow generated during the first stage was used as the feed for the second stage. Therefore, second-stage recovery was calculated relative to the first-stage overflow, while cumulative recovery was calculated relative to the original first-stage feed.

3.8.1. Mass recovery

Mass recovery represents the proportion of the reconstructed flotation feed mass recovered in the overflow product. It was calculated according to Equation 3:

$$Mass\ recovery(\%) = \frac{m_O}{m_{F,rec}} \times 100\% \quad (3)$$

3.8.2 TREO Grade

TREO grade represents the total concentration of rare earth oxides in a feed or flotation product. It was calculated by summing the concentrations of the individual rare earth oxides reported in the ICP-MS analytical dataset, according to Equation 4:

$$TREO\ grade(\%) = \sum individual\ rare\ earth\ oxide\ concentration \quad (4)$$

$$TREO\ grade(\%) = \sum REEO$$

3.8.3 TREO recovery

TREO recovery represents the percentage of the TREO contained in the reconstructed flotation feed that reported to the overflow product.

The TREO content of the overflow product was determined from the dry overflow mass and the corresponding TREO grade:

$$TREO\ recovery(\%) = \frac{m_O \times G_{TREO,O}}{m_{F,rec} \times G_{TREO,F,rec}} \quad (5)$$

3.8.4 Cumulative TREO Recovery

Cumulative TREO recovery represents the percentage of TREO contained in the original first-stage feed that was recovered in the final second-stage overflow product. Therefore, cumulative TREO recovery is only required for second stage groups of experiments, CG_F22B and CG_F27B.

Cumulative recovery was calculated from the first-stage and second-stage TREO recoveries according to Equation 6:

$$R_{TREO,cum}(\%) = \frac{R_{TREO,A} \times R_{TREO,B}}{100} \quad (6)$$

Where:

- $R_{TREO,cum}$ is the cumulative TREO recovery relative to the original feed (%);
- $R_{TREO,A}$ is the TREO recovery obtained during the first flotation stage (%);
- $R_{TREO,B}$ is the TREO recovery during the second flotation stage relative to the first stge overflow (%).

3.8.5 Enrichment ratio

The enrichment ratio (ER) compares the TREO grade of the overflow product with the TREO grade of the material used as flotation feed. It indicates how many times the overflow is richer or poorer in TREO than the feed.

It was calculated according to Equation 7:

$$ER = \frac{G_{TREO,O}}{G_{TREO,F,rec}} \quad (7)$$

The enrichment ratio is dimensionless and is not expressed as a percentage. A value greater than 1 indicates enrichment of TREO in the overflow product. A value equal to 1 indicates no change in TREO grade, while a value below 1 indicates that the overflow product contains a lower TREO grade than the reconstructed feed.

3.9. Limitations of the experimental methodology

Several limitations were identified during the experimental programme. One of the main constraints was the development of a suitable laboratory-scale flotation setup capable of maintaining stable operating conditions throughout each test.

Temperature control represented a particular challenge, especially during experiments conducted at elevated temperatures. Although a thermostatic bath was used, maintaining the pulp at the target temperature during conditioning and flotation was not always possible.

Maintaining the pulp pH at the target value also presented difficulties. Reagent addition, the physicochemical interactions between the ore and the liquid phase resulted in pH variations during conditioning and flotation. Additional pH adjustment was therefore required in some experiments.

The laboratory setup also limited complete control of material losses. Losses may have occurred during pulp conditioning, froth collection and product handling. Manual collection of the froth using an aluminum plate was especially difficult to keep consistent, since part of the froth or attached solid material could remain on the plate or be lost during transfer to the collection container.

Evaluation of reagent performance was limited by the available analytical information. Although XRF and ICP-MS provided the elemental composition of selected feeds and products, the analyses did not directly determine collector or depressant adsorption on mineral surfaces. Consequently, the effectiveness of individual reagents could only be assessed indirectly from changes in product composition, TREO grade, TREO recovery and enrichment ratio.

A further limitation was associated with the turnaround time for TREO quantification by ICP-MS. Samples had to be sent to an external laboratory in Romania, and the analytical results could require more than one month to become available. The delay restricted timely evaluation of the flotation responses obtained under the investigated conditions and limited the use of analytical feedback for planning subsequent experiments. Consequently, some later tests had to be designed without complete TREO results from the preceding experimental series.

Collector dosage selection also represented an experimental limitation. The required dosages corresponded to small masses in the milligram range, increasing the relative influence of weighing uncertainty. Small deviations during reagent preparation and addition may therefore have affected the effective dosage applied in individual tests. In addition, Octanohydroxamic acid (OHA) had to be dissolved in 96% ethanol prior to addition to the pulp. During reagent preparation and transfer, some losses may have occurred, while in other cases slightly more than the target dosage may have been added, meaning that the intended dosage was not necessarily introduced into the flotation system with complete accuracy.

Finally, the complete flotation procedure was time-consuming. Each experiment required feed preparation, pulp heating, pH adjustment, sequential reagent conditioning, flotation, froth collection, filtration, drying, weighing and sample preparation for chemical analysis. The time required for each test limited the number of replicates and the possibility of evaluating a wider range of operating conditions.

4

RESULTS AND DISCUSSION

Chapter 4 presents the experimental results obtained during the beneficiation investigation of rare earth element-bearing ore from the Fen Carbonatite Complex. The results are organised according to the experimental sequence adopted in Chapter 3, beginning with feed characterisation and followed by flotation response under different physico-chemical treatment routes.

A total of 64 flotation experiments were considered in the experimental programme, including tests performed on composites C4 and CG. The results are presented using particle-size distribution, XRF, ICP-MS, SEM-EDS observations and metallurgical calculations. Detailed analytical data and complete experimental conditions are provided in the appendices, while Chapter 4 focuses on the results required to compare the beneficiation routes.

4.1 Feed characterisation

4.1.1 Particle-size distribution of feed materials

The particle-size distribution of the flotation feed materials was evaluated before the flotation tests in order to describe the granulometric conditions of raw and pre-concentrated samples. The characteristic particle-size parameters d10, d50 and d90 are presented in Table 12, while the cumulative particle-size distribution curves are shown in Figure 6.

Table 12: Characteristic particle size parameters (d10, d50, d90) of flotation feed samples (C4 and CG).

	d10	**d50**	**d90**
Feed samples		µm	
C4	1,85	14,80	142,29
C4_ST_R4_C	1,77	16,16	60,16
C4_ST_R4_M	1,67	11,07	37,56
CG_ST_C	1,71	15,84	58,00
CG_ST_M	1,54	12,27	41,51
CG	1,69	12,60	52,39
CG_ST(3)_C	2,97	36,35	79,33
CG_ST(3)_M	N/A	N/A	N/A
CG_B	1,78	14,08	82,82
CG_NMAG	4,99	116,17	274,82

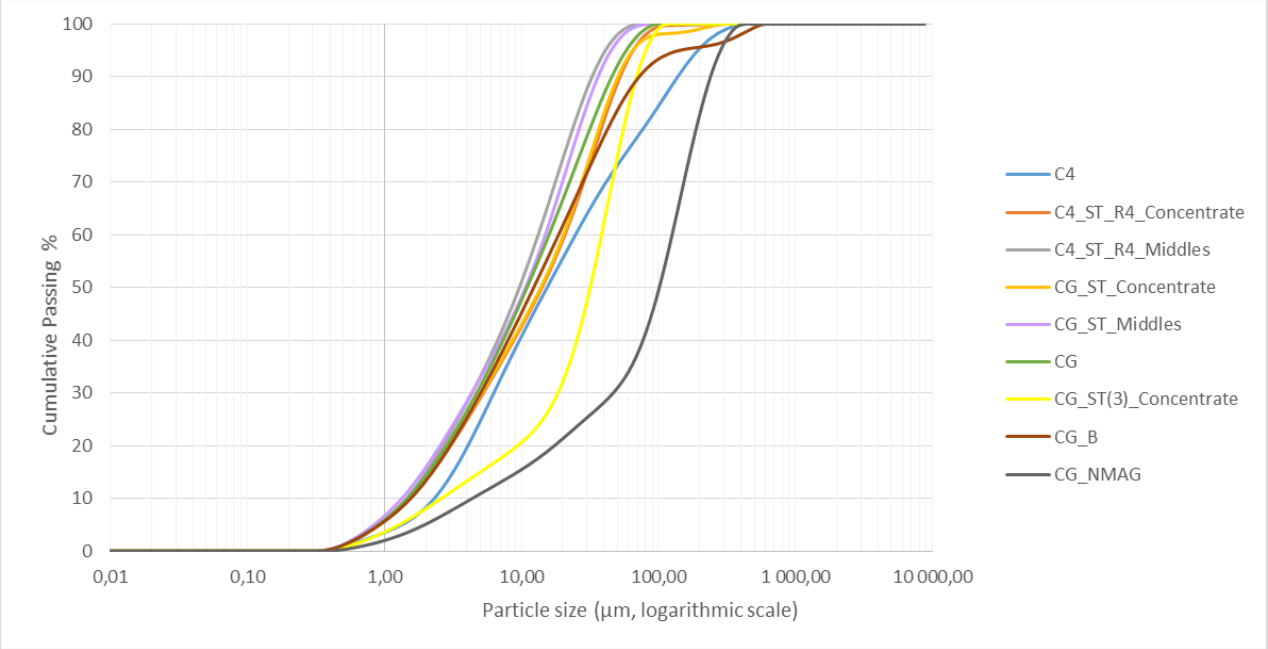

Figure 6:Cumulative particle-size distributions of the C4 and CG flotation feed materials.

The objective of the milling stage was to produce a flotation feed with most particles below 75 µm. The particle-size results show some variability between the feed materials, but this target was achieved for the majority of the samples. Most raw and hydrogravitically pre-concentrated feeds presented d50 values between approximately 11 and 36 µm and d90 values below 75 µm, indicating that most of the particles was within the desired size range. The main exception was the non-magnetic CG fraction, which was considerably coarser, with a d50 of 116,17 µm and a d90 of 274,82 µm.

The two CG feed samples analysed originated from the same composite material, however, they were milled at different times. The differences in particle-size distribution therefore reflect variations in milling performance rather than differences in ore composition. Variability was also observed among the hydrogravitic concentrate and middlings fractions, indicating that the pre-concentration process altered the particle-size characteristics of the material. Particle-size distribution data for CG_ST(3)_Middles could not be obtained and are therefore not included in the table.

Overall, the feeds displayed a wide range of particle sizes, from very fine to relatively coarse distributions. Such variability can influence flotation performance because finer particles may be recovered differently from coarser particles, while particle size also affects mineral liberation and the interaction between particles and bubbles during flotation.

4.1.2 Chemical composition of feed materials by XRF

X-ray fluorescence analysis was used to characterise the bulk elemental composition of the untreated and pre-concentrated flotation feeds. Selected concentrations of Ca, Ti, V, Cr, Mn, Fe, Sr, Ba and Th are presented in Table 13, while their comparative distribution is shown in Figure 7. The selected

elements provide information on compositional variation among carbonate-rich, Fe-bearing, Ba-bearing and trace-element-bearing feed materials.

Table 13: Selected elemental composition of the flotation feed materials determined by XRF.

	Ca	Ti	V	Cr	Mn	Fe	Sr	Ba	Th
					ppm				
C4	214345	11485	2951	836	14619	86002	3616	15559	232
C4_B	219469	11728	3155	866	14909	83615	3626	15279	228
C4_ST_R4_C	175764	12084	3945	1348	12007	98321	2813	13114	316
C4_ST_R4_M	209640	7696	2006	631	14440	75852	3702	11797	171
CG_ST_M	207136	7381	1917	523	14854	79044	3833	11651	176
CG_ST_C	175976	10325	2646	895	12413	123687	3012	12035	249
CG	200783	10295	2417	664	14471	90884	3776	14720	212
CG_ST(3)_M	215023	8765	2278	679	15274	78894	3847	13517	224
CG_ST(3)_C	215126	7651	2178	796	15512	114358	3947	8925	261
CG_B	221547	11185	2641	760	15674	96687	3855	16651	240
CG_NMAG	109500	N/A	26,5	24,4	15656	77730	1982	19200	483

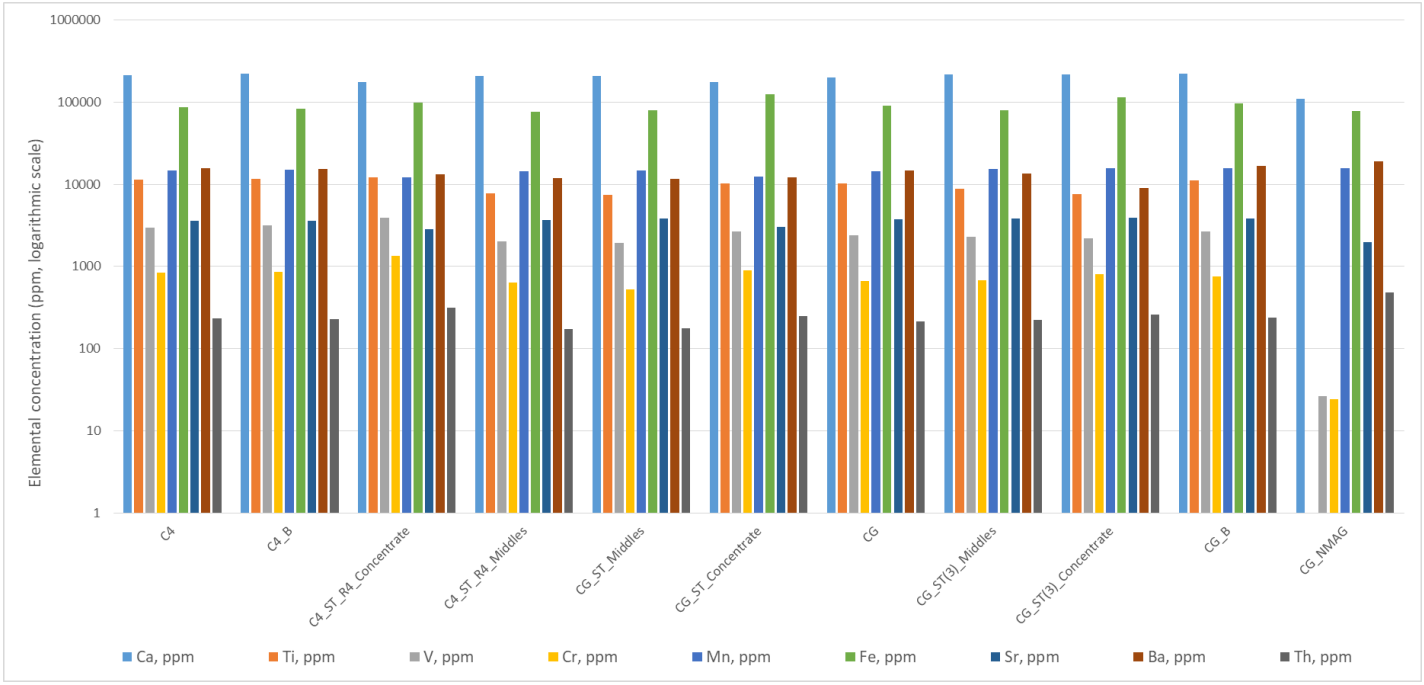

Figure 7: Selected elemental concentrations in the C4 and CG flotation feed materials determined by XRF.

Calcium and Fe were the dominant elements in all samples. Excluding the non-magnetic fraction. Hydrogravitic pre-concentration generally produced concentrates with lower Ca and higher Fe concentrations than the corresponding middlings. For example, C4 concentrate contained 175 764 ppm Ca and 98 321 ppm Fe, compared with 209 640 ppm Ca and 75 852 ppm Fe in the middlings. A similar trend was observed for CG_ST products. In the CG_ST(3) products, Fe was also enriched in the

concentrate (114 358 ppm) relative to the middlings (78 894 ppm), while Ca concentrations remained similar at approximately 215 000 ppm.

The non-magnetic CG fraction showed lower Ca (109 500 ppm) and Fe (77 730 ppm) concentrations than untreated CG, which contained 200 783 ppm Ca and 90 884 ppm Fe. In contrast, the non-magnetic fraction contained the highest Ba and Th concentrations, at 19 200 ppm and 483 ppm, respectively, compared with 14 720 ppm Ba and 212 ppm Th in untreated CG.

Overall, the pre-concentration stages altered the elemental composition of the flotation feeds, with notable variations in Ca, Fe, Ba and Th between the different feed fractions.

4.1.3 TREO composition of feed materials by ICP-MS

ICP-MS analysis was used to determine the light rare earth oxide (LREO), heavy rare earth oxide (HREO) and total rare earth oxide (TREO) contents of the flotation feed materials. The results are summarised in Table 14, while the distribution of the individual rare earth elements and oxides is presented in Figures 8 to 11.

Table 14: LREO, HREO and TREO contents of the flotation feed materials determined by ICP-MS.

	∑LREO	∑HREO	TREO
		%	
C4	0,76	0,02	0,78
C4_B	1,28	0,01	1,29
C4_ST_R4_C	1,92	0,03	1,95
C4_ST_R4_M	0,92	0,01	0,93
CG_ST_M	2,26	0,02	2,28
CG_ST_C	3,57	0,05	3,62
CG	1,28	0,01	1,29
CG_ST(3)_M	N/A	N/A	N/A
CG_ST(3)_C	1,21	0,01	1,22
CG_B	2,27	0,07	2,34
CG_NMAG	1,69	0,07	1,76

The results show that light rare earth oxides represented the dominant contribution to TREO in all analysed feed materials. Heavy rare earth oxide contents were considerably lower, ranging from 0,01% to 0,07%.

CG_ST_Concentrate presented the highest measured TREO grade, at 3,63%, followed by CG_B, at 2,37%, and CG_ST_Middles, at 2,29%. Among the C4 materials, C4_ST_R4_Concentrate presented the highest TREO grade, at 1,96%, while untreated C4 presented the lowest measured grade, at 0,77%.

The hydrogravitic concentrate fractions generally presented higher TREO grades than the corresponding untreated or middlings materials, although this increase was not observed in every CG fraction. The non-magnetic CG fraction presented a TREO grade of 1,77%, exceeding the untreated CG grade of 1,28%.

Overall, the feed materials presented different TREO grades and REE distributions before flotation. However, a higher initial TREO grade did not necessarily produce higher flotation recovery or stronger enrichment, and flotation performance was therefore evaluated using the reconstructed feed grade for each individual test.

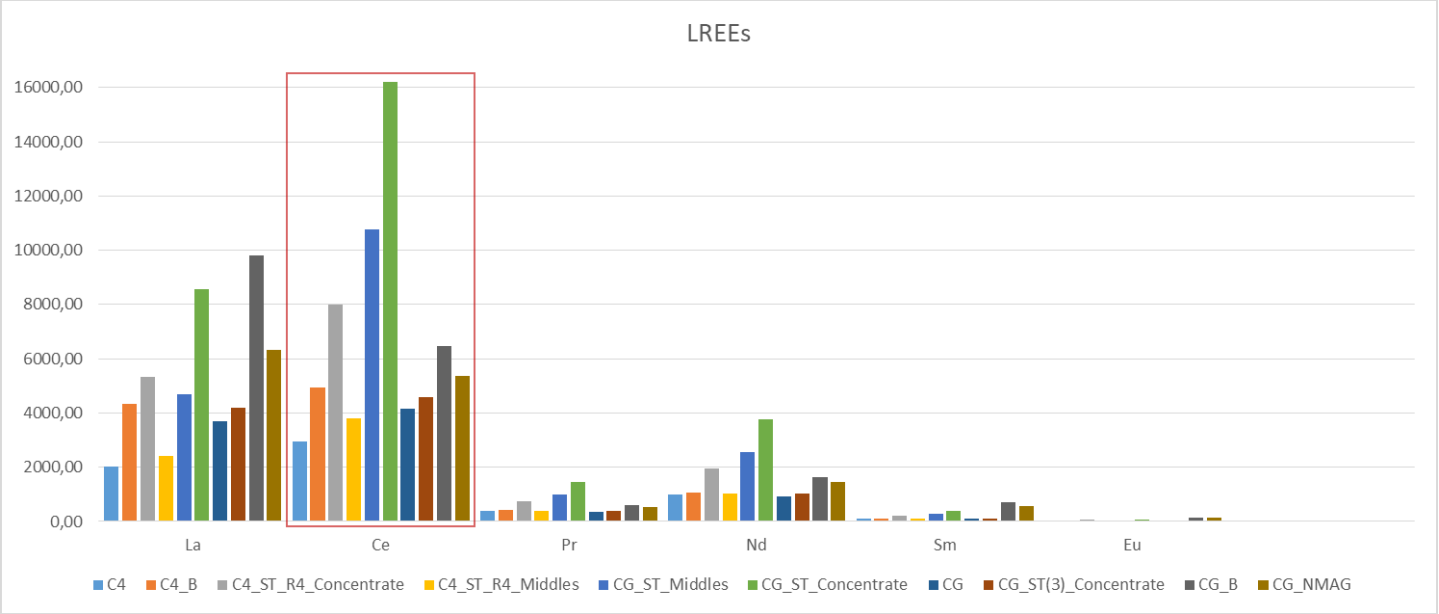

Figure 8: Distribution of light rare earth elements in the C4 and CG flotation feed materials determined by ICP-MS, expressed in ppm.

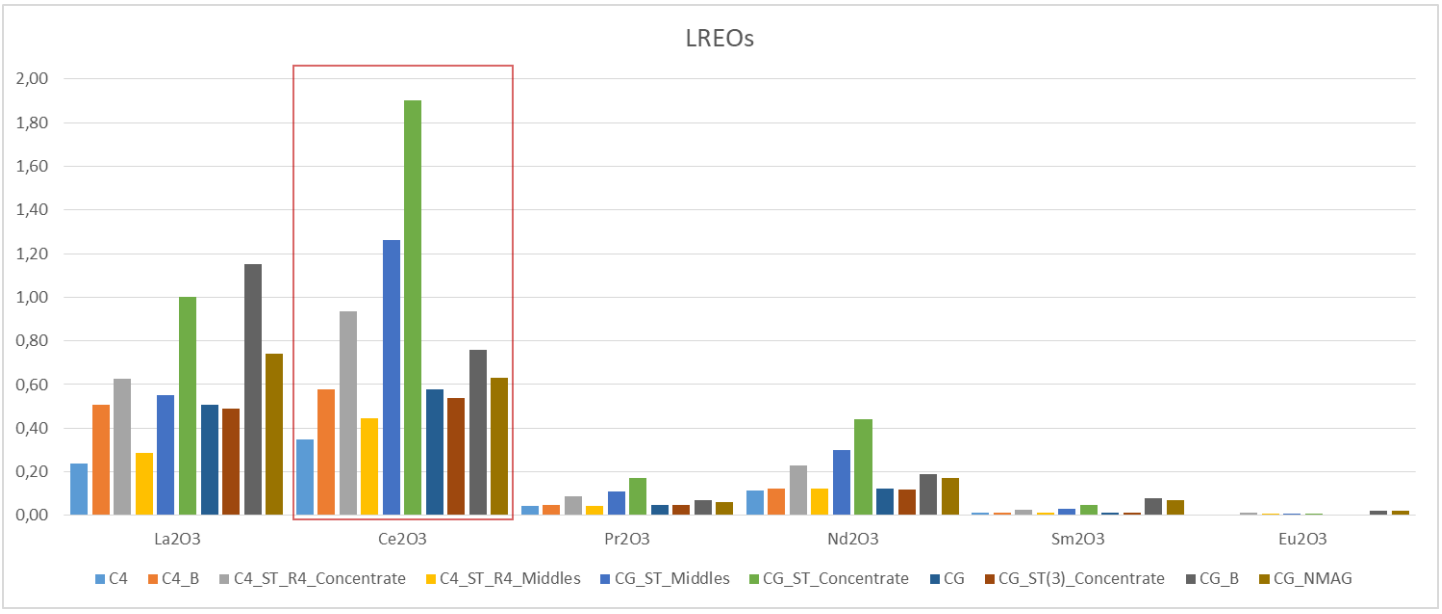

Figure 9: Distribution of light rare earth oxides in the C4 and CG flotation feed materials determined by ICP-MS, expressed in %.

The distribution of individual light rare earth elements and corresponding oxides in the flotation feed materials is presented in Figures 8 and 9. Cerium was the dominant LREE in all analysed samples, followed generally by lanthanum and neodymium, while praseodymium, samarium and europium occurred at substantially lower concentrations. The same compositional trend was observed in the oxide distribution, with Ce_2O_3 representing the largest contribution to total LREO content, followed by La_2O_3 and Nd_2O_3.

Among the analysed materials, CG_ST_Concentrate presented the highest concentrations of the principal LREEs and the highest corresponding oxide contents, particularly for Ce and La. Elevated LREE contents were also observed in CG_ST_Middles and C4_ST_R4_Concentrate relative to the untreated feed materials (C4 and CG). The results indicate that hydrogravitic pre-concentration altered the distribution of LREE-bearing material and produced selected fractions enriched in light rare earth elements. However, the enrichment was not uniform among all pre-concentrated products, as some fractions presented concentrations similar to or lower than the corresponding untreated feeds.

Overall, the REE assemblage was strongly dominated by light rare earth elements, particularly Ce, La and Nd, confirming the LREE-rich character of the Fen carbonatite materials. The predominance of Ce-bearing phases is consistent with the occurrence of minerals such as monazite, parisite and other REE fluorcarbonates identified during mineralogical characterisation.

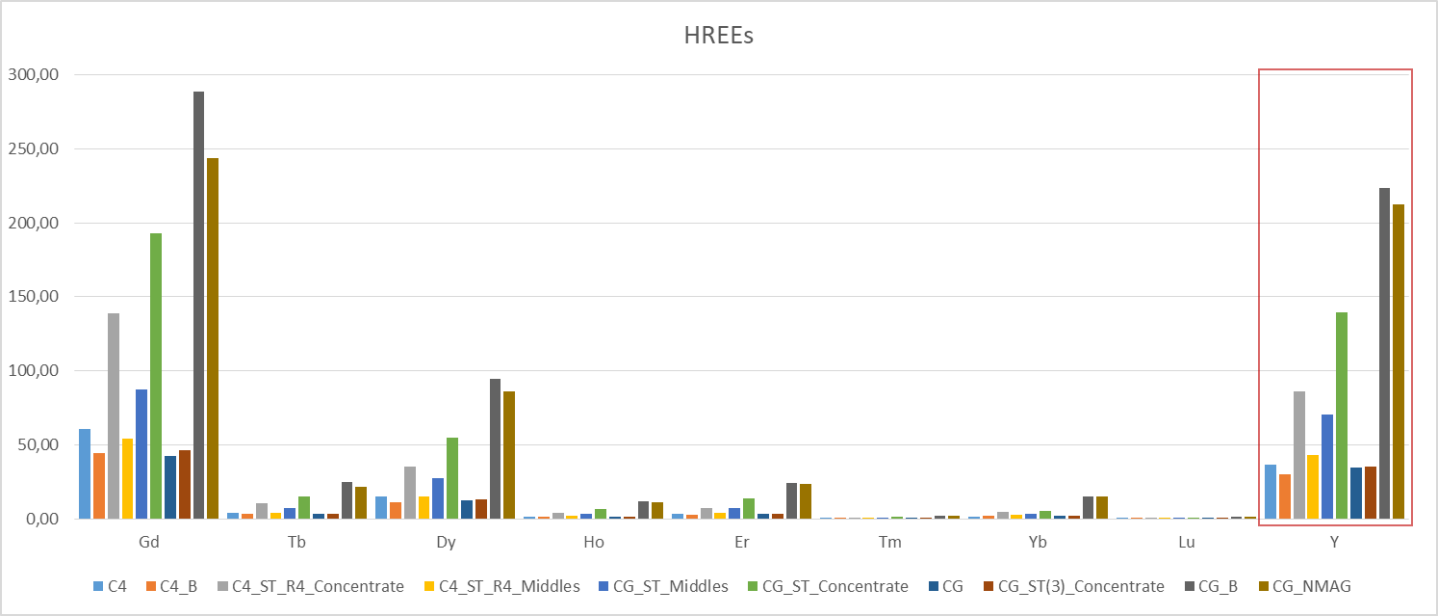

Figure 10: Distribution of heavy rare earth elements in the C4 and CG flotation feed materials determined by ICP-MS, expressed in ppm

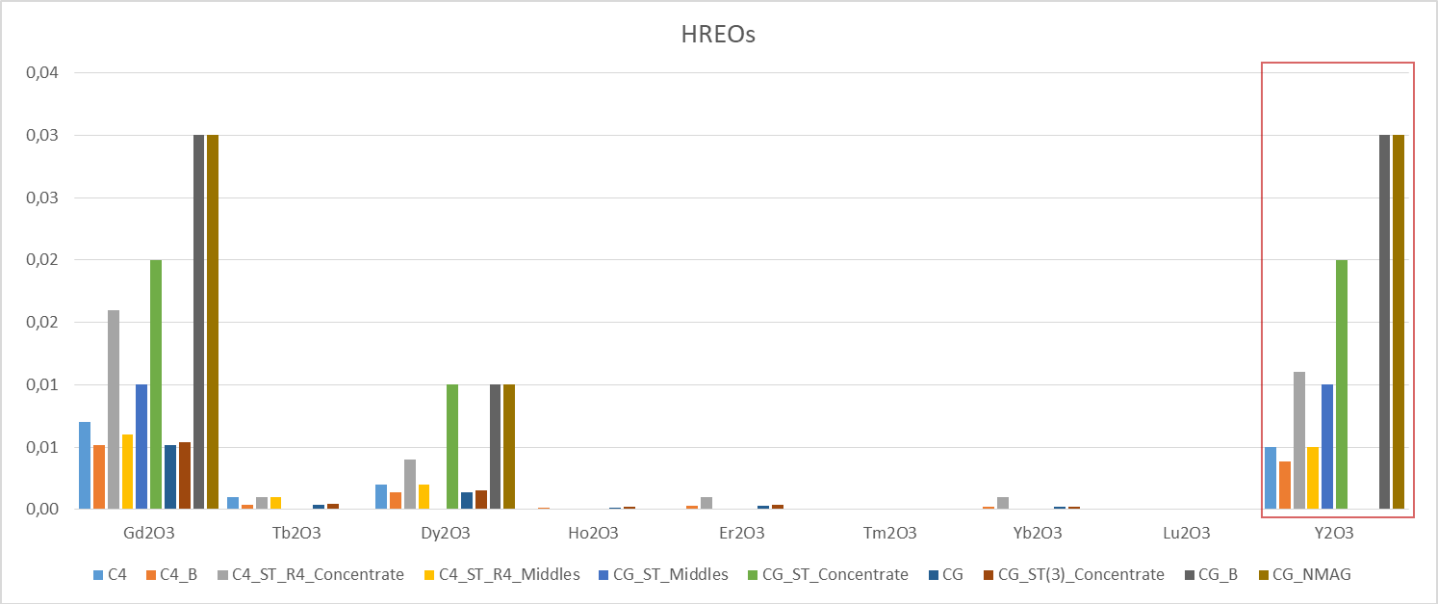

Figure 11: Distribution of heavy rare earth oxides in the C4 and CG flotation feed materials determined by ICP-MS, expressed in %.

The distribution of individual heavy rare earth elements and their corresponding oxides in the flotation feed materials is presented in Figures 10 and 11. Gadolinium and yttrium were the dominant HREEs in all analysed samples, followed by dysprosium, while terbium, holmium, erbium, thulium, ytterbium and lutetium occurred at substantially lower concentrations. The same compositional pattern was observed in the oxide distribution, with Gd_2O_3 and Y_2O_3 representing the largest contributions to the total HREO content, followed by Dy_2O_3.

Among the analysed materials, CG_B presented the highest concentrations of Gd and Y, closely followed by CG_NMAG. Elevated concentrations were also observed in CG_ST_Concentrate and C4_ST_R4_Concentrate relative to the corresponding untreated feed materials. The results indicate that the applied pre-concentration and magnetic separation stages modified the distribution of HREE-bearing material, producing selected fractions enriched in Gd, Y and Dy. However, the enrichment was not uniform across all products, as several fractions retained concentrations similar to or lower than the respective untreated feeds.

Overall, the HREE contents were considerably lower than the LREE contents, confirming the predominantly light rare earth character of the investigated Fen carbonatite materials. Within the HREE group, the distribution was mainly controlled by Gd and Y, whereas the remaining heavy rare earth elements contributed only minor proportions to the total rare earth oxide content.

4.1.4 Mineralogical observations by SEM-EDS

SEM-EDS analysis was used to examine selected mineral phases and textural associations in the C4 and CG flotation feeds. The SEM micrographs show the morphology and contrast of the analysed particles, while the corresponding EDS spectra indicate the characteristic X-ray peaks of the elements detected in each selected zone.

Mineral phases were identified by combining the elemental composition indicated by the EDS spectra in the SEM micrographs. The EDS spectra provide qualitative elemental information to support mineral identification.

Representative SEM micrographs are presented in Figure 13 and corresponding EDS spectra for composite C4 are presented in Figure 14 to 21. The mineral phases assigned to the analysed zones are summarised in Table 15.

- **Composite C4:**

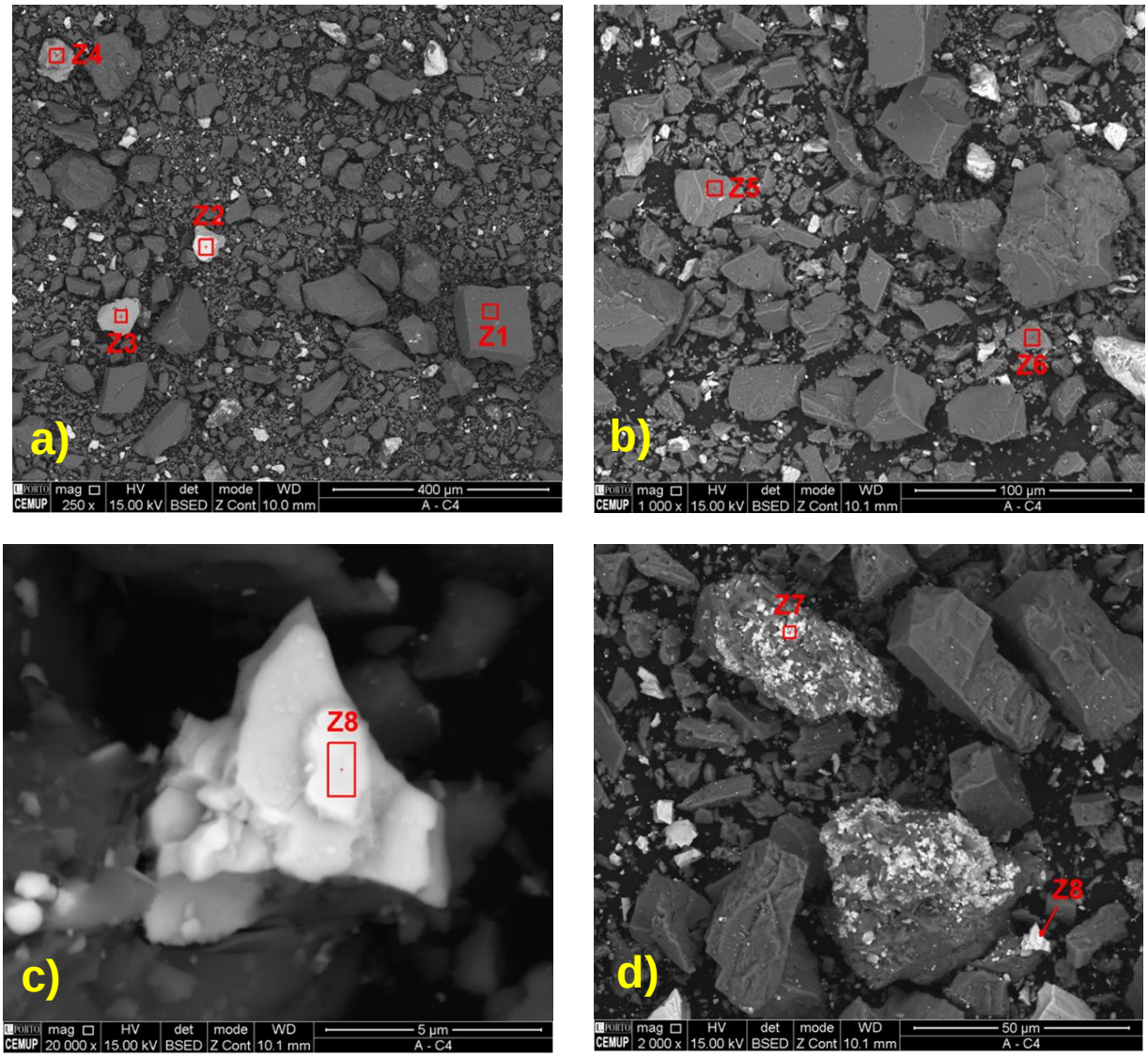

Figure 13: SEM micrographs of the C4 flotation feed showing the mineral phases and textural associations. Images (a–d) represent different analysed areas

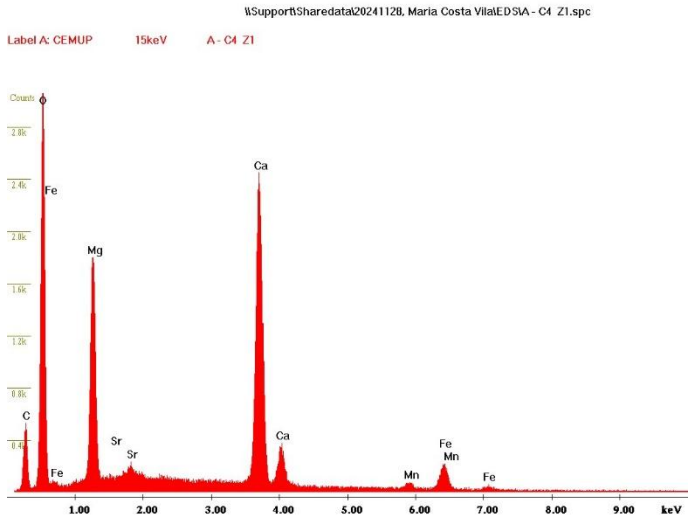

Figure 14: EDS spectrum: C4-Z1

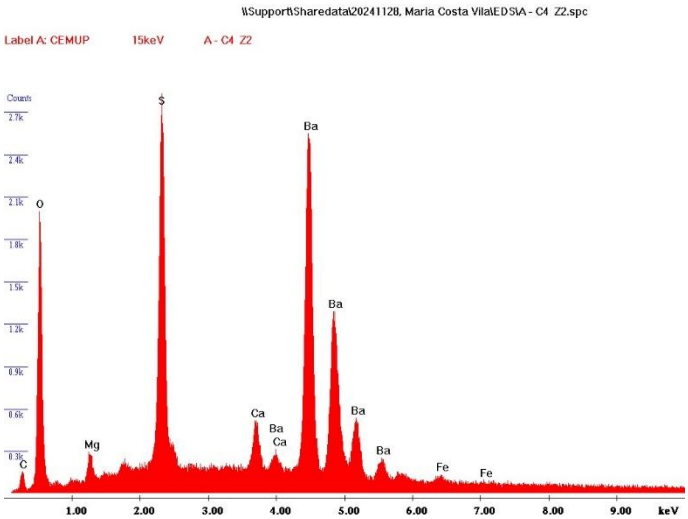

Figure 15: EDS spectrum: C4-Z2

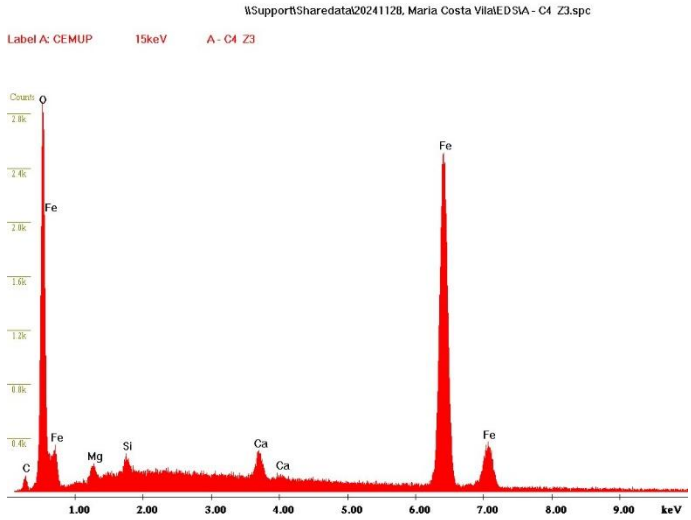

Figure 16: EDS spectrum: C4-Z3

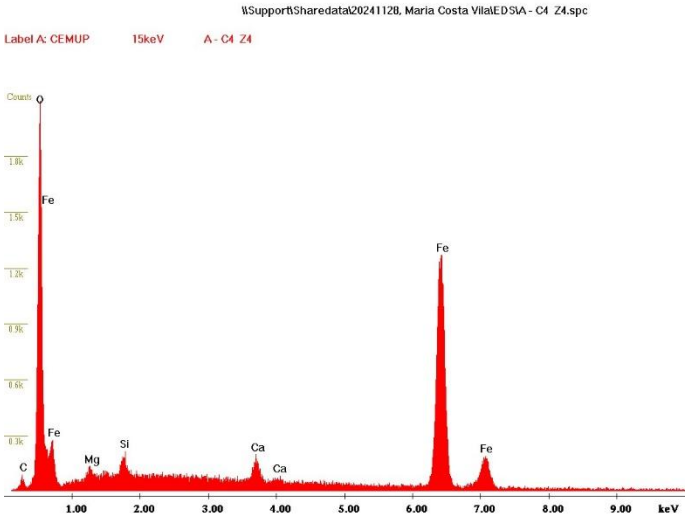

Figure 17: EDS spectrum: C4-Z4

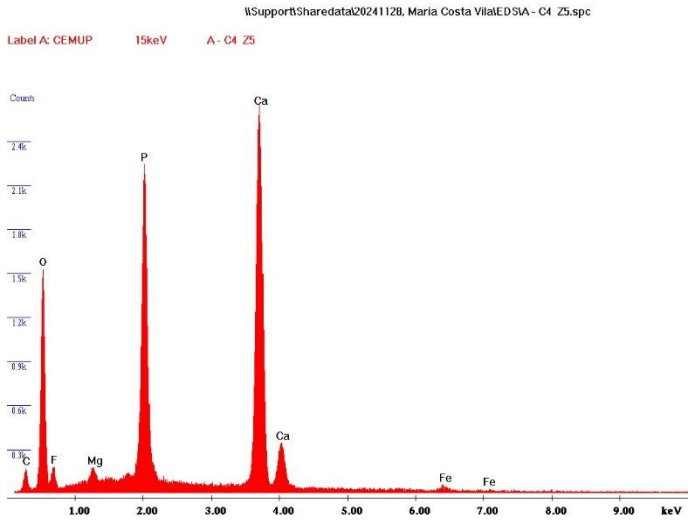

Figure 18: EDS spectrum: C4-Z5

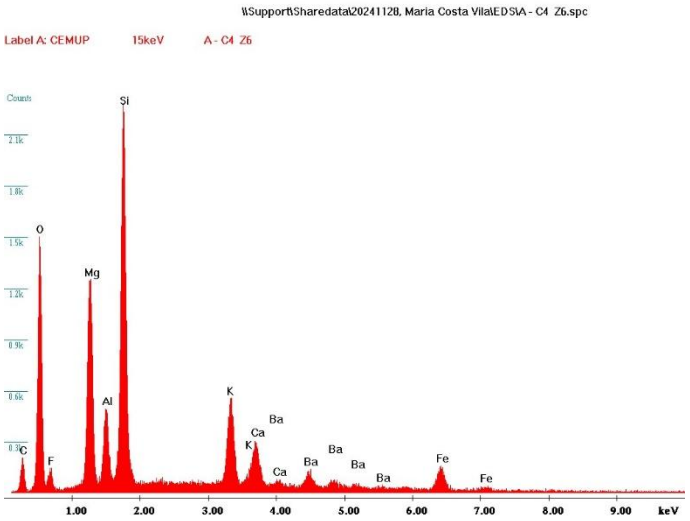

Figure 19: EDS spectrum: C4-Z6

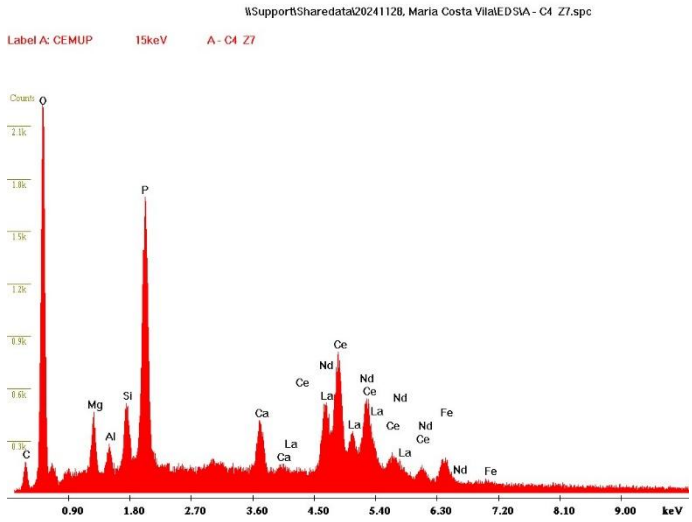

Figure 20: EDS spectrum: C4-Z7

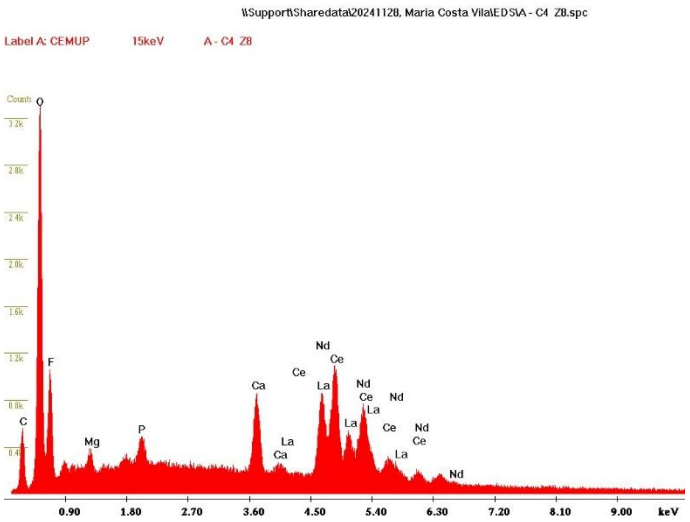

Figure 21: EDS spectrum: C4-Z8

Table 15: Mineral phases identified in selected areas of the C4 flotation feed by SEM-EDS.

Code	Main elements detected	Mineral	Type
Z1	C, Fe, Mg, Sr, Ca, Mn	Ankerite	Carbonate gangue
Z2	C, O, Mg, S, Ca, Ba, Fe	Barite	Sulfate gangue
Z3	C, O, Fe, Mg, Si, Ca	Magnetite	Fe-oxide gangue
Z4	C, O, Fe, Mg, Si, Ca, Fe	Magnetite	Fe-oxide gangue
Z5	C, O, F, Mg, P, Ca, Fe	Fluorapatite	Phosphate mineral / REE host

Z6	C, O, F, Mg, Al, Si, K, Ca, Ba, Fe	Al–Mg silicates	Silicate gangue
Z7	C, O, Mg, Al, Si, P, Ca, La, Ce, Nd, Fe	Monazite	REE phosphate mineral
Z8	C, O, F, Mg, P, Ca, La, Nd, Ce	Parisite	REE fluorocarbonate mineral

The analysed areas of composite C4 contained monazite and parisite as the principal REE-bearing minerals. Associated phases included ankerite, barite, magnetite, fluorapatite and Al–Mg silicates. The observations indicate that REE-bearing minerals occurred together with carbonate, sulphate, phosphate, silicate and Fe-bearing gangue phases.
Representative SEM micrographs are presented in Figure 22 and corresponding EDS spectra for composite CG are presented in Figure 23 to 26. The mineral phases assigned to the analysed zones are summarised in Table 16.

- **Composite CG:**

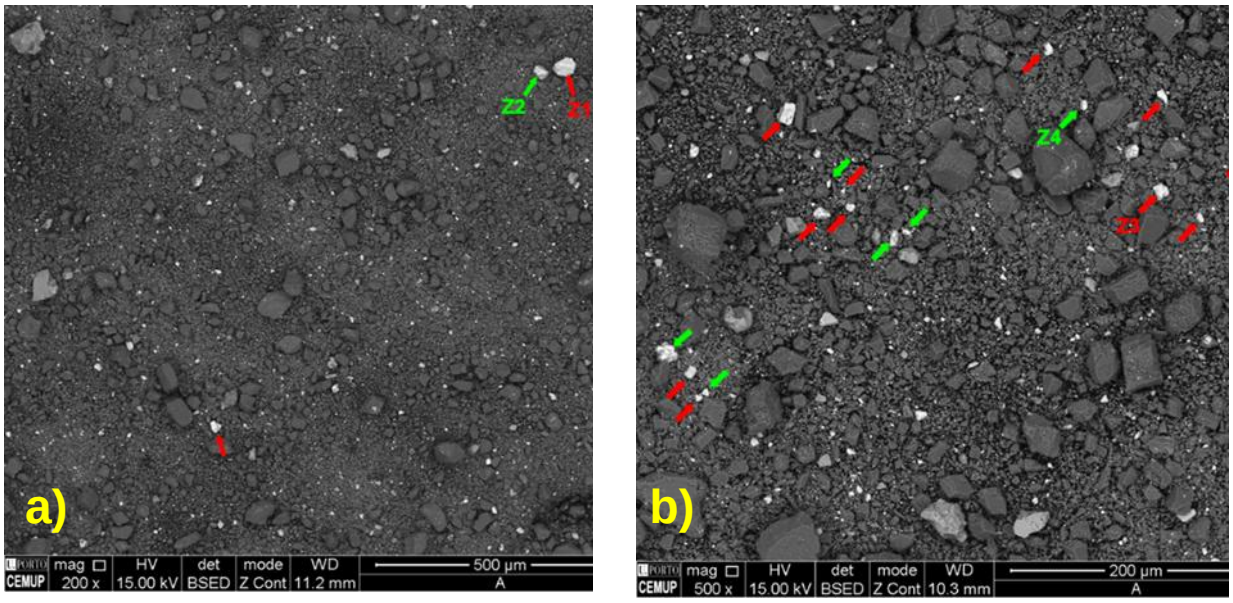

Figure 22:SEM micrographs and corresponding EDS spectra of selected areas of the CG flotation feed. Images (a–b) represent different analysed areas and associated elemental spectra.

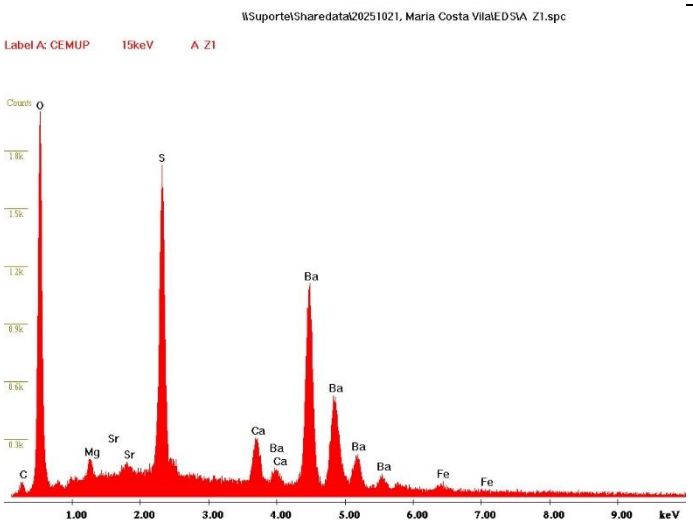

Figure 23: EDS spectrum: CG-Z1.

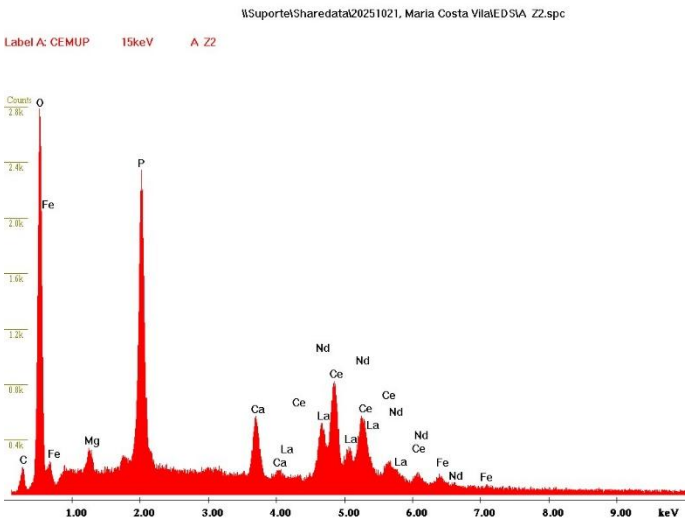

Figure 24: EDS spectrum: CG-Z2

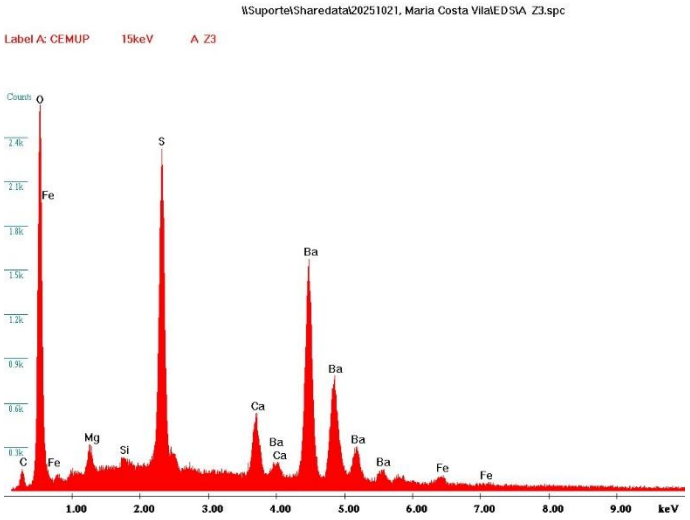

Figure 25: EDS spectrum: CG-Z3

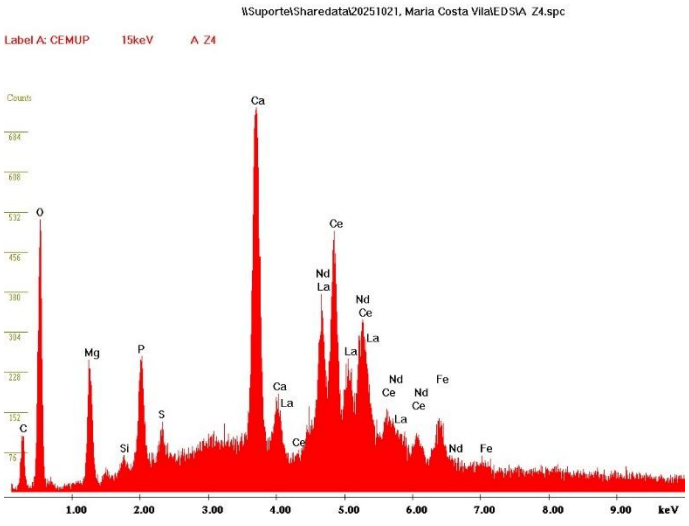

Figure 26: EDS spectrum: CG-Z4

Table 16: Summary of the notation for feed CG.

Zone	Main elements detected	Mineral	Type
Z1	C, O, Mg, Sr, S, Ca, Ba, Fe	Barite	Gangue
Z2	C, O, Fe, Mg, P, Ca, La, Ce, Nd, Fe	Monazite	REE mineral
Z3	C, O, Fe, Mg, Si, S, Ca, Ba, Fe	Barite	Gangue
Z4	C, O, Mg, P, S, Si, Ca, La, Ce, Nd, Fe	Parisite	REE mineral

The analysed areas of composite CG contained monazite and parisite associated mainly with barite. The occurrence of REE-bearing minerals together with gangue phases indicates mineral associations that may influence liberation and flotation selectivity.

The SEM-EDS observations are representative only of the selected analysed areas. Consequently, the results confirm the occurrence and local association of selected mineral phases but do not provide quantitative mineral abundance, liberation degree or complete mineralogical composition of the feed materials.

4.2 Direct flotation response

Direct flotation tests were conducted to evaluate the flotation behavior of untreated C4 and CG composites without prior pre-treatment. The results provide a reference for assessing the effect of the pre-concentration and conditioning routes examined in the subsequent sections.

4.2.1 C4 direct flotation tests

The operating conditions and flotation response of the C4 direct flotation tests are presented in Table 17. The corresponding TREO recoveries are shown in Figure 27.

Table 17:Operating conditions and flotation response of C4 direct flotation tests.

Test code	pH	Temperature (°C)	Collector (mg/kg)		Depressor (mg/kg)		Mass recovery (%)	Overflow TREO grade (%)	TREO recovery (%)	ER
C4_F1	8,5	50	OHA	32	Na_2SiO_3 +NaF	1500 + 12	3,57	1,23	2,80	0,78
C4_F2	9,0	60	Castor oil	210	Na_2SiO_3 +NaF	500 + 13	0,86	1,47	0,92	1,07
C4_F3	9,0	75	OHA	90	Na_2SiO_3	500	15,59	2,33	27,05	1,74
C4_F4	8,0	65	OHA	106	Na_2SiO_3	500	2,84	2,22	4,20	1,48

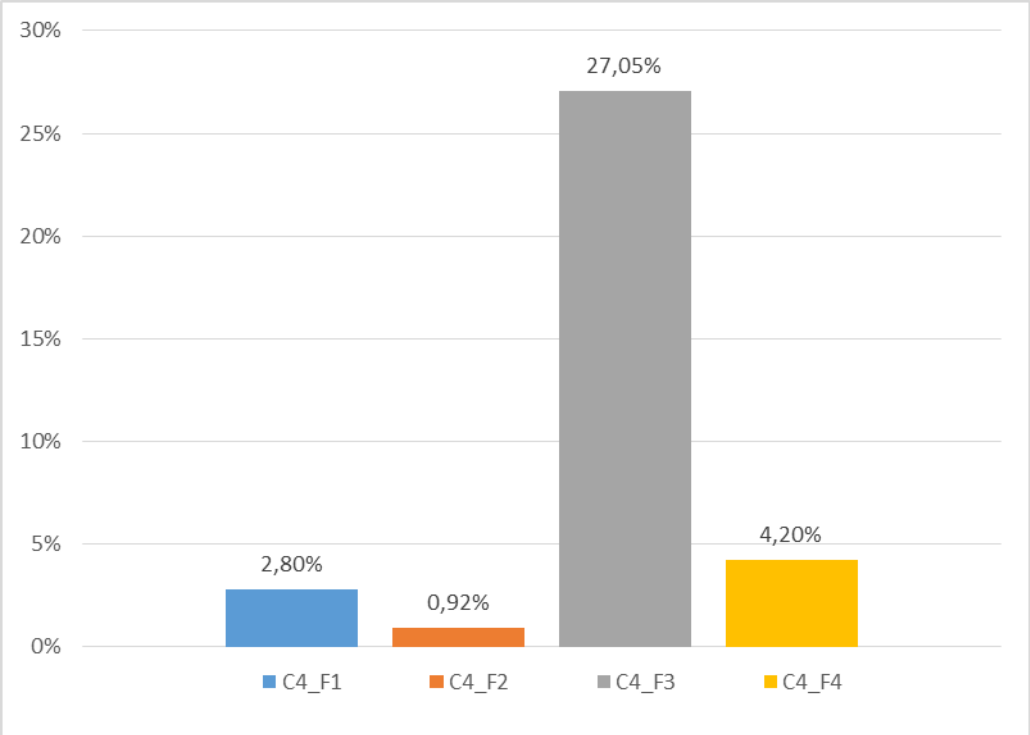

Figure 27: TREO recovery for C4 direct flotation..

The C4 direct flotation tests produced generally low mass and TREO recoveries, although the response varied among the operating conditions. C4_F3 presented the highest TREO recovery, at 27,05%, together with an overflow TREO grade of 2,33% and an enrichment ratio of 1,74. C4_F4 also produced TREO enrichment, but only 4,20% of the reconstructed feed TREO was recovered in the overflow.

C4_F1 presented an enrichment ratio below 1, indicating that the overflow was depleted in TREO relative to the reconstructed feed. Although C4_F3 produced the highest TREO recovery, analysis of the operating conditions does not allow a clear conclusion regarding the factors responsible for this response. Differences in temperature and OHA dosage may have influenced the flotation performance, however, C4_F4 was conducted with a higher OHA dosage but at a lower temperature and produced a substantially lower recovery. Because collector dosage, temperature, pH and depressor conditions varied simultaneously among these preliminary tests, the effect of individual parameters cannot be isolated from this series.

4.2.2 CG direct flotation tests

The operating conditions and flotation response of the CG direct flotation tests are presented in Table 18. The corresponding TREO recoveries are shown in Figure 28..

Table 18: Operating conditions and flotation response of CG direct flotation tests.

Test code	pH	Temperature (°C)	OHA dosage (mg/kg)	Na_2SiO_3 dosage (mg/kg)	Mass recovery (%)	Overflow TREO grade (%)	TREO recovery (%)	ER
CG_F18	9,5	80	1040	1250	37,91	4,46	52,64	1,39
CG_F19	9,0	80	5556	1750	90,89	2,71	87,17	0,96

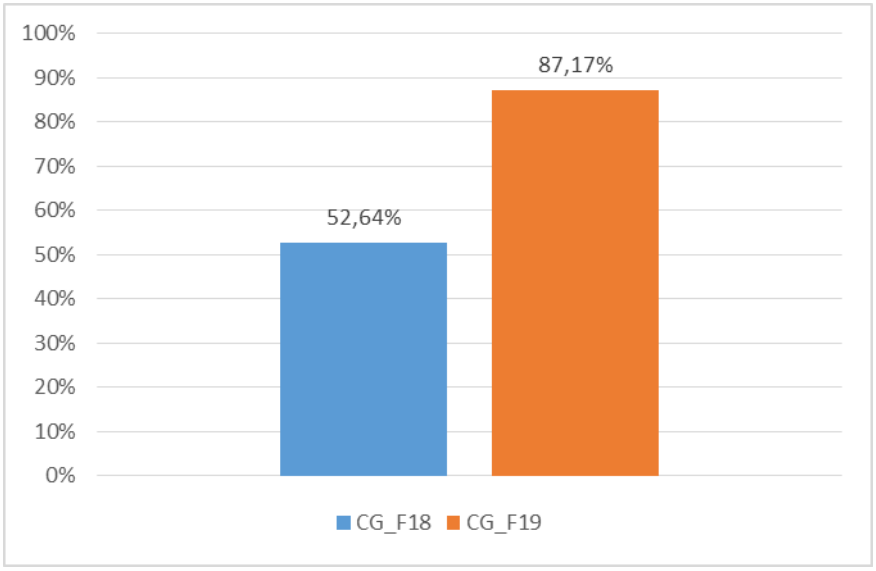

Figure 28: TREO recovery for CG direct flotation.

The CG direct flotation tests produced high mass and TREO recoveries, although the response varied between the operating conditions. CG_F19 presented the highest TREO recovery, at 87.17%, but the associated mass recovery was also very high, at 90.89%, and the enrichment ratio remained below 1. The high TREO recovery therefore reflected the transfer of most of the feed mass to the overflow rather than selective TREO upgrading.

CG_F18 produced a lower TREO recovery of 52.64%, but generated an overflow grade of 4.46% and an enrichment ratio of 1.39. Compared with CG_F19, CG_F18 provided a more selective response because TREO enrichment was achieved while recovering a smaller proportion of the total feed mass.

4.2.3 Comparison between C4 and CG direct flotation

Composite CG exhibited greater overall floatability than C4 under direct flotation conditions, as demonstrated by the higher mass and TREO recoveries obtained in CG_F18 and CG_F19. However, the maximum recovery obtained for CG was associated with limited selectivity, because CG_F19 presented an enrichment ratio below 1.

C4_F3 generated a lower recovery than the CG tests but produced a comparatively stronger enrichment ratio. The direct flotation results therefore indicate different behavior between the composites: CG favored greater transfer of material and TREO to the overflow, whereas the selected C4 condition produced lower recovery but more pronounced relative upgrading. Such differences may be associated not only with variations in feed grade, particle-size distribution and mineralogical composition, but also with the flotation conditions applied. The CG tests were conducted at higher temperature and with higher collector and depressor dosages than the C4 tests, which may have contributed to the higher mass and TREO recoveries obtained. Although C4_F3 exhibited greater relative upgrading, the highest overflow TREO grade was achieved in the CG tests, particularly in CG_F18, highlighting the importance of considering both selectivity and concentrate grade when evaluating flotation performance.

4.3 Hydrogravitic pre-concentration followed by flotation

Hydrogravitic pre-concentration was applied before flotation to evaluate the response of density-separated CG fractions. The concentrate and middlings fractions were used as flotation feeds under different operating conditions. The C4 hydrogravitic products were subjected to dry digestion before flotation and are therefore presented separately in Section 4.4.3.

4.3.1 CG hydrogravitic concentrate and middlings flotation

The operating conditions and flotation response of the CG hydrogravitic route are presented in Table 19. The corresponding TREO recoveries are shown in Figure 29.

Table 19: Operating conditions and flotation responses obtained for CG hydrogravitic pre-concentration followed by flotation.

Test code	pH	Temperature (°C)	OHA dosage (mg/kg)	Na_2SiO_3 dosage (mg/kg)	Mass recovery (%)	Overflow TREO grade (%)	TREO recovery (%)	ER
CG_ST_M_F17	9,5	80	1000	500	51,47	2,47	65,50	1,27
CG_ST(3)_M_F20	9,0	80	5556	1750	86,48	1,74	82,88	0,96
CG_ST(3)_C_F21	9,0	80	5556	1750	94,14	2,48	90,92	0,97
CG_ST(3)_M_F23	8,0	50	504	1750	16,37	2,37	16,03	0,98
CG_ST(3)_C_F24	8,0	50	513	1750	18,89	2,86	17,88	0,95

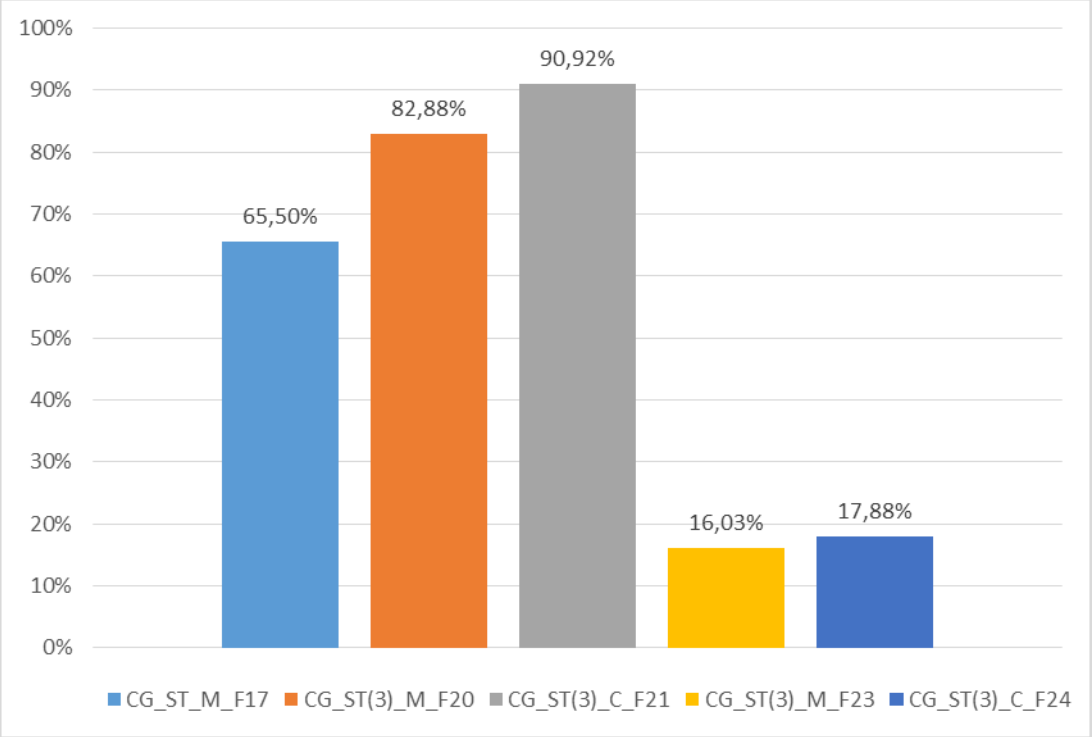

Figure 29: TREO recovery for CG hydrogravitic concentrate and middlings flotation

The hydrogravitic CG fractions produced markedly different flotation responses depending on the operating conditions and the type of hydrogravitic feed fraction. CG_ST(3)_C_F21, which used the hydrogravitic concentrate as flotation feed, presented the highest TREO recovery, at 90,92%, together with a mass recovery of 94,14%. However, the enrichment ratio was 0,97, indicating that most of the feed mass reported to the overflow without selective TREO upgrading. A similar response was observed for CG_ST(3)_M_F20, which presented a TREO recovery of 82,88%, a mass recovery of 86,48% and an enrichment ratio of 0,96.

CG_ST_M_F17, which used the hydrogravitic middlings fraction as flotation feed, produced a lower TREO recovery of 65,50%, but achieved an enrichment ratio of 1,27, representing the only test in the series with clear TREO upgrading. Although CG_ST(3)_C_F21 was operated with the highest collector dosage and produced the highest TREO recovery (90,92%) and a higher overflow TREO grade than CG_ST_M_F17, its enrichment ratio remained below 1 (0,97). This indicates that the increase in TREO grade was accompanied by an even greater transfer of total mass to the overflow, resulting in limited selectivity. In contrast, CG_ST_M_F17 recovered less TREO overall but concentrated TREO more effectively relative to the feed. The difference in flotation response may also have been influenced by the nature of the hydrogravitic feed fractions, since CG_ST(3)_C_F21 was performed on the concentrate fraction whereas CG_ST_M_F17 was performed on the middlings fraction. These fractions likely differed in mineral composition, liberation characteristics and TREO distribution, which may have contributed to the observed differences in recovery and upgrading. Therefore, neither test can be considered unequivocally superior: CG_ST(3)_C_F21 was more effective when maximizing TREO recovery was the primary objective, whereas CG_ST_M_F17 provided the most selective separation and the strongest upgrading of the flotation product. The tests conducted at 50 °C and pH 8 produced considerably lower recoveries, below 18%, while their enrichment ratios also remained below 1, indicating both poor recovery and limited selectivity under those conditions.

4.3.2 Effect of pre-concentrated feed on TREO distribution

Hydrogravitic pre-concentration generated feed fractions with different measured TREO grades and particle-size distributions. However, a higher initial feed grade did not consistently produce a more selective flotation response. For example, the hydrogravitic concentrate used in CG_ST(3)_C_F21 produced the highest TREO recovery, but the enrichment ratio remained below 1.

The comparison between concentrate and middlings fractions also did not show a uniform advantage for either fraction. The concentrate produced the highest overall recovery in CG_ST(3)_C_F21, whereas the middlings fraction produced the strongest upgrading in CG_ST_M_F17. Consequently, flotation performance was influenced not only by the hydrogravitic classification of the feed, but also by the operating conditions and the mineralogical characteristics of each fraction.

4.4 Microwave-assisted digestion followed by flotation

Microwave-assisted digestion was investigated as a pre-conditioning stage before flotation. The experimental routes included wet and dry digestion of untreated C4 material, as well as dry digestion of hydrogravitic pre-concentrated C4 and CG fractions. The results are presented separately according to digestion type and feed condition, followed by a comparison of the main flotation responses

4.4.1 C4 wet digestion route

The operating conditions and flotation response of the C4 wet digestion route are presented in Table 20.

Table 20: Operating conditions and flotation response of C4 wet digestion followed by flotation.

Test code	pH	Temperature (°C)	Depressor (mg/kg)		Mass recovery (%)	Overflow TREO grade (%)	TREO recovery (%)	ER
C4_F7	8,5	75	Phytic acid	90	7,21	1,34	7,16	0,99
C4_F8	9,0	75	Quinic acid	96	7,66	1,42	7,47	0,97

The two wet digestion tests produced similar and generally limited flotation responses. C4_F8 presented the highest TREO recovery, at 7,47%, with an overflow TREO grade of 1,42%. C4_F7 produced a comparable recovery of 7,16% and an overflow grade of 1,34%.

The enrichment ratios were 0,99 for C4_F7 and 0,97 for C4_F8, indicating that neither condition produced TREO upgrading relative to the corresponding reconstructed feed. The similar results obtained with phytic acid and quinic acid suggest that the tested wet digestion conditions had a limited influence on flotation performance. The weak flotation response may also be related to the absence of a collector in these tests, as only depressants were used during flotation.

4.4.2 C4 dry digestion route

The operating conditions and flotation response of the C4 dry digestion route are presented in Table 21. The corresponding TREO recovery is shown in Figure 30.

Table 21: Operating conditions and flotation response of C4 dry digestion followed by flotation.

Test code	pH	Temperature (°C)	Reagents (mg/kg)				Mass recovery (%)	Overflow TREO grade (%)	TREO recovery (%)	ER
C4_F5	8,5	75	Na_2SiO_3	500	OHA	98	5,86	2,43	11,53	1,97
C4_F6	9,0	75	Na_2SiO_3	500	OHA	180	20,09	2,33	36,71	1,83
C4_F10	9,0	80	Na_2SiO_3	500	Phytic acid	186	3,70	3,32	3,66	0,99
C4_F11	9,0	80	Na_2SiO_3	500	Quinic acid	191	2,26	1,86	1,12	0,50

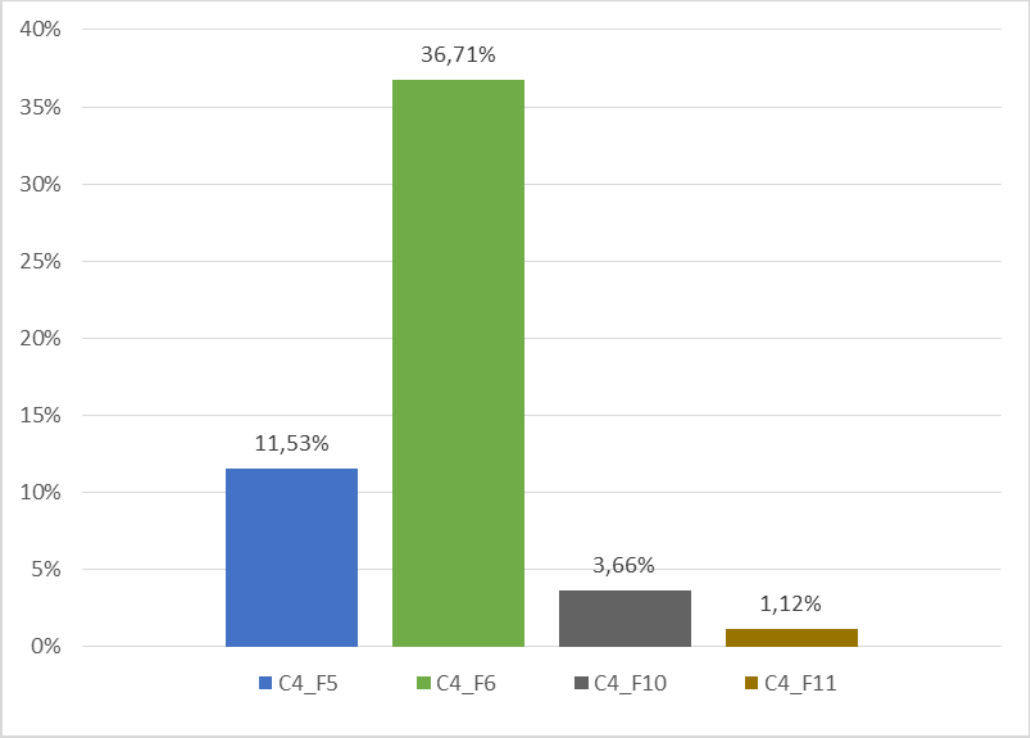

Figure 30: TREO recovery for C4 dry digestion route.

The dry digestion tests produced variable flotation responses across the investigated conditions. C4_F5 and C4_F6, which included OHA as collector, achieved TREO recoveries of 11,53% and 36,71%, respectively, and both produced enrichment ratios greater than 1. In contrast, C4_F10 and C4_F11 yielded substantially lower TREO recoveries of 3,66% and 1,12%, respectively. It should be noted that C4_F10 and C4_F11 were conducted using only the two depressants and did not include OHA collector, which may have influenced their flotation performance and contributed to the lower recoveries obtained. C4_F6 presented the highest TREO recovery, at 36,71%, together with a mass recovery of 20,09%, an overflow TREO grade of 2,33% and an enrichment ratio of 1,83. C4_F5 produced a lower TREO recovery of 11,53%, but presented the highest enrichment ratio within the series, at 1,97.

In contrast, C4_F10 and C4_F11 produced low TREO recoveries of 3,66% and 1,12%, respectively. C4_F10 showed no effective upgrading, with an enrichment ratio of 0,99, while C4_F11 generated an overflow depleted in TREO, with an enrichment ratio of 0,50. Under the tested conditions, the OHA-based tests therefore produced stronger TREO recovery and upgrading than the tests using phytic or

quinic acid. Nevertheless, differences in pH, temperature and reagent dosage prevent attribution of the response exclusively to reagent type.

4.4.3 C4 dry digestion after hydrogravitic pre-concentration

The operating conditions and flotation response of C4 dry digestion after hydrogravitic pre-concentration are presented in Table 22.

Table 22: Operating conditions and flotation response of C4 dry digestion after hydrogravitic pre-concentration followed by flotation.

Test code	pH	Temperature (°C)	OHA dosage (mg/kg)	Na_2SiO_3 (mg/kg)	Mass recovery (%)	Overflow TREO grade (%)	TREO recovery (%)	ER
C4_ST_R4_C_F13	8	80	198	500	9,06	3,57	24,6	2,72
C4_ST_R4_M_F14	8,5	80	189	500	8,86	4,02	14,69	1,66

The two hydrogravitically pre-concentrated C4 fractions produced clear TREO upgrading after dry digestion and flotation. C4_ST_R4_C_F13, conducted using the concentrate fraction, presented the highest TREO recovery, at 24,60%, and the highest enrichment ratio, at 2,72. The overflow grade increased to 3,57%, while only 9,06% of the reconstructed feed mass reported to the overflow.

C4_ST_R4_M_F14, conducted using the middlings fraction, produced a higher overflow TREO grade of 4,02%, but a lower recovery of 14,69% and an enrichment ratio of 1,66. The concentrate-derived feed therefore produced the stronger balance between recovery and relative upgrading, whereas the middlings-derived feed generated the highest overflow grade. The different responses indicate that hydrogravitic fraction type influenced the performance of the combined digestion and flotation route.

4.4.4 CG dry digestion after hydrogravitic pre-concentration

The operating conditions and flotation response of CG dry digestion after hydrogravitic pre-concentration are presented in Table 23.

Table 23: Operating conditions and flotation response of CG dry digestion after hydrogravitic pre-concentration followed by flotation.

Test code	pH	Temperature (°C)	OHA dosage (mg/kg)	Na_2SiO_3 (mg/kg)	Mass recovery (%)	Overflow TREO grade (%)	TREO recovery (%)	ER
CG_ST_M_F15	9,0	80	219	500	21,65	4,07	41,27	1,91
CG_ST_C_F16	9,0	80	206	500	20,15	2,25	13,06	0,65

The two CG fractions produced contrasting flotation responses despite being treated under similar pH, temperature and reagent conditions. CG_ST_M_F15, which used the middlings fraction as feed, presented a TREO recovery of 41,27%, an overflow TREO grade of 4,07% and an enrichment ratio of 1,91. The result indicates both TREO recovery and effective upgrading of the flotation product.

CG_ST_C_F16, which used the concentrate fraction, produced a substantially lower TREO recovery of 13,06% and an enrichment ratio of 0,65, indicating depletion of TREO in the overflow relative to the reconstructed feed.

4.4.5 Comparison between wet and dry digestion routes

The digestion-assisted routes produced different responses according to digestion method and feed preparation. Wet digestion of untreated C4 generated TREO recoveries below 8% and enrichment ratios close to or below 1, indicating limited recovery and no effective upgrading. Dry digestion of untreated C4 produced a stronger response under the OHA-based conditions, particularly in C4_F6, which reached a TREO recovery of 36,71%.

The combination of hydrogravitic pre-concentration, dry digestion and flotation produced the strongest enrichment responses for C4. C4_ST_R4_C_F13 reached the highest enrichment ratio, at 2,72, while C4_ST_R4_M_F14 generated the highest overflow grade, at 4,02%. For CG, the middlings-derived test CG_ST_M_F15 produced both effective upgrading and a TREO recovery of 41,27%, whereas the concentrate-derived test did not produce TREO enrichment.

Overall, dry digestion produced more favourable flotation responses than wet digestion under the investigated conditions. However, the results also demonstrate that digestion method alone did not determine performance, because feed fraction characteristics and reagent conditions varied among the experimental routes.

4.5 Magnetic pre- concentration followed by flotation

Magnetic pre-concentration was evaluated as an additional physical separation stage before flotation of composite CG. The flotation feed corresponded to the non-magnetic fraction obtained after magnetic separation. The operating conditions and flotation response of test CG_NMAG_F25 are presented in Table 24.

Table 24: Operating conditions and flotation response of the non-magnetic fraction after magnetic pre-treatment

Test code	pH	Temperature (°C)	OHA dosage (mg/kg)	Na_2SiO_3 (mg/kg)	Mass recovery (%)	Overflow TREO grade (%)	TREO recovery (%)	ER
CG_NMAG_F25	8	50	504	1750	16,71	3,61	19,4	1,16

The flotation of the non-magnetic fraction produced a mass recovery of 16,71% and a TREO recovery of 19,40%. The overflow presented a TREO grade of 3,61% and an enrichment ratio of 1,16, indicating moderate TREO upgrading relative to the reconstructed flotation feed.

Although the enrichment ratio was greater than 1, most of the TREO remained in the underflow, as indicated by the relatively low recovery. The non-magnetic fraction was also substantially coarser than the remaining flotation feeds, with a d50 of 116,17 µm and a d90 of 274,82 µm. The coarse particle-size distribution may have limited bubble–particle attachment and contributed to the low TREO recovery. However, because only one magnetic pre-concentration test was performed, the individual effects of feed granulometry, magnetic gangue removal and flotation conditions cannot be distinguished.

4.6 Analysis of Taguchi-based flotation response for composite CG

Taguchi-based flotation tests were conducted to evaluate the response of composite CG under controlled variation of selected operating parameters. The CG_F22 series examined the influence of pH,

temperature and OHA dosage, while the CG_F27 series evaluated OHA dosage, depressor type and EDTA addition under fixed pH and temperature conditions.

The CG_F22 and CG_F27 test programmes were conducted in two sequential flotation stages. For each series, the complete operating conditions and metallurgical responses are presented in a table, followed by a graph showing the average TREO recovery associated with each factor level. The average response graphs are used to identify general trends, while selection of the most relevant individual conditions also considers mass recovery, overflow TREO grade, cumulative recovery and enrichment ratio.

4.6.1 CG_F22A series (1st stage)

The operating conditions and metallurgical responses obtained for the first-stage CG_F22A series are presented in Table 25. Figure 32 shows the average TREO recovery associated with each investigated level of pH, temperature and OHA dosage.

Table 25: Operating conditions and flotation response of CG_F22A series.

Test code	pH	Temperature (°C)	OHA dosage (mg/kg)	Mass recovery (%)	TREO grade (%)	TREO recovery (%)	ER
CG_F22_1A	8,0	50	500	11,48	2,67	19,27	1,68
CG_F22_2A	9,5	50	500	31,31	1,32	36,21	1,16
CG_F22_3A	8,0	80	500	23,58	2,49	45,24	1,92
CG_F22_4A	9,5	80	500	29,77	1,4	36,74	1,24
CG_F22_5A	8,0	50	1500	22,27	1,38	26,09	1,17
CG_F22_6A	9,5	50	1500	34,61	1,42	41,95	1,21
CG_F22_7A	8,0	80	1500	46,05	1,21	46,89	1,02
CG_F22_8A	9,5	80	1500	57,77	1,38	59,97	1,04

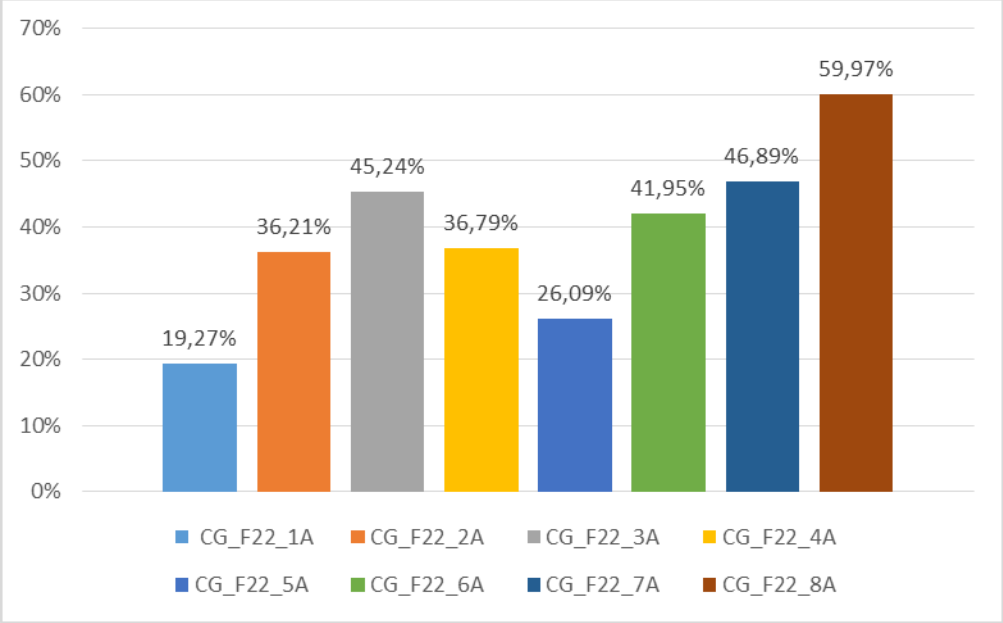

Figure 31: TREO recovery for CG_F22A tests.

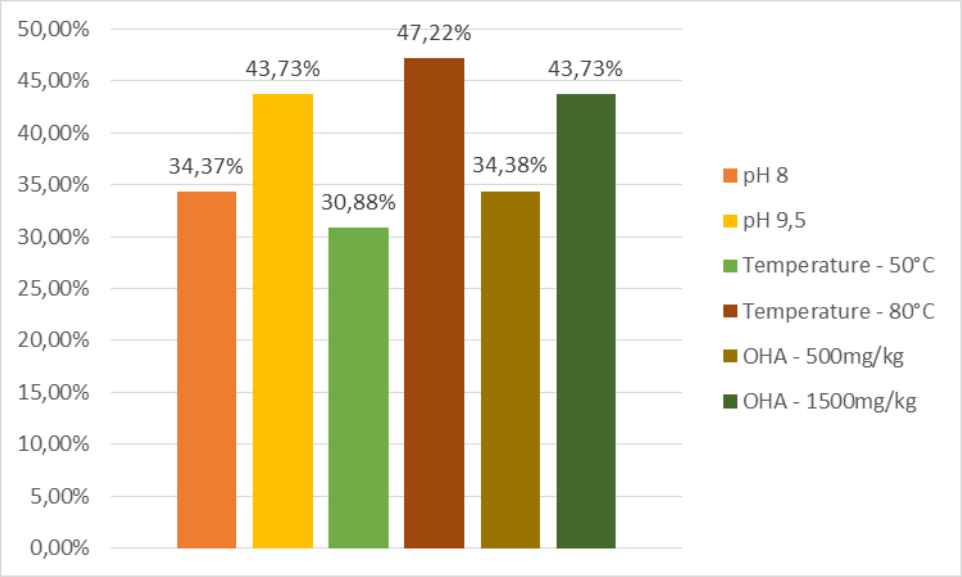

Figure 32: Average TREO recovery obtained at each factor level in the CG_F22A series.

The CG_F22A series produced TREO recoveries ranging from 19,27% to 59,97%, demonstrating substantial variation among the investigated conditions. CG_F22_8A, conducted at pH 9,5, 80 °C and an OHA dosage of 1 500 mg/kg, presented the highest TREO recovery, at 59,97%, together with the highest mass recovery, at 57,77%. However, its enrichment ratio was only 1,04, indicating that the high TREO recovery was accompanied by recovery of a large proportion of the total feed mass and only limited selective upgrading.

CG_F22_1A presented the highest overflow TREO grade, at 2,67%, but its TREO recovery was limited to 19,27%. CG_F22_3A, conducted at pH 8,0, 80 °C and 500 mg/kg OHA, produced a TREO recovery of 45,24% and the highest enrichment ratio, at 1,92. Consequently, different conditions maximised different metallurgical indicators. CG_F22_8A favored maximum recovery, CG_F22_1A produced the highest overflow grade, and CG_F22_3A provided the strongest relative upgrading while maintaining a comparatively high TREO recovery.

The average-response graph shows that temperature produced the largest difference between the investigated factor levels. Average TREO recovery increased from 30,88% at 50 °C to 47,22% at 80 °C. Increasing pH from 8,0 to 9,5 increased average recovery from 34,37% to 43,73%, while increasing OHA dosage from 500 to 1 500 mg/kg produced the almost the same average increase, from 34,38% to 43,73%.

The factor-level averages therefore indicate that pH 9,5, 80 °C and 1 500 mg/kg OHA were associated with the highest average TREO recovery. The same combination was applied in CG_F22_8A, which produced the maximum measured recovery. Nevertheless, the individual results show that maximum recovery did not correspond to maximum selectivity, because CG_F22_3A produced a considerably higher enrichment ratio under the lower OHA dosage and pH condition.

4.6.2 CG_F22B series (2nd stage)

The operating conditions and metallurgical responses obtained for the completed second-stage CG_F22B tests are presented in Table 26. Figure 34 presents the average TREO recovery associated

with each investigated level of pH, temperature and OHA dosage. Cumulative TREO recovery is also reported because the feed to each second-stage test corresponded to the overflow generated during the associated first-stage test.

Table 26: Operating conditions and flotation response of CG_F22B series.

Test code	pH	Temperature (°C)	OHA dosage (mg/kg)	Mass recovery (%)	Overflow TREO grade (%)	TREO recovery (%)	Cumulative TREO recovery (%)	ER
CG_F22_1B	8,0	50	500	17,51	2,89	19,58	3,77	1,12
CG_F22_2B	9,5	50	500	46,54	2,59	43,83	15,87	0,94
CG_F22_3B	8,0	80	500	35,79	2,70	39,45	17,85	1,10
CG_F22_4B	9,5	80	500	11,44	2,32	10,26	3,77	0,90
CG_F22_5B	8,0	50	1500	29,33	2,75	26,98	7,04	0,92
CG_F22_6B	9,5	50	1500	47,26	2,56	45,03	18,89	0,95
CG_F22_7B	8,0	80	1500	N/A	N/A	N/A	N/A	N/A
CG_F22_8B	9,5	80	1500	N/A	N/A	N/A	N/A	N/A

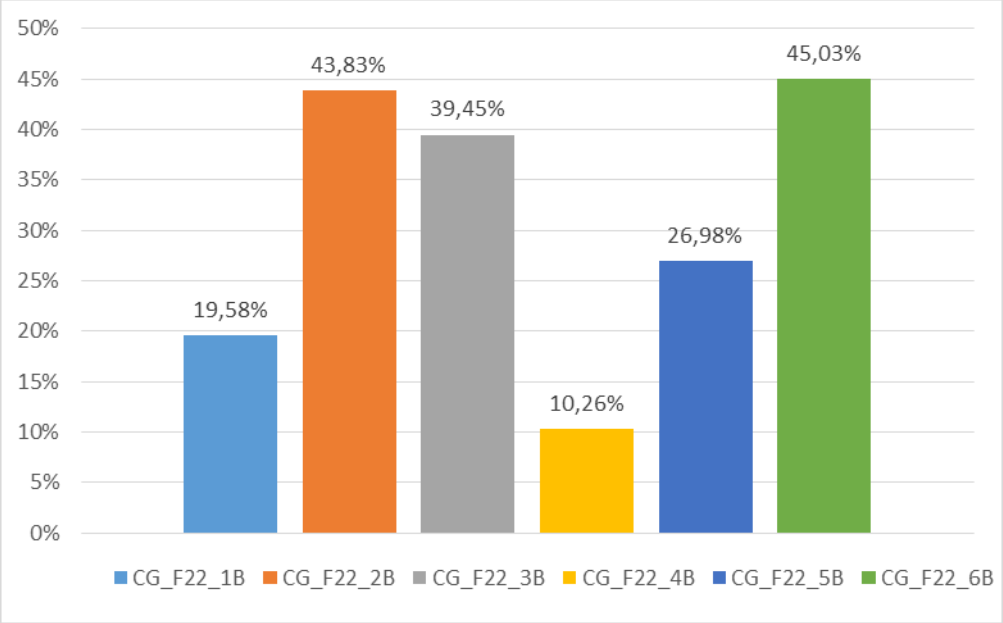

Figure 33: TREO recovery for CG_F22B tests.

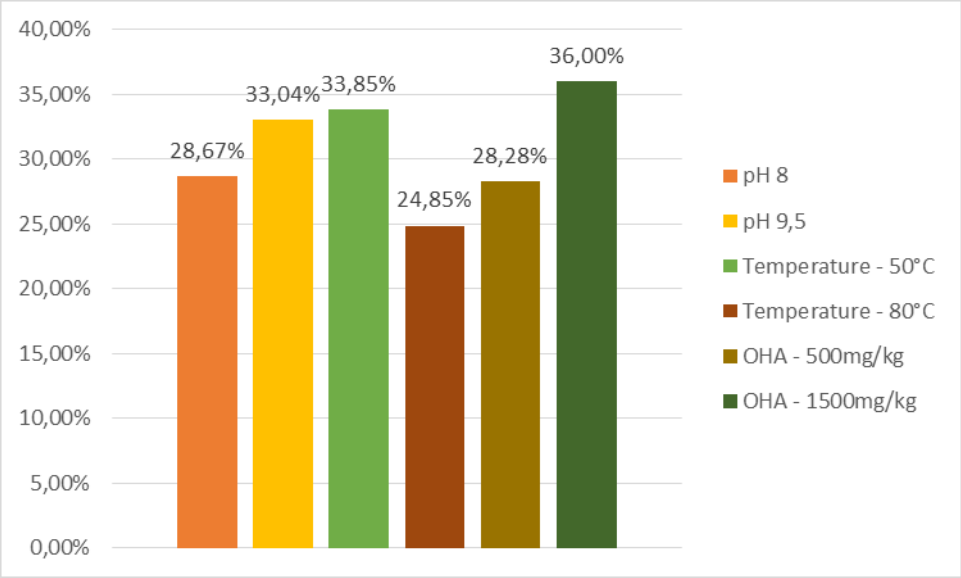

Figure 34: Average TREO recovery obtained at each factor level for the completed CG_F22B tests..

The completed CG_F22B tests produced second-stage TREO recoveries ranging from 10,26% to 45,03%. CG_F22_6B, conducted at pH 9,5, 50 °C and an OHA dosage of 1 500 mg/kg, presented the highest second-stage TREO recovery, at 45,03%, and the highest cumulative TREO recovery, at 18,89%. However, its enrichment ratio was 0,95, indicating that the second-stage overflow was not enriched in TREO relative to its immediate flotation feed.

CG_F22_1B produced the highest overflow TREO grade, at 2,89%, and the highest enrichment ratio, at 1,12, although its cumulative TREO recovery was only 3.77%. CG_F22_3B combined a second stage TREO recovery of 39,45%, a cumulative recovery of 17,85% and an enrichment ratio of 1,10. Among the completed tests, CG_F22_3B therefore provided the most balanced response between recovery from the original feed and selective TREO upgrading.

The average-response graph shows that pH 9,5 was associated with a slightly higher average TREO recovery than pH 8,0, with values of 33,04% and 28,67%, respectively. The average recovery was 33,85% at 50 °C and 24,85% at 80 °C. Similarly, tests conducted with 1 500 mg/kg OHA produced an average recovery of 36,00%, compared with 28,28% for tests conducted with 500 mg/kg OHA.

The apparent higher responses associated with 50 °C and 1 500 mg/kg OHA must be interpreted cautiously because the experimental matrix was incomplete. Both non-performed tests corresponded to combinations of 80 °C and 1 500 mg/kg OHA. Consequently, the lower average at 80 °C and the higher average at 1 500 mg/kg OHA cannot be considered definitive independent factor effects.

Paired comparisons provide a clearer interpretation of the completed tests. At 50 °C and pH 8,0, increasing the OHA dosage from 500 to 1 500 mg/kg increased TREO recovery from 19,58% to 26,98%, but decreased the enrichment ratio from 1,12 to 0,92. At 50 °C and pH 9,5, the same increase in OHA dosage resulted in only a small improvement in TREO recovery, from 43,83% to 45,03%, while the enrichment ratios for both tests remained below 1. Comparing the effect of temperature at pH 8,0 and 500 mg/kg OHA, increasing the temperature from 50 to 80 °C increased second-stage TREO recovery from 19,58% to 39,45% and cumulative TREO recovery from 2,48% to 17,85%, while maintaining an enrichment ratio greater than 1.

Among the completed conditions, CG_F22_6B represented the maximum-recovery condition, CG_F22_1B produced the highest overflow grade and enrichment ratio, and CG_F22_3B provided the most favourable compromise between cumulative recovery and TREO upgrading. Identification of the overall best second-stage factor combination remains restricted by the absence of CG_F22_7B and CG_F22_8B.

4.6.3 CG_F27A series (1st stage)

The CG_F27A series was conducted at a constant pH of 8,0 and a temperature of 50 °C to evaluate the influence of OHA dosage, depressor type and EDTA dosage on flotation response. The operating conditions and metallurgical responses obtained for the first-stage tests are presented in Table 27. Figure 36 presents the average TREO recovery associated with each reagent level investigated.

Table 27: Operating conditions and flotation response of CG_F27A series.

Test code	OHA dosage (mg/kg)	Na_2SiO_3 dosage (mg/kg)	Quinic acid dosage (mg/kg)	EDTA dosage (mg/kg)	Mass recovery (%)	Overflow TREO grade (%)	TREO recovery (%)	ER
CG_F27_1A	500	500	0	0	18,51	2,74	29,74	1,61
CG_F27_2AR	500	500	0	500	8,88	2,18	9,39	1,06
CG_F27_3A	500	0	500	0	13,23	2,06	14,12	1,07
CG_F27_4A	500	0	500	500	8,89	2,09	11,19	1,26
CG_F27_5A	200	500	0	0	7,65	2,13	8,54	1,12
CG_F27_6A	200	500	0	200	7,79	2,38	8,27	1,06
CG_F27_7A	200	0	500	0	8,83	2,27	9,99	1,13
CG_F27_8AR	200	0	500	200	11,43	2,19	12,95	1,13

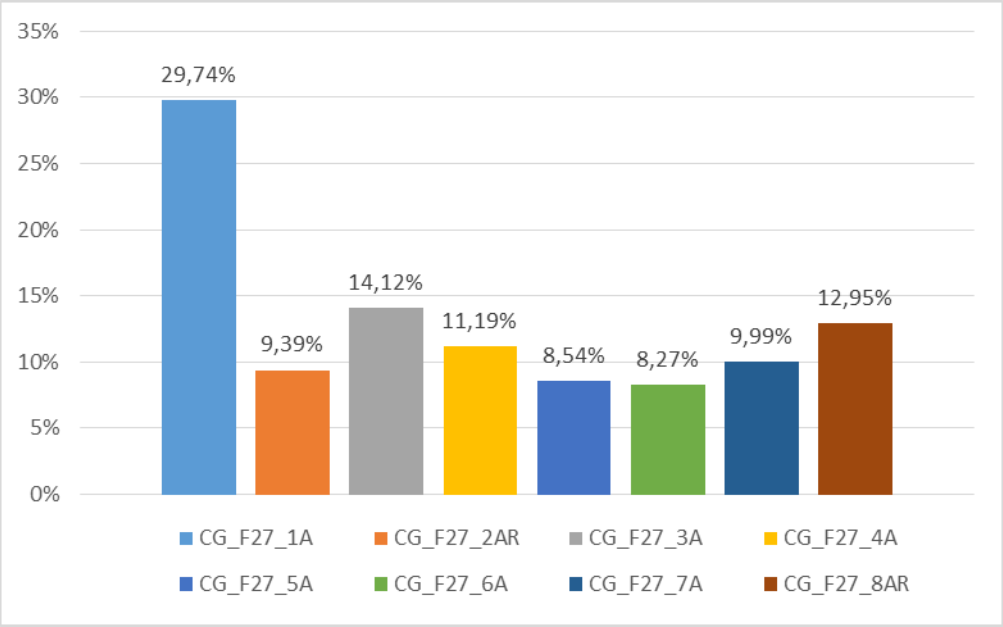

Figure 35: TREO recovery for CG_F27A tests.

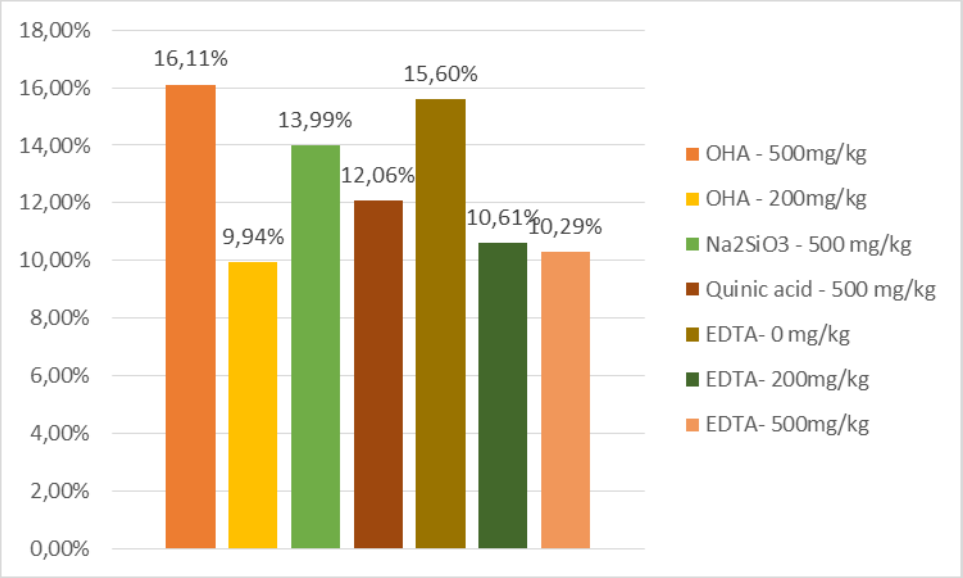

Figure 36: Average TREO recovery associated with the reagent levels investigated in the CG_F27A series.

The CG_F27A tests produced TREO recoveries ranging from 8,27% to 29,74%. CG_F27_1A, conducted with 500 mg/kg OHA, 500 mg/kg sodium silicate and without EDTA, presented the highest TREO recovery, at 29,74%, together with the highest mass recovery, at 18,51%, and the highest enrichment ratio, at 1,61. The same test therefore represented the strongest complete reagent combination evaluated during the first stage.

The mean-response graph indicates that 500 mg/kg OHA produced a higher mean TREO recovery than 200 mg/kg, with values of 16,11% and 9,94%, respectively. Sodium silicate produced a slightly higher mean recovery than quinic acid, at 13,99% compared with 12,06%.

The absence of EDTA was associated with the highest mean recovery, at 15,60%. Mean recovery decreased to 10,61% at 200 mg/kg EDTA and 10,29% at 500 mg/kg EDTA. However, the non-zero EDTA dosages were associated with different OHA dosages: 500 mg/kg EDTA was used with 500 mg/kg OHA, whereas 200 mg/kg EDTA was used with 200 mg/kg OHA. Consequently, the EDTA values represent the mean response of combined reagent conditions rather than an independent EDTA dose–response relationship.

For CG_F27A, the factor-level means and the individual-test results provided the same general indication. The levels associated with the highest mean recovery—500 mg/kg OHA, sodium silicate and absence of EDTA—corresponded to CG_F27_1A, which produced the highest measured TREO recovery and enrichment ratio. Under the investigated first-stage conditions, EDTA addition did not improve flotation performance.

4.6.4 CG_F27B series (2nd stage)

All second-stage tests were performed at pH 8,0 and 50 °C, with depressor dosages reduced from 500 to 250 mg/kg. The operating conditions and metallurgical responses are presented in Table 28. Figure 38 presents the average TREO recovery associated with each reagent level investigated. Cumulative TREO recovery is also reported relative to the original first-stage feed.

Table 28: Operating conditions and TREO response of CG_F27B series.

Test code	OHA dosage (mg/kg)	Na_2SiO_3 dosage (mg/kg)	Quinic acid dosage (mg/kg)	EDTA dosage (mg/kg)	Mass recovery (%)	Overflow TREO grade (%)	TREO recovery (%)	Cumulative TREO recovery (%)	ER
CG_F27_1B	500	250	0	0	18,22	1,59	19,00	5,65	1,04
CG_F27_2B	500	250	0	500	8,81	1,89	9,60	0,90	1,09
CG_F27_3B	500	0	250	0	18,41	1,72	18,24	2,58	0,99
CG_F27_4B	500	0	250	500	13,35	0,78	6,90	0,77	0,52
CG_F27_5B	200	250	0	0	16,19	1,52	14,66	1,25	0,91
CG_F27_6B	200	250	0	200	7,82	2,14	12,42	1,03	1,59
CG_F27_7B	200	0	250	0	12,82	1,97	13,99	1,40	1,09
CG_F27_8B	200	0	250	200	13,55	1,87	18,17	2,35	1,34

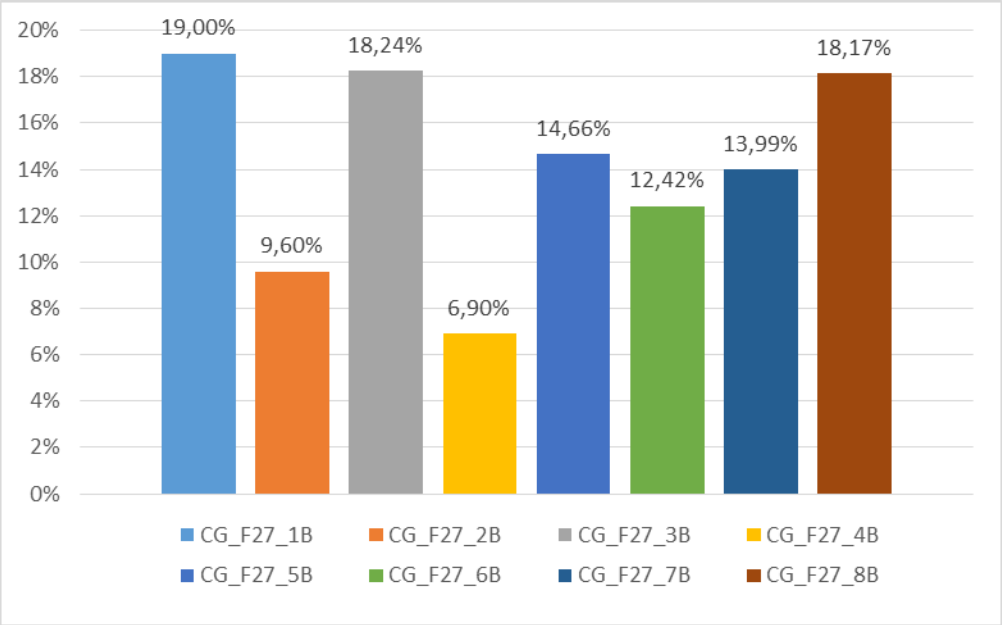

Figure 37: TREO recovery for CG_F27B tests.

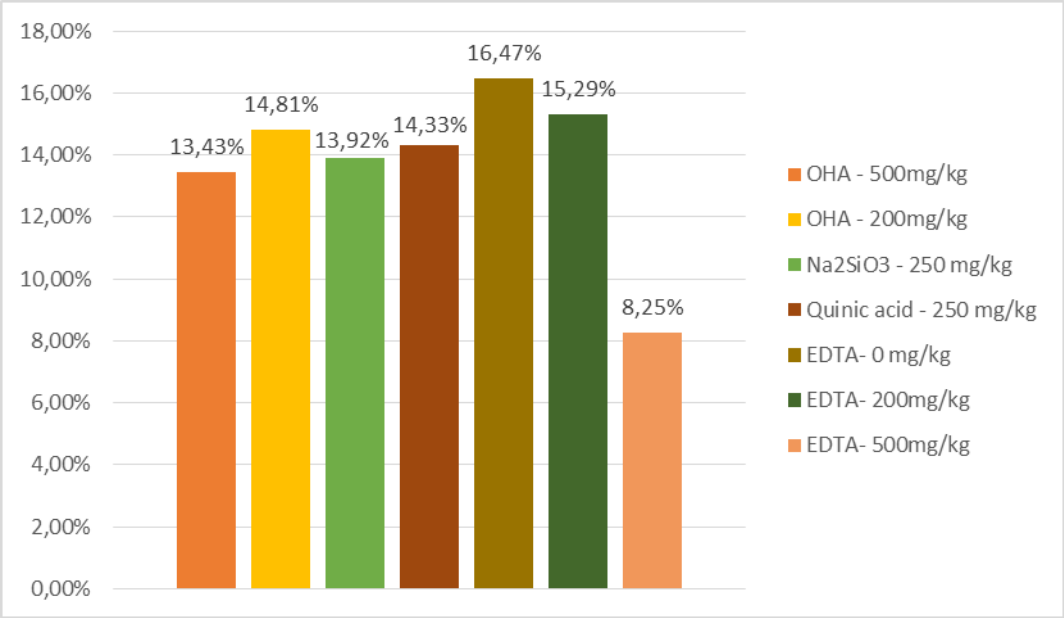

Figure 38: Average TREO recovery associated with the reagent levels investigated in the CG_F27B series.

The CG_F27B tests produced second-stage TREO recoveries ranging from 6,90% to 19,00%. CG_F27_1B, conducted with 500 mg/kg OHA, 250 mg/kg sodium silicate and without EDTA, presented the highest second-stage TREO recovery, at 19,00%, and the highest cumulative recovery, at 5,65%. Its enrichment ratio was 1,04, indicating that the condition favoured recovery but produced only limited TREO upgrading.

CG_F27_6B produced the highest overflow TREO grade, at 2,14%, and the highest enrichment ratio, at 1,59, although its cumulative recovery was only 1,03%. CG_F27_8B showed a balanced performance, with a second-stage TREO recovery of 18,17%, a cumulative recovery of 2,35% and an enrichment ratio of 1,34. Consequently, CG_F27_1B represented the maximum-recovery condition, CG_F27_6B represented the maximum-upgrading condition, and CG_F27_8B provided an intermediate response between recovery and enrichment.

The mean-response graph indicates that 200 mg/kg OHA produced a slightly higher mean TREO recovery than 500 mg/kg, with values of 14,81% and 13,43%, respectively. Quinic acid produced a slightly higher mean recovery than sodium silicate, at 14,33% compared with 13,92%. The absence of EDTA generated the highest mean recovery, at 16,47%, while mean recovery decreased to 15,29% at 200 mg/kg EDTA and 8,25% at 500 mg/kg EDTA.

The mean factor responses and the individual-test results provided different indications. The factor-level means suggest that 200 mg/kg OHA, quinic acid and absence of EDTA were generally associated with higher recovery across the complete experimental matrix. However, the exact combination of such levels, applied in CG_F27_7B, produced a TREO recovery of 13,99%, while the highest individual recovery of 19,00% was obtained in CG_F27_1B using 500 mg/kg OHA, sodium silicate and no EDTA.

The difference occurs because each factor-level mean combines results obtained under several conditions of the remaining variables. For example, the mean response for 500 mg/kg OHA included the high recoveries obtained in CG_F27_1B and CG_F27_3B, together with the substantially lower recoveries obtained when 500 mg/kg EDTA was present in CG_F27_2B and CG_F27_4B. Such lower-performing combinations reduced the overall mean response associated with 500 mg/kg OHA.

The factor-level means therefore describe the general performance of each reagent level across several combinations, whereas the individual tests identify the performance of each complete reagent system. The highest mean levels cannot be combined automatically and considered the optimum condition because the response of one reagent depended on the levels of the remaining reagents.

Accordingly, CG_F27_1B was identified as the best tested condition for maximum second-stage and cumulative TREO recovery. The mean responses associated with 200 mg/kg OHA and quinic acid remain relevant as general trends and may guide additional optimisation tests, but they do not demonstrate that their combined use represents the optimum reagent condition.

Although selected second-stage tests produced enrichment ratios above 1, cumulative TREO recoveries remained below 6% throughout the CG_F27B series. The second flotation stage therefore produced additional upgrading only in the tests where the enrichment ratio exceeded 1, while recovering only a limited proportion of the TREO initially present in the first-stage feed. In tests with enrichment ratios below 1, no upgrading was achieved despite the additional TREO recovery.

4.6.5 Main parameter trends based on TREO recovery and enrichment ratio

The Taguchi-based flotation results demonstrate that factor-level means and individual-test responses provide complementary but distinct information. The mean-response graphs describe the general TREO recovery associated with each factor level across several experimental combinations, whereas the individual-test tables describe the response of each complete combination of pH, temperature and reagents. Consequently, the factor levels presenting the highest mean recoveries cannot be combined automatically and described as the optimum condition when interactions among variables are present.

In the CG_F22A series, the highest mean responses were associated with pH 9,5, 80 °C and 1 500 mg/kg OHA. The same complete combination was used in CG_F22_8A, which produced the highest individual recovery, at 59,97%. Nevertheless, CG_F22_3A produced the highest enrichment ratio, at 1,92, confirming that maximum recovery and maximum upgrading were achieved under different conditions.

In the CG_F22B series, CG_F22_6B produced the highest second-stage and cumulative TREO recoveries, while CG_F22_3B provided a more favourable balance between cumulative recovery and enrichment. The mean factor responses were interpreted cautiously because CG_F22_7B and CG_F22_8B were not performed, resulting in an incomplete and unbalanced comparison of temperature and OHA dosage.

In the CG_F27A series, the factor-level means and the individual-test results were consistent. The levels associated with the highest mean recovery—500 mg/kg OHA, sodium silicate and absence of EDTA—corresponded to CG_F27_1A, which produced the highest individual recovery and enrichment ratio.

In the CG_F27B series, the factor-level means and the maximum individual recovery differed. Although 200 mg/kg OHA and quinic acid produced slightly higher mean recoveries, CG_F27_1B, conducted with 500 mg/kg OHA and sodium silicate, produced the highest individual and cumulative recoveries. The difference indicates interaction among OHA dosage, depressor type and EDTA addition.

Across both CG_F27 stages, absence of EDTA was associated with the highest mean recovery. EDTA addition did not improve the overall flotation response under the investigated conditions, particularly at 500 mg/kg, although the effect of EDTA cannot be evaluated independently because each EDTA dosage was tested together with specific OHA dosages and depressor systems.

Selection of the most relevant operating condition was therefore based primarily on the individual-test results, because each individual test represents a complete operating combination that was experimentally evaluated. Factor-level means were used to identify general tendencies and potential

directions for further optimisation. The final evaluation also considered mass recovery, overflow TREO grade, enrichment ratio and, for second-stage tests, cumulative TREO recovery.

4.7 Comparative evaluation of beneficiation routes

The investigated routes were compared using mass recovery, overflow TREO grade, TREO recovery and enrichment ratio. Direct flotation included preliminary single-stage tests and the two-stage Taguchi-based series, while the remaining routes involved hydrogravitic, magnetic or microwave-assisted treatment before flotation.

4.7.1 Influence of pre-concentration and pre-treatment relative to direct flotation

For composite C4, selected pre-treatment routes improved flotation performance relative to direct flotation. C4_F3 represented the strongest direct-flotation response, with a TREO recovery of 27,05% and an enrichment ratio of 1,74. Dry digestion followed by flotation increased recovery to 36,71% in C4_F6, while hydrogravitic pre-concentration combined with dry digestion produced the highest enrichment ratio, at 2,72, in C4_ST_R4_C_F13. Wet digestion was not beneficial, because recovery remained below 8% and no effective upgrading was achieved.

The C4 results therefore indicate that dry digestion was advantageous when recovery was prioritised, while hydrogravitic pre-concentration followed by dry digestion was more favourable for selective upgrading. Pre-treatment did not improve performance uniformly, and its contribution depended on the treatment method and feed fraction.

For composite CG, direct flotation included the preliminary CG_F18 and CG_F19 tests and the two-stage CG_F22 and CG_F27 series. The preliminary direct-flotation tests demonstrated that untreated CG could produce either high recovery with limited selectivity or a lower but more selective response. The first-stage Taguchi tests confirmed that untreated CG could also achieve meaningful recovery and enrichment under controlled operating conditions. CG_F22_3A, for example, combined a TREO recovery of 45,24% with an enrichment ratio of 1,92.

The second flotation stages did not increase overall TREO recovery because only the overflow from the first stage was reprocessed. Their principal purpose was additional upgrading of the first-stage concentrate. In the CG_F22B series, selected tests increased overflow grade or maintained enrichment above 1, but cumulative recoveries remained below 19%. In the CG_F27B series, cumulative recoveries remained below 6%. The second stage therefore produced limited additional upgrading at the expense of substantial TREO loss from the original feed.

Hydrogravitic pre-concentration generated the highest CG recoveries, including 90,92% in CG_ST(3)_C_F21. However, the associated mass recovery was 94,14% and the enrichment ratio was 0,97, indicating limited selectivity. Hydrogravitic pre-concentration followed by dry digestion produced a more selective response in CG_ST_M_F15, with a recovery of 41,27% and an enrichment ratio of 1,91. Magnetic pre-concentration produced moderate upgrading but limited recovery.

No pre-concentration or pre-treatment route was consistently superior to direct flotation for composite CG. Direct flotation remained competitive in terms of recovery, overflow grade and enrichment, particularly in CG_F18 and CG_F22_3A. Hydrogravitic pre-concentration produced the highest total recovery but limited upgrading, while the combined hydrogravitic and dry-digestion route generated a selective response comparable with the strongest direct-flotation conditions.

4.7.2 Overall response of C4 and CG feed materials

Composite C4 generally presented lower mass and TREO recoveries than CG, indicating lower overall transfer of solids and REE-bearing particles to the overflow. Nevertheless, selected C4 routes produced pronounced enrichment, particularly after hydrogravitic pre-concentration and dry digestion. The response of C4 was therefore characterised by comparatively limited flotation recovery potential but greater relative upgrading under selected pre-treatment conditions.

Composite CG presented greater overall floatability and produced the highest TREO recoveries and overflow grades obtained during the experimental programme. However, several high-recovery CG tests were also associated with high mass recovery and enrichment ratios close to or below 1. Such behaviour indicates simultaneous recovery of REE-bearing particles and gangue, particularly under conditions involving elevated collector dosage.

The higher absolute overflow grades obtained for CG were also influenced by the higher initial TREO grades of several CG feed materials. Consequently, overflow grade alone cannot be used to compare the two composites. Enrichment ratio provides a more appropriate measure of relative upgrading, while TREO and mass recoveries indicate whether upgrading was accompanied by selective separation.

Overall, CG showed greater potential for TREO recovery, while C4 showed greater potential for relative enrichment under selected combined treatment conditions. For CG, optimisation should prioritise control of mass recovery and gangue flotation. For C4, further investigation should focus on feed preparation and dry-digestion conditions capable of improving recovery without reducing the enrichment achieved.

4.7.3 Integrated interpretation of route performance

The comparison of the metallurgical indicators indicates that the relevance of each experimental condition depended on the intended function of the flotation stage. Conditions producing high TREO recovery together with high mass recovery and enrichment ratios close to or below 1 favored transfer of REE bearing material to the overflow but provided limited separation from gangue. Such responses are more consistent with a rougher stage objective, in which recovery is prioritised over concentrate grade.

Conditions that produced lower mass recovery but enrichment ratios above 1 showed better selectivity, meaning that REE bearing minerals were concentrated more effectively relative to gangue minerals. Such responses are therefore more suitable for a cleaning stage, where the aim is to improve concentrate quality rather than maximise recovery.

In the CG_F22 and CG_F27 routes, the second flotation stage treated the overflow product generated during the first stage. Selected second-stage tests produced additional upgrading, although several conditions presented enrichment ratios below 1. Cleaning also rejected part of the TREO recovered during the first stage, resulting in lower cumulative recovery relative to the original feed. The second-stage results therefore demonstrate a recovery grade trade-off rather than a consistent improvement in concentrate quality.

The variable responses obtained among the routes are consistent with the mineralogical complexity of Fen carbonatite material. SEM-EDS observations identified parisite and monazite associated with barite, fluorapatite, carbonates, silicates and Fe-bearing minerals. Recovery of composite or insufficiently liberated particles may therefore have transferred REE-bearing minerals and gangue simultaneously to the overflow, limiting grade improvement (Dahlgren, 2019; Al-Ali et al., 2020; Akyildiz et al., 2026).

Particle size distribution and reagent conditions also influenced flotation behavior. Fine particles feeds may have favored entrainment of gangue particles, whereas the coarse non-magnetic fraction may have

reduced bubble particle attachment. Elevated temperature increased mean TREO recovery in the CG_F22A series, while higher OHA dosage generally favored recovery but did not consistently improve enrichment. Such responses agree with literature describing the influence of temperature, collector adsorption and gangue depression on hydroxamate-based REE flotation (Jordens et al., 2013; Marion et al., 2020).

Table 29: Most relevant tested routes and operating conditions according to the principal metallurgical objectives.

Processing objective	Test code	Route and operating conditions	Mass recovery (%)	Overflow TREO grade (%)	TREO recovery (%)	ER
Most balanced direct-flotation response	C4_F3	Direct flotation; pH 9,0; 75 °C; OHA 90 mg/kg; Na_2SiO_3 500 mg/kg	15,59	2,33	27,05	1,74
Highest TREO recovery	C4_F6	Dry digestion followed by flotation; pH 9,0; 75 °C; OHA 180 mg/kg; Na_2SiO_3 500 mg/kg	20,09	2,33	36,71	1,83
Maximum relative upgrading	C4_ST_R4_C_F13	Hydrogravitic concentrate, dry digestion and flotation; pH 8,0; 80 °C; OHA 198 mg/kg; Na_2SiO_3 500 mg/kg	9,06	3,57	24,60	2,72
High overflow TREO grade	C4_ST_R4_M_F14	Hydrogravitic middlings, dry digestion and flotation; pH 8,5; 80 °C; OHA 189 mg/kg; Na_2SiO_3 500 mg/kg	8,86	4,02	14,69	1,66
High overflow TREO grade	CG_ST_M_F17	Hydrogravitic middlings followed by flotation; pH 9,5; 80 °C; OHA 1000 mg/kg; Na_2SiO_3 250 mg/kg	51,47	2,47	65,50	1,27
Maximum TREO recovery	CG_ST(3)_C_F21	Hydrogravitic concentrate followed by flotation; pH 9,0; 80 °C; OHA 5 556 mg/kg; Na_2SiO_3 1 750 mg/kg	94,14	2,48	90,92	0,97
Maximum overflow TREO grade	CG_F18	Direct flotation; pH 9,5; 80 °C; OHA 1 040 mg/kg; Na_2SiO_3 1 250 mg/kg	37,91	4,46	52,64	1,39

Most balanced direct-flotation response	CG_F22_3A	First-stage Taguchi-based direct flotation; pH 8,0; 80 °C; OHA 500 mg/kg; Na_2SiO_3 1 750 mg/kg	23,58	2,49	45,24	1,92
Highest TREO recovery	CG_F22_8A	First-stage Taguchi-based direct flotation; pH 9,5; 80 °C; OHA 1500 mg/kg	57,77	1,38	59,97	1,04
Most balanced combined-route response	CG_ST_M_F15	Hydrogravitic middlings, dry digestion and flotation; pH 9,0; 80 °C; OHA 219 mg/kg; Na_2SiO_3 500 mg/kg	21,65	4,07	41,27	1,91
Most balanced direct-flotation response	CG_F27_1A	First-stage Taguchi-based direct flotation; pH 8,0; 50 °C; OHA 500 mg/kg;	18,51	2,74	29,74	1,61

The listed conditions in table 29 represent the most relevant responses among the experiments performed. They should not be interpreted as definitive optimum conditions because confirmation tests, replication and scale-up validation were not conducted.

Overall, the experimental results indicate that route performance was controlled by the interaction between feed characteristics, pre-concentration method and flotation conditions.

5

CONCLUSIONS

The present investigation evaluated the applicability of direct flotation and combined physico-chemical beneficiation routes to rare earth element-bearing materials from the Fen Carbonatite Complex. Two ore composites, C4 and CG, were examined through direct flotation, hydrogravitic pre-concentration, magnetic pre-concentration, microwave-assisted digestion and sequential flotation under different reagent and operating conditions.

Feed characterisation demonstrated considerable variability in particle-size distribution, elemental composition and TREO grade. Light rare earth oxides represented the dominant contribution to TREO in all analysed materials. SEM-EDS observations identified monazite and parisite as the principal REE-bearing minerals in the selected areas, associated with barite, fluorapatite, carbonates, silicates and Fe-bearing phases. Differences in feed granulometry and mineral associations contributed to the variable recovery and selectivity observed among the beneficiation routes.

Direct flotation provided the reference response for evaluating the contribution of pre-concentration and pre-treatment. Composite C4 produced moderate TREO recovery and enrichment under direct flotation, with C4_F3 reaching a recovery of 27,05% and an enrichment ratio of 1,74. Composite CG exhibited greater flotation recovery potential. CG_F18 produced a recovery of 52,64%, an overflow TREO grade of 4,46% and an enrichment ratio of 1,39, while CG_F19 produced a substantially higher recovery of 87,17% but no effective enrichment.

Hydrogravitic pre-concentration altered the TREO grade, particle-size distribution and composition of the flotation feeds. For composite CG, hydrogravitic pre-concentration followed by flotation generated the highest TREO recovery obtained during the experimental programme. CG_ST(3)_C_F21 reached a recovery of 90,92%, however, the associated mass recovery was 94,14% and the enrichment ratio was 0,97. Hydrogravitic pre-concentration therefore increased recovery under selected conditions but did not necessarily improve flotation selectivity.

The hydrogravitic middlings fraction showed a more selective response in CG_ST_M_F17, achieving a TREO recovery of 65,50% and an enrichment ratio of 1,27. The differing results between the concentrate and middlings fractions indicate that flotation performance depended not only on the hydrogravitic product type but also on the applied flotation conditions.

Microwave-assisted digestion produced different responses according to digestion method and feed condition. Wet digestion of untreated C4 did not improve flotation performance, since TREO recoveries remained below 8% and enrichment ratios remained close to or below unity. The absence of collector during the corresponding flotation tests may also have contributed to the limited response.

Microwave-assisted dry digestion produced a more favorable response for untreated C4. C4_F6 reached the highest C4 TREO recovery, at 36,71%, with an enrichment ratio of 1,83. The result exceeded the maximum recovery obtained through direct C4 flotation, indicating that dry digestion improved recovery under the applied flotation conditions.

The combination of hydrogravitic pre-concentration, dry digestion and flotation produced the strongest C4 upgrading responses. C4_ST_R4_C_F13 presented an enrichment ratio of 2,72 and a TREO recovery of 24,60%, while C4_ST_R4_M_F14 produced the highest C4 overflow TREO grade, at 4,02%. The combined route was therefore more favourable than direct flotation when selective upgrading was prioritised, although recovery remained lower than the maximum obtained after dry digestion of untreated C4.

For composite CG, hydrogravitic pre-concentration followed by dry digestion generated contrasting results according to the flotation feed fraction. CG_ST_M_F15 produced a TREO recovery of 41,27%, an overflow grade of 4,07% and an enrichment ratio of 1,91, representing one of the strongest recovery–upgrading balances obtained during the investigation. In contrast, the concentrate-derived test CG_ST_C_F16 produced limited recovery and an enrichment ratio below unity. The combined route was effective for the CG middlings fraction but not for the concentrate fraction, showing that its performance depended on the pre-concentrated product treated.

Magnetic pre-concentration followed by flotation produced moderate TREO upgrading of the non-magnetic CG fraction. CG_NMAG_F25 reached an enrichment ratio of 1,16, although TREO recovery remained limited to 19,40%. The substantially coarser particle-size distribution of the non-magnetic feed may have reduced flotation recovery. Because only one magnetic pre-concentration test was performed, the contribution of magnetic separation could not be evaluated independently from particle-size and flotation-condition effects.

The Taguchi-based tests represented structured direct flotation of untreated CG rather than pre-concentration routes. The CG_F22 series investigated the influence of pH, temperature and OHA dosage on flotation performance. Elevated temperature produced the largest difference between the investigated factor-level mean responses, while higher pH and OHA dosage also increased mean recovery. CG_F22_8A, conducted at pH 9,5, 80 °C and 1 500 mg/kg OHA, produced the highest individual recovery within the series, at 59,97%, but its enrichment ratio remained close to unity. CG_F22_3A, conducted at pH 8,0, 80 °C and 500 mg/kg OHA, produced a recovery of 45,24% and an enrichment ratio of 1,92. The comparison confirms that maximum recovery and maximum selective upgrading required different operating conditions.

The CG_F27 series investigated the influence of OHA dosage, depressor type and EDTA addition on flotation performance. Analysis of the factor-level mean responses indicated that the absence of EDTA was associated with the highest mean recovery in both flotation stages, while flotation performance also varied according to collector dosage and depressor selection. CG_F27_1A, conducted using 500 mg/kg OHA, sodium silicate and no EDTA, produced the strongest first-stage response, reaching a TREO recovery of 29,74% and an enrichment ratio of 1,61. As observed in the CG_F22 series, the results demonstrated that flotation performance was sensitive to operating conditions and reagent combinations. However, EDTA dosage was linked to specific OHA dosages and depressor conditions, preventing complete isolation of its individual effect.

The second stages of both the CG_F22 and CG_F27 series treated first-stage overflow products and therefore functioned as cleaning stages. In both series, selected conditions produced additional upgrading, while several conditions generated enrichment ratios below unity. Cleaner flotation also

rejected part of the TREO recovered during the first stage, resulting in substantially lower cumulative recoveries relative to the original feed.

Composite CG generally presented higher TREO recovery and overflow grades than composite C4. However, several high-recovery CG conditions were accompanied by high mass recovery and limited enrichment, indicating simultaneous recovery of REE-bearing particles and gangue. Composite C4 produced lower overall recoveries but stronger relative upgrading under selected combined pre-treatment conditions.

Across the experimental programme, high TREO recovery was frequently associated with high mass recovery and limited selectivity. Conversely, stronger enrichment generally occurred at lower mass recovery and lower overall TREO recovery. Evaluation of beneficiation performance therefore requires combined consideration of mass recovery, overflow TREO grade, TREO recovery and enrichment ratio.

The applicability of combined physico-chemical beneficiation depended on composite type, feed fraction and processing objective. For C4, microwave-assisted dry digestion improved TREO recovery, while hydrogravitic pre-concentration followed by dry digestion produced the strongest relative upgrading. For CG, hydrogravitic pre-concentration alone produced very high but poorly selective recovery, while hydrogravitic pre-concentration followed by dry digestion produced a favourable selective response only for the middlings fraction.

Direct flotation remained competitive for composite CG. CG_F18 produced the highest overflow TREO grade, while CG_F22_3A produced the strongest selective direct-flotation response. Therefore, additional pre-concentration or pre-treatment did not consistently improve CG performance relative to direct flotation.

No single route simultaneously maximised TREO recovery, overflow grade and enrichment ratio. C4_F6 represented the principal recovery-oriented condition for C4, while C4_ST_R4_C_F13 represented the principal upgrading-oriented condition. For CG, CG_ST(3)_C_F21 represented the maximum-recovery condition but presented limited selectivity. CG_F22_3A and CG_ST_M_F15 represented the strongest selective responses obtained through direct and combined beneficiation routes, respectively.

The experimental objectives were achieved through characterisation of the flotation feeds, evaluation of direct flotation, assessment of physical and physico-chemical pre-concentration routes, investigation of operating variables and identification of the principal recovery and selectivity constraints. The results demonstrate that combined beneficiation can improve selected aspects of Fen carbonatite processing, although no combined route was universally superior.

The experimental programme identified promising laboratory-scale recovery-oriented and upgrading-oriented routes but did not establish a definitive optimum beneficiation flowsheet. Complete route recoveries relative to the original untreated feed, confirmation testing, closed-circuit evaluation and scale-up validation remain necessary before industrial route selection. Future work should therefore prioritise confirmation of the most relevant recovery-oriented and upgrading-oriented conditions through replicate testing under improved control of pH, temperature, reagent dosage, air flow and froth collection. Further investigation should include independent evaluation of existing reagents and testing of new collectors, depressants, modifiers and other flotation reagents, together with assessment of EDTA effects, particle-size and liberation optimisation, and development of a rougher–cleaner–scavenger circuit.

REFERENCES

Akyildiz, E., Silva, C. M., Lode, S., Tobiczyk, K., & Kowalczuk, P. B. (2026). Linking mineralogical variability to processing: Strategies for a rare earth carbonatite deposit. *Physicochemical Problems of Mineral Processing, 62*(1), 217430.

Akyildiz, E., Silva, C. M., Tobiczyk, K., Lode, S., Aasly, K., & Kowalczuk, P. B. (2026). Flotation response of parisite, monazite, bastnäsite and synchysite from a carbonatite deposit. *Powder Technology, 471,* 122112.

Al-Ali, S., Wall, F., Fitzpatrick, R., Broom-Fendley, S., Rollinson, G., Brady, A. E., Pickles, J. R., Williams, A., & Dawes, W. (2020). Key process mineralogy parameters for rare earth fluorcarbonate-bearing carbonatite deposits: The example of Songwe Hill, Malawi. *Minerals Engineering, 159,* 106617.

Balaram, V. (2019). Rare earth elements: A review of applications, occurrence, exploration, analysis, recycling, and environmental impact. *Geoscience Frontiers, 10,* 1285–1303.

Bulatovic, S. (2005). *Process for separation of bastnaesite from weathered bastnaesite barite fluorite ores* (U.S. Patent No. 6,874,640 B2). U.S. Patent and Trademark Office.

Bulatovic, S. M. (2010). *Handbook of flotation reagents: Chemistry, theory and practice: Volume 2: Flotation of gold, PGM and oxide ores*. Elsevier.

Chen, P., Ilton, E. S., Wang, Z., Rosso, K. M., & Zhang, X. (2024). Global rare earth element resources: A concise review. *Applied Geochemistry, 175,* 106158.

Cheng, S., Li, W., Han, Y., Sun, Y., Gao, P., & Zhang, X. (2024). Recent process developments in beneficiation and metallurgy of rare earths: A review. *Journal of Rare Earths, 42,* 629–642.

Coint, N., & Dahlgren, S. (2019). *Rare earth elements (REE) in two long drill-cores from the Fen Carbonatite Complex, Telemark, Norway (preliminary version)* (NGU Report No. 2019.008). Geological Survey of Norway.

Dahlgren, S. (2019). *REE mineralization in the Fen Carbonatite Complex, Telemark, Norway: A world-class exploration target for the Hi-Tech and "Green-shift" industry?* (Report from the Geological Advisor No. 1-2019). Buskerud Telemark Vestfold County Councils.

Dushyantha, N., Batapola, N., Ilankoon, I. M. S. K., Rohitha, S., Premasiri, R., Abeysinghe, B., Ratnayake, N., & Dissanayake, K. (2020). The story of rare earth elements (REEs): Occurrences, global distribution, genesis, geology, mineralogy and global production. *Ore Geology Reviews, 122,* 103521.

Everly, D. (2018). *Surface chemistry of novel collectors and their application to froth flotation of rare earth minerals* [Master's thesis, Colorado School of Mines].

Gupta, C. K., & Krishnamurthy, N. (2005). *Extractive metallurgy of rare earths*. CRC Press.

Jha, M. K., Kumari, A., Panda, R., Kumar, J. R., Yoo, K., & Lee, J. Y. (2016). Review on hydrometallurgical recovery of rare earth metals. *Hydrometallurgy, 165,* 2–26.

Jordens, A., Cheng, Y. P., & Waters, K. E. (2013). A review of the beneficiation of rare earth element bearing minerals. *Minerals Engineering, 41,* 97–114.

Leite, M. R. M. (1986). *Fragmentação e classificação de rochas e minérios* [Course manual]. Faculdade de Engenharia da Universidade do Porto.

Liu, C., Xu, L., Deng, J., Tian, J., Wang, D., Xue, K., Zhang, X., Wang, Y., Fang, J., & Liu, J. (2023). A review of flotation reagents for bastnäsite-(Ce) rare earth ore. *Advances in Colloid and Interface Science, 321*, 103029.

Liu, S.-L., Fan, H.-R., Liu, X., Meng, J., Butcher, A. R., Lahaye, Y., Yang, K.-F., & Li, X.-C. (2023). Global rare earth elements projects: New developments and supply chains. *Ore Geology Reviews, 157*, 105428.

Marion, C., Li, R., & Waters, K. E. (2020). A review of reagents applied to rare-earth mineral flotation. *Advances in Colloid and Interface Science, 279*, 102142.

Nkiawete, M. M., & Vander Wal, R. L. (2025). Rare earth elements: Sector allocations and supply chain considerations. *Journal of Rare Earths, 43*, 1–8.

O'Connor, C., Hu, Y., & Han, L. (2026). Review of the recent history and current status of flotation practice in China. *Minerals Engineering, 235*, 109829.

Ragonnaud, G. (2024a, June). *Critical raw materials act* (PE 747.898). European Parliamentary Research Service.

Ragonnaud, G. (2024b, November). *Implementing the EU's Critical Raw Materials Act* (PE 766.253). European Parliamentary Research Service.

Shuai, Z., Zhu, Y., Gao, P., & Han, Y. (2024). Rare earth elements resources and beneficiation: A review. *Minerals Engineering, 218*, 109011.

Szabadvary, F. (1988). The history of the discovery and separation of the rare earths. In K. A. Gschneidner, Jr. & L. Eyring (Eds.), *Handbook on the physics and chemistry of rare earths* (Vol. 11, pp. 33–80). Elsevier.

Weeks, M. E. (1956). *Discovery of the elements* (H. M. Leicester, Ed.; 6th ed.). Journal of Chemical Education.

Wills, B. A., & Napier-Munn, T. (2006). *Wills' mineral processing technology: An introduction to the practical aspects of ore treatment and mineral recovery* (7th ed.). Butterworth-Heinemann.

APPENDICES

A. COMPLETE EXPERIMENTAL CONDITIONS

A.1 OPERATING CONDITIONS FOR C4 DIRECT FLOTATION TESTS

	Conditioning sequence	Time (min)	Reagent	mg/g	pH	Temperature (°C)	RPM	Air flowrate (mL/min)	Products	Sample dry mass (g)	Liquid (mL)	Solids %	Loss (%)
C4_F1	1ºConditioning	6	NaHCO3	52 mg	8,85	35	400		**Feed**	167	520	24,31%	
	2ºConditioning	6	Na_2SiO_3+NaF	6+2 mg	8,878	44	400		**C4_F1_O**	5,8			
	3ºConditioning	6	OHA	5.3 mg	8,66	47,3	400		**C4_F1_U**	156,8			
			MIBC	1 drop					**C4_F1_W**		375	29,48%	3%
	Froth flotation	3			8,48	56	400	1,599					
C4_F2	1ºConditioning	15	NaHCO3	102 mg	8,691	60,4	400		**Feed**	167	520	24,31%	
	2ºConditioning	6	Na_2SiO_3+NaF	2 drops +2,2 mg of NaF	8,313	61,9	400		**C4_F2_O**	1,4			
	3ºConditioning	6	Castor oil	35 mg dissolved in 1 drop of ethanol	9,163	61,9	400		**C4_F2_U**	161,7			
			MIBC	7 drops					**C4_F2_W**		425	27,56%	2%
	Froth flotation	4		3	8,658	73,7	400	2,7					
C4_F3	1ºConditioning	10	NaHCO3	103,6	9,18	69,4	450		**Feed**	167	560	23,0%	
	2ºConditioning	10	Na_2SiO_3	2 drops	9,06	70,2	450		**C4_F3_O**	24,5			
	3ºConditioning	10	OHA	15,1	8,962	69,8	450		**C4_F3_U**	132,7			
			MIBC	4 drops					**C4_F3_W**		400	24,91%	6%
	Froth flotation	10			8,987	68,2	450	5,33					
C4_F4	1ºConditioning	10	Na2CO3	100,4	-	-	450		**Feed**	167	560	23,0%	
	2ºConditioning	10	Na_2SiO_3	2 drops	-	-	450		**C4_F4_O**	4,4			
	3ºConditioning	10	OHA	17,7	-	-	450		**C4_F4_U**	150,4			
			MIBC	4 drops					**C4_F4_W**		400	27,33%	7%
	Froth flotation	10			8,33	68,5	450	5,33					

A.2 OPERATING CONDITIONS FOR C4 HYDROGRAVITIC AND MICROWAVE-ASSISTED ROUTES

	Conditioning sequence	Time (min)	Reagent	mg/g	pH	Eh	Temperature (°C)	RPM	Air flowrate (mL/min)	Products	Sample dry mass (g)	Liquid (mL)	Solids %	Loss (g)	Loss (%)
C4_F5	Microwave (dried ore 2 times- 46,6 minutes)									**Feed**	167	560	23,0%		
	1ºConditioning	10	Na2CO3	104,6	8,923	9,3	74,2	400		**C4_F5_O**	9,6				
	2ºConditioning	10	Na_2SiO_3	2 drops	8,836	8,2	76,6	400		**C4_F5_U**	154,3				
	3ºConditioning	10	OHA	16,3	8,699	17,7	76,9	400		**C4_F5_W**		400	27,84%	3,1	2%
		3	MIBC	4 drops	8,675	22	75	400							
	Froth flotation	10			8,733	7,1	76,8	400	5,33						
C4_F6	Microwave (dried ore- 23,3 minutes, 195ºC)									**Feed**	167	560	23,0%		
	1ºConditioning	10	Na2CO3	110,5	9,244	-110,6	75,2	400		**C4_F6_O**	30,1				
	2ºConditioning	10	Na_2SiO_3	2 drops	9,063	-38	75	400		**C4_F6_U**	119,7				
	3ºConditioning	10	OHA	30	9,007	-36,1	75,6	400		**C4_F6_W**		400	23,03%	17,2	10%
		3	MIBC	4 drops	8,981	-25,5	76,2								
	Froth flotation	10			8,996	-6,4	74,7	400	5,33						
C4_F7	Microwave (pulp- 167g ore + 560 ml H2O)	23,3 minutes	Na2CO3	108,1	8,778	-98,6	75,3	450		**Feed**	167	560	23,0%		
			Na_2SiO_3	2 drops						**C4_F7_O**	11,6				
	Conditioning	10	Phytic acid	14,9	8,519	-82	75,2	450		**C4_F7_U**	149,2				
		3	MIBC	4 drops	8,587	2,7	74			**C4_F7_W**		400	27,17%	6,2	4%
	Froth flotation	10			8,64	1	70,3	450	5,33						
C4_F8	Microwave (pulp- 167g ore + 560 ml H2O)	23,3 minutes	Na2CO3	103,4	9,11	-98,3	74,3	450		**Feed**	167	560	23,0%		
			Na_2SiO_3	2 drops						**C4_F8_O**	10,8				
	Conditioning	10	Quinic acid	16,2	8,918	-113	74,4	450		**C4_F8_U**	130,2				
		3	MIBC	4 drops	8,74	-56,2	75			**C4_F8_W**		400	24,56%	26	16%

	Conditioning sequence	Time (min)	Reagent	mg/g	pH	Eh	Temperature (°C)	RPM	Air flowrate (mL/min)	Products	Sample dry mass (g)	Liquid (mL)	Solids %	Loss (%)
C4_F10	Microwave (dried ore- 22,3 minutes, 195ºC)									**Feed**	167	560	23,0%	
	1ºConditioning	10	Na2CO3	100,8	8,951	-41,2	80,2	400		**C4_F10_O**	4,7			
	2ºConditioning	10	Na_2SiO_3	2 drops (118,8)	8,917	-32,8	80,1	400		**C4_F10_U**	122,2			
	3ºConditioning	10	Phytic acid	31,6	8,79	-11,8	80,4	400		**C4_F10_W**		400	23,40%	
		3	MIBC	4 drops	8,779	-1,6	79,5							
	Froth flotation	10			8,623	-27,3	75,2	400	5,33					24%
C4_F11	Microwave (dried ore- 22,3 minutes, 195ºC)									**Feed**	167	560	23,0%	
	1ºConditioning	10	Na2CO3	102,6	8,849	-63,2	78,9	400		**C4_F11_O**	3,5			
	2ºConditioning	10	Na_2SiO_3	2 drops (118,8)	8,829	-17	79	400		**C4_F11_U**	151,4			
	3ºConditioning	10	Quinic acid	31,9	8,621	-3,6	78,5	400		**C4_F11_W**		400	27,46%	
		3	MIBC	4 drops	8,61	1,3	78,5							
	Froth flotation	10			8,61	18,6	77	400	5,33					7%
C4_ST_R4_C_F13	Microwave (dried ore- 44,6 minutes, 195ºC)									**Feed**	167	560	23,0%	
	1ºConditioning	10	Na2CO3	101,7	8,001	-185,5	79,3	400		**C4_ST_R4_C_F13_O**	13,5			
	2ºConditioning	10	Na_2SiO_3	2 drops (120)	7,946	-126,8	76,2	400		**C4_ST_R4_C_F13_U**	135,5			
	3ºConditioning	10	OHA	33	7,944	-74	77,1	400		**C4_ST_R4_C_F13_W**		360	27,35%	
		3	MIBC	4 drops	7,931	-54,6	80,8							
	Froth flotation	10			7,96	-34,6	80,6	400	5,33					11%
C4_ST_R4_M_F14	Microwave (dried ore- 44,6 minutes, 195ºC)									**Feed**	167	560	23,0%	
	1ºConditioning	10	Na2CO3	102,9	8,726	-37	74,8	400		**C4_ST_R4_M_F14_O**	13,8			
	2ºConditioning	10	Na_2SiO_3	2 drops (120)	8,788	-10,8	74,9	400		**C4_ST_R4_M_F14_U**	141,9			
	3ºConditioning	10	OHA	31,5	8,638	-10,1	76,7	400		**C4_ST_R4_M_F14_W**		360	28,27%	
		3	MIBC	4 drops	8,682	-31,1	78							
	Froth flotation	10			8,531	-1,3	79,6	400	5,33					7%

A.3 OPERATING CONDITIONS FOR CG DIRECT FLOTATION AND HYDROGRAVITIC TESTS

	Conditioning sequence	Time (min)	Reagent	mg/g	pH	Eh	Temperature (°C)	RPM	Air flowrate (mL/min)	Products	Sample dry mass (g)	Liquid (mL)	Solids (%)	Loss (%)
CG_ST_M_F15	Microwave (dried ore- 44,6 minutes, 195ºC)									**Feed**	167	560	23,0%	
	1ºConditioning	10	Na2CO3	111,4	9,095	-76	78,8	400		**CG_ST_M_F15_O**	33,9			
	2ºConditioning	10	Na_2SiO_3	2 drops (120)	8,974	-83,2	78,7	400		**CG_ST_M_F15_U**	122,7			
	3ºConditioning	10	OHA	36,6	8,881	-85,7	80,1	400		**CG_ST_M_F15_W**		315	28,03%	6%
		3	MIBC	4 drops	8,829	-95,4	78,5							
	Froth flotation	10			8,908	-11,9	80,3	400	5,33					
CG_ST_C_F16	Microwave (dried ore- 44,6 minutes, 195ºC)									**Feed**	167	560	23,0%	
	1ºConditioning	10	Na2CO3	104,2	8,29	-274,3	77	400		**CG_ST_C_F16_O**	29,6			
	2ºConditioning	10	Na_2SiO_3	2 drops (120)	8,228	-218	77,1	400		**CG_ST_C_F16_U**	117,3			
	3ºConditioning	10	OHA	34,4	9,231	-360,6	77,2	400		**CG_ST_C_F16_W**		345	25,37%	12%
		3	MIBC	4 drops	-	-	-							
	Froth flotation	10			8,788	-66,2	78,6	400	5,33					
CG_ST_M_F17	1ºConditioning	12	Na2CO3	723,5	9,738	-212,5	80,7	400		**Feed**	180	547,273	24,7%	
	2ºConditioning	12	Na_2SiO_3	299,9	9,611	-197	81	400		**CG_ST_M_F17_O**	73,6			
	3ºConditioning	12	OHA	180,6	9,538	-147,8	82,4	400		**CG_ST_M_F17_U**	69,4			
		3	MIBC	4 drops	9,541	-174,8	81,8			**CG_ST_M_F17_W**		240	22,43%	21%
	Froth flotation	19			9,466	-66,8	78	400	5,33					
CG_F18	1ºConditioning	12	Na2CO3	736,7	9,725	-328,4	81,2	400		**Feed**	180	547,273	24,7%	
	2ºConditioning	12	Na_2SiO_3	5 drops	9,617	-250,1	80,7	400		**CG_F18_O**	59,6			
	3ºConditioning	12	OHA	186,9	9,53	-162,4	80,2	400		**CG_F18_U**	97,6			
		3	MIBC	4 drops	9,589	-154,4	79,8	400		**CG_F18_W**		310	23,95%	13%
	Froth flotation	17			9,566	-81,8	77,2	400	5,33					

	Conditioning sequence	Time (min)	Reagent	mg/g	pH	Eh	Temperature (°C)	RPM	Air flowrate (mL/min)	Products	Sample dry mass (g)	Liquid (mL)	Solids (%)	Loss (%)
CG_F19	1ºConditioning	12	Na2CO3	409,7	9,54	-312,3	81,1	400		**Feed**	180	547,273	24,7%	
	2ºConditioning	12	Na_2SiO_3	7 drops	9,471	-449,3	80,4	400		**CG_F19_O**	151,7			
	3ºConditioning	12	OHA	1,0105 g	8,709	-94,4	81,4	400		**CG_F19_U**	15,2			
		3	MIBC	4 drops	9,495	-128,3	80,2	400		**CG_F19_W**		180	7,79%	7%
	Froth flotation	12			8,921	-75,4	80,5	400	5,33					
CG_ST(3)_M_F20	1ºConditioning	12	Na2CO3	406,2	9,404	-193,2	81,5	400		**Feed**	180	547,273	24,7%	
	2ºConditioning	12	Na_2SiO_3	7 drops	9,445	-116,4	81,9	400		**CG_ST(3)_M_F20_O**	126,7			
	3ºConditioning	12	OHA	1,008 g	8,762	-102,7	80,9	400		**CG_ST(3)_M_F20_U**	19,8			
		3	MIBC	4 drops	8,761	-100,7	81,2	400		**CG_ST(3)_M_F20_W**		140	12,39%	19%
	Froth flotation	12			8,894	-62,6	82,7	400	5,33					
CG_ST(3)_C_F21	1ºConditioning	12	Na2CO3	410,8	9,602	-472,1	79,4	400		**Feed**	180	547,273	24,7%	
	2ºConditioning	12	Na_2SiO_3	7 drops	9,43	-244,4	80,3	400		**CG_ST(3)_C_F21_O**	131,8			
	3ºConditioning	12	OHA	1,0023 g	8,721	-152,2	79,8	400		**CG_ST(3)_C_F21_U**	8,2			
		3	MIBC	4 drops	8,807	-119,2	79,3	400		**CG_ST(3)_C_F21_W**		330	2,42%	22%
	Froth flotation	11			8,813	-205	77,6	400	5,33					
CG_ST(3)_M_F23	1ºConditioning	12	Na_2SiO_3	7 drops	8,538	55,4	54,5	400		**Feed**	178,9	547,273	24,6%	
	2ºConditioning	12	OHA	90,2 mg + 1,5 ml etanol 96%	8,09	91	51,6	400		**CG_ST(3)_M_F23_O**	24,7			
		3	MIBC	5 drops				400		**CG_ST(3)_M_F23_U**	126,2			
	Froth flotation	6			8,218	104,9	49	400	5,33	**CG_ST(3)_M_F23_W**		361	25,9%	16%
CG_ST(3)_C_F24	1ºConditioning	12	Na_2SiO_3	7 drops	8,628	104,4	54,5	400		**Feed**	180	547,273	24,7%	
	2ºConditioning	12	OHA	92,4 mg + 1,5 ml etanol 96%	8,448	99,4	51,6	400		**CG_ST(3)_C_F24_O**	33,5			
		3	MIBC	4 drops	8,131	124,1		400		**CG_ST(3)_C_F24_U**	143,8			
	Froth flotation	6			8,234	130,1	49	400	5,33	**CG_ST(3)_C_F24_W**		415	25,7%	1%

A.4 OPERATING CONDITIONS FOR THE CG_F22 TAGUCHI SERIES

	Conditioning sequence	Time (min)	Reagent	mg/g	pH	Eh	Temperature (°C)	RPM	Air flowrate (mL/min)	Products	Sample dry mass (g)	Liquid (mL)	Solids (%)	Loss (%)
CG_F22_1A	1ºConditioning	12	Na_2SiO_3	7 drops	8,76	-	51,6	400		**Feed**	181	547,273	24,9%	
	2ºConditioning	12	OHA	90,1 + 1,5 ml etanol 96%	8,587	-	51,3	400		**CG_F22_1_O**	19,8			
		3	MIBC	4 drops	8,08	-	50,5	400		**CG_F22_1_U**	152,7			
										CG_F22_1_W		390	28,14%	5%
	Froth flotation	6			8,137	-1,5	50,7	400	5,33					
CG_F22_2A	1ºConditioning	12	Na2CO3	204,1	9,399	-116	50,8	400		**Feed**	180	547,273	24,7%	
	2ºConditioning	12	Na_2SiO_3	7 drops	9,553	-63,2	50	400		**CG_F22_2_O**	54,7			
	3ºConditioning	12	OHA	90,1 + 1,5 ml etanol 96%	9,533	-19,1	50,1	400		**CG_F22_2_U**	120			
		3	MIBC	4 drops	-	-12,3	-	400		**CG_F22_2_W**		310	27,91%	3%
	Froth flotation	6			9,478	35,5	49,2	400	5,33					
CG_F22_3A	1ºConditioning	12	Na_2SiO_3	7 drops	8,32	21,3	77,4	400		**Feed**	180	547,273	24,7%	
	2ºConditioning	12	OHA	90,1 + 1,5 ml etanol 96%	8,115	30,8	80	400		**CG_F22_3_O**	31,6			
		3	MIBC	4 drops	8,013	49,2	79,9	400		**CG_F22_3_U**	102,4			
	Froth flotation	6			8,148	39,2	85,4	400	5,33	**CG_F22_3_W**		375	21,4%	26%
CG_F22_4A	1ºConditioning	12	Na2CO3	204,6	8,746	7,4	82,2	400		**Feed**	180	547,273	24,7%	
	2ºConditioning	12	Na_2SiO_3	7 drops	9,266	-26,7	81,7	400		**CG_F22_4_O**	39,6			
	3ºConditioning	12	OHA	90 + 1,5 ml etanol 96%	9,399	-33,4	81,5	400		**CG_F22_4_U**	93,4			
		3	MIBC	4 drops	9,344	-26	81,1	400		**CG_F22_4_W**		355	20,8%	26%
	Froth flotation	6			9,38	-14,8	81,3	400	5,33					
CG_F22_1AR	1ºConditioning	12	Na_2SiO_3	7 drops	8,905	154,4	52,8	400		**Feed**	180	547,273	24,7%	
	2ºConditioning	12	OHA	90,2 + 1,5 ml etanol 96%	8,313	171,3	51,5	400		**CG_F22_1R_O**	11,8			
		3	MIBC	4 drops	8,334	160	51,6			**CG_F22_1R_U**	116,4			
	Froth flotation	6			8,291	146	50,9	400	5,33	**CG_F22_1R_W**		420	21,7%	29%

	Conditioning sequence	Time (min)	Reagent	mg/g	pH	Eh	Temperature (°C)	RPM	Air flowrate (mL/min)	Products	Sample dry mass (g)	Liquid (mL)	Solids (%)	Loss (%)
CG_F22_5A	1ºConditioning	12	Na_2SiO_3	7 drops	8,605	122,5	53,3	400		**Feed**	180	547,273	24,7%	
	2ºConditioning	12	OHA	270,8 + 2 ml etanol 96%	8,234	118,4	50,9	400		**CG_F22_5_O**	39,3			
		3	MIBC	4 drops	8,066	122,6	49,8	400		**CG_F22_5_U**	137,2			
	Froth flotation	6			8,143	118,8	49	400	5,33	**CG_F22_5_W**		340	28,8%	2%
CG_F22_6A	1ºConditioning	12	Na2CO3	600	9,963	-141,6	52,5	400		**Feed**	180	547,273	24,7%	
	2ºConditioning	12	Na_2SiO_3	7 drops	9,524	-6,7	52,6	400		**CG_F22_6_O**	56,2			
	3ºConditioning	12	OHA	298 + 2 ml etanol 96%	9,292	33,7	52,6	400		**CG_F22_6_U**	106,2			
		3	MIBC	4 drops	9,446	28,1	52,5	400		**CG_F22_6_W**		349	23,3%	10%
	Froth flotation	6			9,435	31,8	52,2	400	5,33					
CG_F22_7A	1ºConditioning	12	Na_2SiO_3	7 drops	8,27	54,1	78,6	400		**Feed**	180	547,273	24,7%	
	2ºConditioning	12	OHA	270,3 + 2 ml etanol 96%	8,022	59,7	76,1	400		**CG_F22_7_O**	77,6			
		3	MIBC	4 drops	8,042	55,2	77,3	400		**CG_F22_7_U**	90,9			
	Froth flotation	6			8,118	48,9	80,1	400	5,33	**CG_F22_7_W**		355	20,4%	6%
CG_F22_8A	1ºConditioning	12	Na2CO3	599,7	9,637	-180	81,1	400		**Feed**	180	547,273	24,7%	
	2ºConditioning	12	Na_2SiO_3	7 drops	9,529	-93	80,5	400		**CG_F22_8_O**	82,2			
	3ºConditioning	12	OHA	270,3 + 2 ml etanol 96%	9,362	-66,4	80,2	400		**CG_F22_8_U**	60,1			
		3	MIBC	4 drops	9,512	-79,3	79,9	400		**CG_F22_8_W**		316	16,0%	21%
	Froth flotation	6			9,463	-41,4	81,6	400	5,33					

	Conditioning sequence	Time (min)	Reagent	mg/g	pH	Eh	Temperature (°C)	RPM	Air flowrate (mL/min)	Products	Sample dry mass (g)	Liquid (mL)	Solids (%)	Loss (%)
CG_F22_1B	1ºConditioning	6	Na_2SiO_3	7 drops	8,88	78	52,2	400		**Feed**	116,76	355	24,7%	
	2ºConditioning	6	OHA	59 mg + 1,5 ml etanol 96%	8,1	83,3	50,5	400		**CG_F22_1B_O**	20,4			
		3	MIBC	4 drops	8,115	84,6	50,2	400		**CG_F22_1B_U**	96,1			
	Froth flotation	6			8,24	100,2	46,3	400	5,33	**CG_F22_1B_W**		200	32,5%	0%
CG_F22_2B	1ºConditioning	6	Na_2SiO_3	7 drops	9,464	64,3	30,9	400		**Feed**	101,96	328	23,7%	
	2ºConditioning	6	OHA	51,1 mg + 1,5 ml etanol 96%	9,361	63	24,8	400		**CG_F22_2B_O**	46,4			
		3	MIBC	4 drops	9,376	61,7	25,2	400		**CG_F22_2B_U**	53,3			
	Froth flotation	6			9,402	57,9	41,3	400	5,33	**CG_F22_2B_W**		185	22,4%	2%
CG_F22_3B	1ºConditioning	6	Na_2SiO_3	7 drops	8,691	30,2	79	400		**Feed**	100	328	23,4%	
	2ºConditioning	6	OHA	52,8 mg + 1,5 ml etanol 96%	8,058	42,5	78,6	400		**CG_F22_3B_O**	35			
		3	MIBC	4 drops	8,078	44,6	76,9	400		**CG_F22_3B_U**	62,8			
	Froth flotation	6			8,179	60,6	72,4	400	5,33	**CG_F22_3B_W**		218	22,4%	2%
CG_F22_4B	1ºConditioning	6	Na_2SiO_3	7 drops	9,348	-102,9	77,8	400		**Feed**	87,16	265	24,8%	
	2ºConditioning	6	OHA	43,7 mg + 1,5 ml etanol 96%	9,418	-56,5	79	400		**CG_F22_4B_O**	9,7			
		3	MIBC	4 drops	9,404	-42,9	79	400		**CG_F22_4B_U**	75,1			
	Froth flotation	6			9,408	-2,7	76,5	400	5,33	**CG_F22_4B_W**		144	34,3%	3%
CG_F22_5B	1ºConditioning	6	Na_2SiO_3	7 drops	9,075	52,5	54,2	400		**Feed**	107	320	25,1%	
	2ºConditioning	6	OHA	160,3 mg+1 ml etanol 96%	8,017	69	52,7	400		**CG_F22_5B_O**	30,8			
		3	MIBC	4 drops	8,047	74,7	52,1	400		**CG_F22_5B_U**	74,2			
	Froth flotation	6			8,139	115,15	49,5	400	5,33	**CG_F22_5B_W**		195	27,6%	2%
CG_F22_6B	1ºConditioning	6	Na_2SiO_3	7 drops	9,588	16,1	49,5	400		**Feed**	103,3	310	25,0%	
	2ºConditioning	6	OHA	154,9 mg + 1 ml etanol 96%	9,302	0,7	50,5	400		**CG_F22_6B_O**	47,4			

		3	MIBC	4 drops	9,332	0,8	50,8	400		**CG_F22_6B_U**	52,9			
	Froth flotation	6			9,321	10,2	49,1	400	5,33	**CG_F22_6B_W**		175	23,2%	3%

A.5 OPERATING CONDITIONS FOR MAGNETIC PRE-CONCENTRATION AND SEQUENTIAL FLOTATION TESTS

	Conditioning sequence	**Time (min)**	**Reagent**	**mg/g**	**pH**	**Eh**	**Temperature (°C)**	**RPM**	**Air flowrate (mL/min)**	**Products**	**Sample dry mass (g)**	**Liquid (mL)**	**Solids (%)**	**Loss (%)**
C4_F9A	Microwave (pulp- 167g ore + 560 ml H2O)	37	Na_2SiO_3 (4 drops)	238 mg	10,25	-344,1	74,5	400		**Feed**	167	560	23,0%	
			BaCl2.2H2O	36,2 mg				400		**C4_F9A_O**	1,6			
		3	MIBC	5 drop	10,06	-277	75,4			**C4_F9A_U**				
	Froth flotation	10			9,948	-81,5	72,7	400	4,797					
C4_F9B	C4_F9A_Underflow + 89 ml H2O				9,908	-245,3	70,6	400		**Feed**	165,4	560	22,8%	
	Conditioning	10	OHA	32 mg	9,637	-236,3	75,4	400		**C4_F9B_O**	23,2			
		3	MIBC	2 drop	9,574	-237,1	75,7			**C4_F9B_U**	120,2			
	Froth flotation	10			9,556	-40,8	71,9	400	4,797	**C4_F9B_W**		400	23,11%	13%
C4_F12A	1ºConditioning	10	Na_2SiO_3	4 drops	8,934	-53,2	79,6	400		**Feed**	167	560	23,0%	
	2ºConditioning	10	BaCl2	42,1 mg	8,826	-29,1	79,8	400		**C4_F12A_O**	3,2			
		3	MIBC	4 drops	8,767	-16,6	79,6	400		**C4_F12A_U**	138,5			
	Froth flotation	10			8,709	1,7	79,3	400	5,33	**C4_F12A_W**		400	25,72%	15%
C4_F12B	1ºConditioning	10	OHA	32,2 mg	8,977	-70,2	78,6	400		**Feed**	138,5	588,5	19,1%	
		3	MIBC	2 drops	8,901	-67,4	78,5	400		**C4_F12B_O**	19,2			
	Froth flotation	10			8,754	5,1	79,4	400	5,33	**C4_F12B_U**	103			
										C4_F12B_W		364	22,06%	12%
CG_NMAG_F25	1ºConditioning	12	Na_2SiO_3	7 drops	8,503	84,4	52,2	400		**Feed**	180	547,273	24,7%	
	2ºConditioning	12	OHA	90,7 + 1,5 ml etanol 96%	8,05	44,9	50,2	400		**CG_NMAG_F25_O**	29,9			

		3	MIBC	4 drops	8,063	77,4	51,4	400		**CG_NMAG_F25_U**	149			
										CG_NMAG_F25_W		435	25,5%	1%
	Froth flotation	6			8,127	81,1	52,7	400	5,33					
CG_F26A	1ºConditioning	6	Na2CO3	103,1 mg	8,982	104,5	55,3	400		**Feed**	181,9	547,273	24,9%	
	2ºConditioning	6	Na_2SiO_3	4 drops	9,44	82,3	53,6	400		**CG_F26A_O**	0,8			
	3ºConditioning	6	BaCl2	92,1 + 1,5 ml etanol 96%	9,419	81,5	51,9	400		**CG_F26A_U**	181			
		3	MIBC	4 drops	9,436	73,8	50,9	400		**CG_F26A_W**		391	31,6%	0%
	Froth flotation	6			9,399	68,7	48,2	400	5,33					
CG_F26B	1ºConditioning	6	EDTA	90 mg	9,43	124	54,4	400		**Feed**	181	547,273	24,9%	
	2ºConditioning	6	OHA	90,1 + 1,5 ml etanol 96%	8,389	119,2	53,8	400		**CG_F26B_O**	11,8			
		3	MIBC	4 drops	8,422	113,7	52,4	400		**CG_F26B_U**	169,7			
	Froth flotation	6			8,525	74,3	50,9	400	5,33	**CG_F26B_W**		400	29,8%	0%

A.6 OPERATING CONDITIONS FOR THE CG_F27 TAGUCHI SERIES

	Conditioning sequence	Time (min)	Reagent	mg/g	pH	Eh	Temperature (°C)	RPM	Air flowrate (mL/min)	Products	Sample dry mass (g)	Liquid (mL)	Solids (%)	Loss (%)
CG_F27_1A_T	1ºConditioning	6	Na_2SiO_3	2 drops	8,982	104,5	55,3	400		**Feed**	180	547,273	24,70%	
	2ºConditioning	6	OHA	90+1,5ml etanol 96%	9,44	82,3	53,6	400		**CG_F27_1A_T _O**	10,6			
		3	MIBC	3 drops	9,436	73,8	50,9	400		**CG_F27_1A_T _U**	167,8			
	Froth flotation	6			9,399	68,7	48,2	400	5,33	**CG_F27_1A_T _W**		410	29,00%	1%
CG_F27_1A	1ºConditioning	6	Na_2SiO_3	2 drops	8,982	104,5	55,3	400		**Feed**	180	547,273	24,70%	
	2ºConditioning	6	OHA	90+1,5ml etanol 96%						**CG_F27_1A_O**	33			
		3	MIBC	3 drops	9,436	73,8	50,9	400		**CG_F27_1A_U**	145,3			
	Froth flotation	6			9,399	68,7	48,2	400	5,33	**CG_F27_1A_W**		390	27,10%	1%
CG_F27_2A	1ºConditioning	6	Na_2SiO_3	2 drops	8,982	104,5	55,3	400		**Feed**	180	547,273	24,70%	
	2ºConditioning	6	OHA	90+1,5ml etanol 96%	9,44	82,3	53,6	400		**CG_F27_2A_O**	18,2			
	3ºConditioning	6	EDTA	90 mg	9,419	81,5	51,9	400		**CG_F27_2A_U**	160,2			
		3	MIBC	3 drops	9,436	73,8	50,9	400		**CG_F27_2A_W**		360	30,80%	1%
	Froth flotation	6			9,399	68,7	48,2	400	5,33					
CG_F27_3A	1ºConditioning	6	Quinic acid	90 mg	8,982	104,5	55,3	400		**Feed**	180	547,273	24,70%	
	2ºConditioning	6	OHA	90+1,5ml etanol 96%	9,44	82,3	53,6	400		**CG_F27_3A_O**	23,6			
		3	MIBC	3 drops	9,436	73,8	50,9	400		**CG_F27_3A_U**	154,8			
	Froth flotation	6			9,399	68,7	48,2	400	5,33	**CG_F27_3A_W**		355	30,40%	1%
CG_F27_4A	1ºConditioning	6	Quinic acid	90 mg	8,982	104,5	55,3	400		**Feed**	180	547,273	24,70%	
	2ºConditioning	6	EDTA	90 mg	9,44	82,3	53,6	400		**CG_F27_4A_O**	15,6			
	3ºConditioning	6	OHA	90+1,5ml etanol 96%	9,419	81,5	51,9	400		**CG_F27_4A_U**	159,8			
		3	MIBC	3 drops	9,436	73,8	50,9	400		**CG_F27_4A_W**		360	30,70%	3%
	Froth flotation	6			9,399	68,7	48,2	400	5,33					

	Conditioning sequence	Time (min)	Reagent	mg/g	pH	Eh	Temperature (°C)	RPM	Air flowrate (mL/min)	Products	Sample dry mass (g)	Liquid (mL)	Solids (%)	Loss (%)
CG_F27_5A	1ºConditioning	6	Na_2SiO_3	2 drops	8,982	104,5	55,3	400		**Feed**	180	547,273	24,70%	
	2ºConditioning	6	OHA	36 + 1,5 ml etanol 96%	9,419	81,5	51,9	400		**CG_F27_5A_O**	13,7			
		3	MIBC	3 drops	9,436	73,8	50,9	400		**CG_F27_5A_U**	165,3			
	Froth flotation	6			9,399	68,7	48,2	400	5,33	**CG_F27_5A_W**		350	32,10%	1%
CG_F27_6A	1ºConditioning	6	Na_2SiO_3	2 drops	8,982	104,5	55,3	400		**Feed**	180	547,273	24,70%	
	2ºConditioning	6	EDTA	36	9,44	82,3	53,6	400		**CG_F27_6A_O**	13,9			
	3ºConditioning	6	OHA	36 + 0,6 ml etanol 96%	9,419	81,5	51,9	400		**CG_F27_6A_U**	164,5			
		3	MIBC	3 drops	9,436	73,8	50,9	400		**CG_F27_6A_W**		335	32,90%	1%
	Froth flotation	6			9,399	68,7	48,2	400	5,33					
CG_F27_7A	1ºConditioning	6	Quinic acid	90	8,982	104,5	55,3	400		**Feed**	180	547,273	24,70%	
	2ºConditioning	6	OHA	36+0,6 ml etanol 96%	9,44	82,3	53,6	400		**CG_F27_7A_O**	15,8			
		3	MIBC	3 drops	9,436	73,8	50,9	400		**CG_F27_7A_U**	163,2			
	Froth flotation	6			9,399	68,7	48,2	400	5,33	**CG_F27_7A_W**		385	29,80%	1%
CG_F27_8A	1ºConditioning	6	Quinic acid	90	8,982	104,5	55,3	400		**Feed**	180	547,273	24,70%	
	2ºConditioning	6	EDTA	36	9,44	82,3	53,6	400		**CG_F27_8A_O**	15,6			
	3ºConditioning	6	OHA	36+0,6 ml etanol 96%	9,419	81,5	51,9	400		**CG_F27_8A_U**	163,1			
		3	MIBC	3 drops	9,436	73,8	50,9	400		**CG_F27_8A_W**		360	31,20%	1%
	Froth flotation	6			9,399	68,7	48,2	400	5,33					
CG_F27_2AR	1ºConditioning	6	Na_2SiO_3	2 drops	8,982	104,5	55,3	400		**Feed**	180	547,273	24,70%	
	2ºConditioning	6	EDTA	90	9,44	82,3	53,6	400		**CG_F27_2AR_O**	16,3			
	3ºConditioning	6	OHA	90+1,5 ml etanol 96%	9,419	81,5	51,9	400		**CG_F27_2AR_U**	167,3			
		3	MIBC	3 drops	9,436	73,8	50,9	400		**CG_F27_2AR_W**		332	33,50%	-2%
	Froth flotation	6			9,399	68,7	48,2	400	5,33					

	Conditioning sequence	Time (min)	Reagent	mg/g	pH	Eh	Temperature (°C)	RPM	Air flowrate (mL/min)	Products	Sample dry mass (g)	Liquid (mL)	Solids (%)	Loss (%)
CG_F27_8AR	1ºConditioning	6	Quinic acid	90	8,982	104,5	55,3	400		**Feed**	180	547,273	24,70%	
	2ºConditioning	6	EDTA	36	9,44	82,3	53,6	400		**CG_F27_8AR_O**	20,4			
	3ºConditioning	6	OHA	36+0,6ml etanol 96%	9,419	81,5	51,9	400		**CG_F27_8AR_U**	158			
		3	MIBC	3 drops	9,436	73,8	50,9	400		**CG_F27_8AR_W**		405	28,10%	1%
	Froth flotation	6			9,399	68,7	48,2	400	5,33					
CG_F27_1B	1ºConditioning	6	Na_2SiO_3	1 drops	8,982	104,5	55,3	400		**Feed**	100	547,273	15,40%	
	2ºConditioning	6	OHA	50+0,8ml etanol 96%	9,419	81,5	51,9	400		**CG_F27_1B_O**	18			
		3	MIBC	3 drops	9,436	73,8	50,9	400		**CG_F27_1B_U**	80,8			
	Froth flotation	6			9,399	68,7	48,2	400	5,33	**CG_F27_1B_W**		435	15,70%	1%
CG_F27_2B	1ºConditioning	6	Na_2SiO_3	1 drops	8,982	104,5	55,3	400		**Feed**	100	547,273	15,40%	
	2ºConditioning	6	EDTA	50	9,44	82,3	53,6	400		**CG_F27_2B_O**	8,5			
	3ºConditioning	6	OHA	50+0,8ml etanol 96%	9,419	81,5	51,9	400		**CG_F27_2B_U**	88			
		3	MIBC	3 drops	9,436	73,8	50,9	400		**CG_F27_2B_W**		420	17,30%	4%
	Froth flotation	6			9,399	68,7	48,2	400	5,33					
CG_F27_3B	1ºConditioning	6	Quinic acid	25+1,5ml etanol 96%	8,982	104,5	55,3	400		**Feed**	100	547,273	15,40%	
	2ºConditioning	6	OHA	50+0,8ml etanol 96%	9,44	82,3	53,6	400		**CG_F27_3B_O**	18,1			
		3	MIBC	3 drops	9,436	73,8	50,9	400		**CG_F27_3B_U**	80,2			
	Froth flotation	6			9,399	68,7	48,2	400	5,33	**CG_F27_3B_W**		420	16,00%	2%
CG_F27_4B	1ºConditioning	6	Quinic acid	25+1,5ml etanol 96%	8,982	104,5	55,3	400		**Feed**	100	547,273	15,40%	
	2ºConditioning	6	EDTA	50	9,44	82,3	53,6	400		**CG_F27_4B_O**	13,2			
	3ºConditioning	6	OHA	50+0,8ml etanol 96%	9,419	81,5	51,9	400		**CG_F27_4B_U**	85,7			
		3	MIBC	3 drops	9,436	73,8	50,9	400		**CG_F27_4B_W**		445	16,10%	1%
	Froth flotation	6			9,399	68,7	48,2	400	5,33					

	Conditioning sequence	Time (min)	Reagent	mg/g	pH	Eh	Temperature (°C)	RPM	Air flowrate (mL/min)	Products	Sample dry mass (g)	Liquid (mL)	Solids (%)	Loss (%)
CG_F27_5B	1ºConditioning	6	Na_2SiO_3	1 drops	8,982	104,5	55,3	400		**Feed**	100	547,273	15,40%	
	2ºConditioning	6	OHA	20+0,3ml etanol 96%	9,419	81,5	51,9	400		**CG_F27_5B_O**	16			
		3	MIBC	3 drops	9,436	73,8	50,9	400		**CG_F27_5B_U**	82,8			
	Froth flotation	6			9,399	68,7	48,2	400	5,33	**CG_F27_5B_W**		432	16,10%	1%
CG_F27_6B	1ºConditioning	6	Na_2SiO_3	1 drops	8,982	104,5	55,3	400		**Feed**	100	547,273	15,40%	
	2ºConditioning	6	EDTA	20	9,44	82,3	53,6	400		**CG_F27_6B_O**	7,7			
	3ºConditioning	6	OHA	20+0,3ml etanol 96%	9,419	81,5	51,9	400		**CG_F27_6B_U**	90,8			
		3	MIBC	3 drops	9,436	73,8	50,9	400		**CG_F27_6B_W**		432	17,40%	2%
	Froth flotation	6			9,399	68,7	48,2	400	5,33					
CG_F27_7B	1ºConditioning	6	Quinic acid	25+1,5ml etanol 96%	7,971	85,1	51,4	400		**Feed**	100	547,273	15,40%	
	2ºConditioning	6	OHA	20+0,3ml etanol 96%	8,022	85,6	50,5	400		**CG_F27_7B_O**	12,7			
		3	MIBC	3 drops	8,041	87,7	50,1	400		**CG_F27_7B_U**	86,4			
	Froth flotation	6			8,13	86,3	49,7	400	5,33	**CG_F27_7B_W**		391	18,10%	1%
CG_F27_8B	1ºConditioning	6	Quinic acid	25+1,5ml etanol 96%	7,938	99,9	51,3	400		**Feed**	100	547,273	15,40%	
	2ºConditioning	6	EDTA	20	7,767	103,2	50,7	400		**CG_F27_8B_O**	13,4			
	3ºConditioning	6	OHA	20+0,3ml etanol 96%	7,976	98,5	50,7	400		**CG_F27_8B_U**	85,5			
		3	MIBC	3 drops	7,982	99,7	50,8	400		**CG_F27_8B_W**		470	15,40%	1%
	Froth flotation	6			8,122	45,5	49	400	5,33					

B. XRF RESULTS FOR ANALYSED FLOTATION PRODUCTS

B.1 XRF RESULTS FOR C4 DIRECT FLOTATION TESTS

	Ca	Ti	V	Cr	Mn	Fe	Sr	Ba	Th
	ppm								
C4_F1_O	176583	14677	3940	885	12011	60864	2854	15475	230
C4_F1_U	152818	7437	2179	663	11468	69351	2942	11513	185
C4_F2_O	189621	10662	2764	817	12868	71804	3087	8062	194
C4_F2_U	184064	9587	2579	729	12092	70766	2808	11710	183
C4_F3_O	112492	13000	3861	823	7471	34083	1471	6337	161
C4_F3_U	155760	5787	1795	628	11976	72536	3109	10103	172
C4_F4_O	182619	21619	6023	1198	12274	59629	2794	26071	266
C4_F4_U	44973	2236	702	254	3839	23062	926	3183	63

B.2 XRF RESULTS FOR C4 HYDROGRAVITIC PRE-CONCENTRATION AND MICROWAVE-ASSISTED ROUTE

	Ca	Ti	V	Cr	Mn	Fe	Sr	Ba	Th
	ppm								
C4_F5_O	140914	17753	5037	1188	10247	47392	2445	24542	308
C4_F5_U	155760	5787	1795	628	11976	72536	3109	10103	172
C4_F6_O	187050	21586	6178	1515	12394	59574	2876	28775	335
C4_F6_U	103632	3387	1103	402	9189	58207	2576	6905	138
C4_F7_O	198043	17987	4746	908	13565	72911	3251	22954	213
C4_F7_U	101040	4796	1503	492	8814	54319	2500	8483	156
C4_F8_O	190663	21803	5857	983	13184	67192	3055	32082	229
C4_F8_U	151838	6485	1981	650	11366	67709	2938	10365	177
C4_F10_O	215375	13106	3314	765	14319	81996	3571	17095	216
C4_F10_U	158164	7743	2156	729	11552	69697	2985	10745	192
C4_F11_O	205044	16746	4426	875	14033	76023	3383	22928	210
C4_F11_U	192358	9416	2736	778	13470	79221	3455	12835	206
C4_ST_R4_C_F13_O	178064	13744	4544	1571	12020	114763	2666	15588	352
C4_ST_R4_C_F13_U	178554	10977	3786	1421	12746	112665	3025	14129	348
C4_ST_R4_M_F14_O	205126	14940	3962	1117	13909	66832	3349	19795	263
C4_ST_R4_M_F14_U	204634	7285	1982	603	14067	73781	3570	10894	152

B.3 XRF RESULTS FOR CG DIRECT FLOTATION AND HYDROGRAVITIC PRE-CONCENTRATION TESTS

	Ca	Ti	V	Cr	Mn	Fe	Sr	Ba	Th
	ppm								
CG_ST_M_F15_O	204370	16004	4239	1571	14024	64715	3444	21466	278
CG_ST_M_F15_U	213743	5117	1185	412	15248	83948	4009	7783	146
CG_ST_C_F16_O	170081	18059	5228	1508	11393	92665	2647	21843	348
CG_ST_C_F16_U	177613	7445	2020	773	12840	165745	3276	8593	256
CG_ST_M_F17_O	211505	9636	2247	644	14294	76677	3451	12300	184
CG_ST_M_F17_U	205505	5506	1185	389	14607	75660	3807	8190	137

	Ca	Ti	V	Cr	Mn	Fe	Sr	Ba	Th
	ppm								
CG_F18_O	213991	13443	3726	936	15066	79463	3658	21841	262
CG_F18_U	202621	6824	1539	523	14750	110305	3732	10158	207
CG_F19_O	194014	8968	2218	634	14044	87461	3522	13807	213
CG_F19_U	164650	8444	2089	600	10627	90459	2401	8421	217
CG_ST(3)_M_F20_O	200438	8535	2127	655	14631	74391	3562	12619	218
CG_ST(3)_M_F20_U	220541	10210	2649	830	15496	79795	3795	15174	253
CG_ST(3)_C_F21_O	195505	5752	1750	641	13967	104556	3580	7921	227
CG_ST(3)_C_F21_U	185711	9538	2672	978	12711	134318	3010	9274	312
CG_ST(3)_M_F23_O	176731	9977	2698	557	13010	59227	3238	17629	208
CG_ST(3)_M_F23_U	147140	5439	1536	507	11283	60053	2835	8711	175
CG_ST(3)_C_F24_O	166244	9768	3427	1198	12055	62076	3050	12364	279
CG_ST(3)_C_F24_U	150135	3661	1084	451	11900	102182	3132	4910	188

B.4 XRF RESULTS FOR THE CG_F22 TAGUCHI SERIES

	Ca	Ti	V	Cr	Mn	Fe	Sr	Ba	Th
	ppm								
CG_F22_1A_O	99639	7775	2343	607	8709	42586	2219	14431	194
CG_F22_1A_U	159922	5668	1591	521	12388	82861	3152	9005	187
CG_F22_2A_O	122155	7203	2089	536	10417	52761	2719	15304	192
CG_F22_2A_U	67323	2670	789	296	6990	53539	1968	5084	129
CG_F22_3A_O	169483	11113	3130	804	12176	58828	3039	18471	244
CG_F22_3A_U	60043	2614	791	283	6641	46439	1827	5371	119
CG_F22_4A_O	103984	7030	2178	581	9144	44823	2481	15475	189
CG_F22_4A_U	158369	5126	1335	446	12235	89928	3138	8362	184
CG_F22_5A_O	221571	12482	3080	814	15737	82873	3881	20627	244
CG_F22_5A_U	95044	4583	1288	434	8760	61607	2372	9424	159
CG_F22_6A_O	109769	5585	1691	526	9833	53507	2718	12482	180
CG_F22_6A_U	157273	7088	1745	520	12187	87385	3129	11467	192
CG_F22_7A_O	175629	8970	2337	618	13100	70200	3360	15561	196
CG_F22_7A_U	154704	7905	1977	544	12041	83898	3015	12736	211
CG_F22_8A_O	183362	8466	2229	601	13518	70970	3414	14369	205
CG_F22_8A_U	145194	7111	1776	522	11391	92136	2898	11943	206

	Ca	Ti	V	Cr	Mn	Fe	Sr	Ba	Th
	ppm								
CG_F22_1B_O	181118	7233	1889	581	13719	72873	3464	11966	186
CG_F22_1B_U	147136	4023	1122	497	11767	114310	3084	5616	194
CG_F22_2B_O	157022	9508	2543	635	11490	56166	2712	14765	196
CG_F22_2B_U	159457	5121	1368	502	12141	83176	3142	6932	180
CG_F22_3B_O	154300	7083	1886	468	11816	61111	3047	10631	170

	Ca	Ti	V	Cr	Mn	Fe	Sr	Ba	Th
	ppm								
CG_F22_3B_U	144491	4513,5	1135	410	10810	86404,5	2545,5	5186	148,5
CG_F22_4B_O	131986	5777	1528	417	10530	63334	2673	8028	158
CG_F22_4B_U	160235	5205	1386	477	12404	91876	3174	8197	183
CG_F22_5B_O	185698	9963	2430	608	13488	77826	3353	14576	184
CG_F22_5B_U	149005	6659	1695	531	11499	80585	2880	10447	189
CG_F22_6B_O	166740	7214	1777,5	491	12060,5	71794,5	3050,5	10370	170,5
CG_F22_6B_U	141048	6946	1791	528	10915	86754	2601	10386	188
CG_F22_7_O	**N/A**								
CG_F22_7_U									
CG_F22_8_O									
CG_F22_8_U									

B.5 XRF RESULTS FOR MAGNETIC PRE-CONCENTRATION AND SEQUENTIAL FLOTATION TESTS

	Ca	Ti	V	Cr	Mn	Fe	Sr	Ba	Th
	ppm								
C4_F9A _O	188467	11485	2951	836	14619	86002	3068	29266	198
C4_F9B_O	181478	21261	5991	1313	12428	65729	2730	29904	194
C4_F9B_U	199703	5920	1769	591	13916	83079	3639	8811	189
C4_F12A_O	206213	12929	3294	876	13894	76835	3255	13990	216
C4_F12B_O	203905	16708	4778	1382	14058	76042	3180	22063	313
C4_F12B_U	201769	7416	1884	567	14191	86868	3698	11426	176
CG_NMAG_F25_O	165385	11275	3213	563	12788	66439	3189	22927	196
CG_NMAG_F25_U	125301	5254	1298	496	10762	146121	2683	8953	213
CG_F26A_O	206627	10618	2544	634	13721	83776	3011	5805	192
CG_F26B_O	208092	15308	3927	934	4370	75298	3365	21746	263
CG_FB26_U	154108	6774	1783	519	11625	74434	2905	12254	183

B.4 XRF RESULTS FOR THE CG_F27 TAGUCHI SERIES

	Ca	Ti	V	Cr	Mn	Fe	Sr	Ba	Th
	ppm								
CG_F27_1A_T_O	109902	13481	4713	1559	8134	41911	1859	18417	391
CG_F27_1A_T_U	170343	9848	2269	457	13274	98294	3251	21192	206
CG_F27_1A_O	174236	16126	4575	920	13329	67731	3132	31134	310
CG_F27_1A_U	169002	9606	2201	466	12966	105954	3135	19709	203
CG_F27_2A_O	152045	10997	2989	782	11475	81402	2625	17719	274
CG_F27_2A_U	170351	10848	2430	536	13272	96449	3204	22613	223
CG_F27_3A_O	172326	9638	2519	718	12276	71576	2917	13839	213
CG_F27_3A_U	169354	7644	1874	584	12559	84047	3191	12003	203
CG_F27_4A_O	166461	11357	3059	721	11761	62134	2806	17077	231

	Ca	Ti	V	Cr	Mn	Fe	Sr	Ba	Th
	ppm								
CG_F27_4A_U	175372	7638	1895	612	12925	88855	3271	11360	194
CG_F27_5A_O	134880	9366	2449	524	8189	38908	1747	10440	151
CG_F27_5A_U	178643	8087	2032	655	13302	87750	3303	12583	204
CG_F27_6A_O	172538	12113	3205	709	12442	65092	3006	19108	230
CG_F27_6A_U	173879	7650	1985	602	12784	86201	3209	13058	205
CG_F27_7A_O	174154	11807	3212	723	12240	62662	2926	16366	234
CG_F27_7A_U	183066	8168	2107	618	13299	87748	3344	11570	215
CG_F27_8A_O	173595	11245	2949	691	12514	67392	3027	18467	244
CG_F27_8A_U	178430	8163	2002	638	13093	84652	3304	11480	202
CG_F27_2AR_O	179598	12105	3104	775	13007	71202	3186	18742	236
CG_F27_2AR_U	178009	7487	1864	621	12842	88639	3271	12700	213
CG_F27_8AR_O	173441	12560	3252	742	13161	87990	3105	21677	282
CG_F27_8AR_U	169223	10676	2482	523	12945	99137	3074	21689	211

C. ICP-MS RESULTS FOR ANALYSED FLOTATION PRODUCTS

C.1 RARE EARTH ELEMENT, RARE EARTH OXIDE (LREO, HREO AND TREO) RESULTS FOR C4 DIRECT FLOTATION TESTS

	Light Rare Earth Elements (LREEs)						Heavy Rare Earth Elements (HREEs)									
	mg/kg	mg/kg	mg/kg	mg/kg	mg/kg	mg/kg	mg/kg	mg/kg	mg/kg	mg/kg	mg/kg	mg/kg	mg/kg	mg/kg	mg/kg	mg/kg
Sample C4	**La**	**Ce**	**Pr**	**Nd**	**Sm**	**Eu**	**Gd**	**Tb**	**Dy**	**Ho**	**Er**	**Tm**	**Yb**	**Lu**	**Y**	**Sc**
C4_F1_O	3120	4869	552	1393	234	57,7	91,6	7,39	25,9	3,33	6,87	0,77	5,5	0,62	82,9	45,3
C4_F1_U	4172	6129	723	1825	278	68	109	8,39	28,5	3,47	6,61	0,68	4,78	0,5	91,7	42,1
C4_F2_O	3898,1	5909,2	650,3	1683,8	161,4	51,7	81,5	6,4	21,75	2,67	5,3	0,56	3,91	0,43	57,3	25,3
C4_F2_U	3557,7	5623,3	536,1	1588,8	153,2	50,1	78,4	6,2	21,67	2,7	5,44	0,59	4,09	0,45	59,7	25,8
C4_F3_O	6387,9	9223,6	1011,2	2597,7	248,2	73,8	121,1	9,2	30,69	3,64	6,87	0,7	4,65	0,51	83,6	19,5
C4_F3_U	2967	4738,2	502,7	1341,9	129	36	61	4,8	16,75	2,11	4,23	0,45	2,93	0,34	45,9	22,5
C4_F4_O	6227,4	8716	964	2486,7	238,2	73,1	120,2	9,1	30,36	3,6	6,74	0,68	4,39	0,48	81,3	3,4
C4_F4_U	3868,6	5968,3	660,3	1708,8	164	44,7	73,5	5,8	19,98	2,49	4,99	0,54	3,61	0,41	52	22,4

	Light Rare Earth Elements (LREE) Oxides						TLREO	Heavy Rare Earth Elements (HREE) Oxides									THREO	TREO
	%	%	%	%	%	%		%	%	%	%	%	%	%	%	%		
Sample C4	**La_2O_3**	**Ce_2O_3**	**Pr_2O_3**	**Nd_2O_3**	**Sm_2O_3**	**Eu_2O_3**	%	**Gd_2O_3**	**Tb_2O_3**	**Dy_2O_3**	**Ho_2O_3**	**Er_2O_3**	**Tm_2O_3**	**Yb_2O_3**	**Lu_2O_3**	**Y_2O_3**	**Sc_2O_3**	%	%
C4_F1_O	0,366	0,57	0,065	0,162	0,027	0,009	1,199	0,011	0,001	0,003	0	0,001	0	0,001	0	0,011	0,007	0,035	**1,23**
C4_F1_U	0,489	0,718	0,085	0,213	0,032	0,011	1,548	0,013	0,001	0,003	0	0,001	0	0,001	0	0,012	0,006	0,037	**1,58**
C4_F2_O	0,457	0,692	0,076	0,196	0,019	0,008	1,448	0,009	0,001	0,002	0	0,001	0	0	0	0,007	0,004	0,024	**1,47**
C4_F2_U	0,417	0,659	0,063	0,185	0,018	0,008	1,35	0,009	0,001	0,002	0	0,001	0	0	0	0,008	0,004	0,025	**1,37**
C4_F3_O	0,749	1,08	0,118	0,303	0,029	0,012	2,291	0,014	0,001	0,004	0	0,001	0	0,001	0	0,011	0,003	0,035	**2,33**
C4_F3_U	0,348	0,555	0,059	0,157	0,015	0,006	1,14	0,007	0,001	0,002	0	0	0	0	0	0,006	0,003	0,019	**1,16**
C4_F4_O	0,73	1,021	0,113	0,29	0,028	0,012	2,194	0,014	0,001	0,003	0	0,001	0	0	0	0,01	0,001	0,03	**2,22**
C4_F4_U	0,454	0,699	0,077	0,199	0,019	0,007	1,455	0,008	0,001	0,002	0	0,001	0	0	0	0,007	0,003	0,022	**1,48**

C.2 RARE EARTH ELEMENT, RARE EARTH OXIDE (LREO, HREO AND TREO) RESULTS FOR C4 HYDROGRAVITIC PRE-CONCENTRATION AND MICROWAVE-ASSISTED ROUTE

	Light Rare Earth Elements (LREEs)						Heavy Rare Earth Elements (HREEs)									
	mg/kg	mg/kg	mg/kg	mg/kg	mg/kg	mg/kg	mg/kg	mg/kg	mg/kg	mg/kg	mg/kg	mg/kg	mg/kg	mg/kg	mg/kg	mg/kg
Sample C4	**La**	**Ce**	**Pr**	**Nd**	**Sm**	**Eu**	**Gd**	**Tb**	**Dy**	**Ho**	**Er**	**Tm**	**Yb**	**Lu**	**Y**	**Sc**
C4_F5_O	6590,7	9653,6	1072,7	2679,7	270,6	82,5	140,1	10,9	36,49	4,44	8,59	0,97	5,92	0,76	92,9	23,7
C4_F5_U	3003,6	4693,5	517,5	1308,4	129,5	36,5	62,2	4,9	16,93	2,13	4,32	0,47	3,02	0,36	46,9	21,8
C4_F6_O	6376,3	9322,3	959	2591	259,2	70,5	121,6	9,4	31,35	3,75	7,13	0,73	4,68	0,54	80,1	21,2
C4_F6_U	2622,4	4083,7	449,9	1141,9	112,3	31,5	54,7	4,4	15,36	1,96	4,04	0,44	2,9	0,35	42,1	22,1
C4_F7_O	3546,7	5403,5	592,6	1534,2	148,8	40,1	65,9	5,2	17,92	2,23	4,49	0,48	3,22	0,37	47	20,3
C4_F7_U	3548	5456,8	579,1	1547,2	150,5	40	70,2	5,5	18,83	2,33	4,64	0,49	3,15	0,38	50,4	20,4
C4_F8_O	3724,5	5771,3	633,2	1634,2	157,6	38,2	67	5,2	17,89	2,21	4,42	0,47	3	0,36	47	17,7
C4_F8_U	3917,8	5812,5	641,4	1668,2	161,7	40,8	72,1	5,6	19,13	2,37	4,69	0,5	3,17	0,38	50,3	21,3
C4_F10_O	7765	15171	1346	3429	329	38,8	86	6,4	22,2	2,8	5,69	0,61	3,41	0,47	63,6	30
C4_F10_U	8195	14774	1431	3667	355	38,6	85,4	6,4	22,4	2,81	5,74	0,61	3,43	0,47	63,2	28,8
C4_F11_O	4111	8538	815	2064	194	21,7	48,2	3,5	11,7	1,41	2,69	0,27	1,56	0,2	32,1	13,2
C4_F11_U	8632	17597	1496	3821	369	46,2	107,1	8,1	28	3,51	7,13	0,76	4,08	0,59	79,3	36,3
C4_ST_R4_C_F13_O	9772	14627	1427	3726	328	82,6	208,2	15,1	49,2	5,78	10,46	1,01	4,9	0,7	127,2	34,4
C4_ST_R4_C_F13_U	3075	4392	335	890	65	72,7	185,5	13,4	44	5,24	9,58	0,93	4,46	0,65	113,3	33,4
C4_ST_R4_M_F14_O	10371	17242	1676	4234	407	50,9	126,8	9,5	32	3,91	7,68	0,8	3,98	0,61	85,1	32,6
C4_ST_R4_M_F14_U	4806	10629	969	2470	238	34,3	87,8	6,8	23,7	3,09	6,44	0,7	3,43	0,57	68,2	41,8

	Light Rare Earth Elements (LREE) Oxides						**TLREO**	**Heavy Rare Earth Elements (HREE) Oxides**										**THREO**	**TREO**
	%	**%**	**%**	**%**	**%**	**%**		**%**	**%**	**%**	**%**	**%**	**%**	**%**	**%**	**%**	**%**		
Sample C4	**La_2O_3**	**Ce_2O_3**	**Pr_2O_3**	**Nd_2O_3**	**Sm_2O_3**	**Eu_2O_3**	**%**	**Gd_2O_3**	**Tb_2O_3**	Dy_2O_3	**Ho_2O_3**	**Er_2O_3**	**Tm_2O_3**	**Yb_2O_3**	**Lu_2O_3**	**Y_2O_3**	**Sc_2O_3**	**%**	**%**
C4_F5_O	0,773	1,131	0,126	0,313	0,031	0,013	2,387	0,016	0,001	0,004	0,001	0,001	0	0,001	0	0,012	0,004	0,04	**2,43**
C4_F5_U	0,352	0,55	0,061	0,153	0,015	0,006	1,137	0,007	0,001	0,002	0	0	0	0	0	0,006	0,003	0,019	**1,16**
C4_F6_O	0,748	1,092	0,112	0,302	0,03	0,011	2,295	0,014	0,001	0,004	0	0,001	0	0,001	0	0,01	0,003	0,034	**2,33**
C4_F6_U	0,308	0,478	0,053	0,133	0,013	0,005	0,99	0,006	0,001	0,002	0	0	0	0	0	0,005	0,003	0,017	**1,01**
C4_F7_O	0,416	0,633	0,069	0,179	0,017	0,006	1,32	0,008	0,001	0,002	0	0,001	0	0	0	0,006	0,003	0,021	**1,34**
C4_F7_U	0,416	0,639	0,068	0,18	0,017	0,006	1,326	0,008	0,001	0,002	0	0,001	0	0	0	0,006	0,003	0,021	**1,35**
C4_F8_O	0,437	0,676	0,074	0,191	0,018	0,006	1,402	0,008	0,001	0,002	0	0,001	0	0	0	0,006	0,003	0,021	**1,42**
C4_F8_U	0,459	0,681	0,075	0,195	0,019	0,006	1,435	0,008	0,001	0,002	0	0,001	0	0	0	0,006	0,003	0,021	**1,46**
C4_F10_O	0,91	1,78	0,16	0,4	0,04	0,01	3,3	0,01	0	0	0	0	0	0	0	0,01	0	0,02	**3,32**
C4_F10_U	0,96	1,73	0,17	0,43	0,04	0,01	3,34	0,01	0	0	0	0	0	0	0	0,01	0	0,02	**3,36**
C4_F11_O	0,48	1	0,1	0,24	0,02	0	1,84	0,01	0	0	0	0	0	0	0	0	0	0,01	**1,86**
C4_F11_U	1,01	2,06	0,18	0,45	0,04	0,01	3,75	0,01	0	0	0	0	0	0	0	0,01	0,01	0,03	**3,78**
C4_ST_R4_C_F13_O	1,15	1,71	0,17	0,43	0,04	0,01	3,51	0,02	0	0,01	0	0	0	0	0	0,02	0,01	0,06	**3,57**
C4_ST_R4_C_F13_U	0,36	0,51	0,04	0,1	0,01	0,01	1,03	0,02	0	0,01	0	0	0	0	0	0,01	0,01	0,05	**1,08**
C4_ST_R4_M_F14_O	1,22	2,02	0,2	0,49	0,05	0,01	3,99	0,01	0	0	0	0	0	0	0	0,01	0,01	0,03	**4,02**
C4_ST_R4_M_F14_U	0,56	1,24	0,11	0,29	0,03	0,01	2,24	0,01	0	0	0	0	0	0	0	0,01	0,01	0,03	**2,27**

C.3 RARE EARTH ELEMENT, RARE EARTH OXIDE (LREO, HREO AND TREO) RESULTS FOR CG DIRECT FLOTATION AND HYDROGRAVITIC PRE-CONCENTRATION TESTS

	Light Rare Earth Elements (LREEs)						Heavy Rare Earth Elements (HREEs)									
	mg/kg	mg/kg	mg/kg	mg/kg	mg/kg	mg/kg	mg/kg	mg/kg	mg/kg	mg/kg	mg/kg	mg/kg	mg/kg	mg/kg	mg/kg	mg/kg
Sample CG	**La**	**Ce**	**Pr**	**Nd**	**Sm**	**Eu**	**Gd**	**Tb**	**Dy**	**Ho**	**Er**	**Tm**	**Yb**	**Lu**	**Y**	**Sc**
CG_ST_M_F15_O	9215	19049	1546	4026	418	59,2	155,7	12,6	45	5,76	11,48	1,2	5,42	0,86	127,4	39,5
CG_ST_M_F15_U	3369	7338	677	1776	187	29,1	78,2	6,6	25,6	3,53	7,56	0,84	3,76	0,62	79	44,1
CG_ST_C_F16_O	5953	9344	811	2169	189	105,5	283,2	20,9	68,8	8,18	15,07	1,47	6,47	0,98	171,8	36
CG_ST_C_F16_U	8574	17680	1426	3729	383	56	149,8	11,7	41,2	5,22	10,12	1,03	4,52	0,72	106,2	36,3
CG_ST_M_F17_O	5184	11318	1061	2763	290	53,5	148,2	12,1	44,8	5,93	12,13	1,29	5,58	0,94	127,4	50,5
CG_ST_M_F17_U	2879	6276	616	1605	169	22	60,1	5,2	20,3	2,84	6,08	0,67	2,89	0,51	59,7	34,2
CG_F18_O	10081	20936	1680	4372	449	70	198,5	15,5	53,3	6,69	13	1,34	5,44	0,95	138,2	40,5
CG_F18_U	5207	11047	1127	2844	301	43,2	119,6	9,9	37,2	4,92	10,05	1,06	4,56	0,76	99,8	40,5
CG_F19_O	6225	12063	1150	2999	314	48,5	132,1	10,9	39,8	5,19	10,52	1,12	4,74	0,8	104,9	38
CG_F19_U	9287	17865	1601	4191	449	69,4	205,6	17,3	63,5	8,28	16,36	1,7	6,64	1,18	158,9	40
CG_ST(3)_M_F20_O	5120	6955	628	1651	189	43,49	78,86	6,6	25,1	3,18	6,7	0,64	4,71	0,43	80,74	38,32
CG_ST(3)_M_F20_U	6438	9581	870	2273	179	43,51	71,86	5,96	22,08	2,74	5,58	0,52	4,11	0,33	64,74	26,07
CG_ST(3)_C_F21_O	7193	10167	928	2436	180	44,05	72,22	5,73	20,9	2,54	5,05	0,45	3,67	0,27	56,97	22,72
CG_ST(3)_C_F21_U	18662	10993	1012	2649	264	62,86	105,62	8,45	30,15	3,67	7,08	0,64	4,86	0,4	77,46	21,39
CG_ST(3)_M_F23_O	6602	9866	906	2380	252	28,74	70,94	5,85	21,79	2,84	5,81	0,62	2,82	0,43	64,17	24,18
CG_ST(3)_M_F23_U	6648	10235	940	2418	254	27,23	67,02	5,46	20,17	2,55	5,22	0,55	2,5	0,37	56,16	22,59
CG_ST(3)_C_F24_O	10347	11374	393	1674	179	64,2	154,63	11,08	36	4,14	7,55	0,73	3,36	0,46	90,63	20,83
CG_ST(3)_C_F24_U	8073	13509	1114	2926	296	29,3	73,02	5,9	21,15	2,69	5,34	0,53	2,44	0,35	54,7	20,62

	Light Rare Earth Elements (LREE) Oxides						**TLREO**	**Heavy Rare Earth Elements (HREE) Oxides**										**THREO**	**TREO**
	%	**%**	**%**	**%**	**%**	**%**		**%**	**%**	**%**	**%**	**%**	**%**	**%**	**%**	**%**	**%**		
Sample CG	**La_2O_3**	**Ce_2O_3**	**Pr_2O_3**	**Nd_2O_3**	**Sm_2O_3**	**Eu_2O_3**	**%**	**Gd_2O_3**	**Tb_2O_3**	Dy_2O_3	**Ho_2O_3**	**Er_2O_3**	**Tm_2O_3**	**Yb_2O_3**	**Lu_2O_3**	**Y_2O_3**	**Sc_2O_3**	**%**	**%**
CG_ST_M_F15_O	1,08	2,23	0,18	0,47	0,05	0,01	4,02	0,02	0	0,01	0	0	0	0	0	0,02	0,01	0,06	**4,07**
CG_ST_M_F15_U	0,4	0,86	0,08	0,21	0,02	0	1,57	0,01	0	0	0	0	0	0	0	0,01	0,01	0,03	**1,6**
CG_ST_C_F16_O	0,7	1,09	0,09	0,25	0,02	0,02	2,17	0,03	0	0,01	0	0	0	0	0	0,02	0,01	0,07	**2,25**
CG_ST_C_F16_U	1,01	2,07	0,17	0,43	0,04	0,01	3,73	0,02	0	0	0	0	0	0	0	0,01	0,01	0,04	**3,78**
CG_ST_M_F17_O	0,61	1,33	0,12	0,32	0,03	0,01	2,42	0,02	0	0,01	0	0	0	0	0	0,02	0,01	0,06	**2,47**
CG_ST_M_F17_U	0,34	0,74	0,07	0,19	0,02	0	1,36	0,01	0	0	0	0	0	0	0	0,01	0,01	0,03	**1,38**
CG_F18_O	1,18	2,45	0,2	0,51	0,05	0,01	4,4	0,02	0	0,01	0	0	0	0	0	0,02	0,01	0,06	**4,46**
CG_F18_U	0,61	1,29	0,13	0,33	0,03	0,01	2,4	0,01	0	0	0	0	0	0	0	0,01	0,01	0,03	**2,45**
CG_F19_O	0,73	1,41	0,13	0,35	0,04	0,01	2,67	0,02	0	0	0	0	0	0	0	0,01	0,01	0,04	**2,71**
CG_F19_U	1,09	2,09	0,19	0,49	0,05	0,01	3,92	0,02	0	0,01	0	0	0	0	0	0,02	0,01	0,06	**3,98**
CG_ST(3)_M_F20_O	0,6	0,81	0,07	0,19	0,02	0,01	1,7	0,01	0	0	0	0	0	0	0	0,01	0,01	0,03	**1,74**
CG_ST(3)_M_F20_U	0,76	1,12	0,1	0,27	0,02	0,01	2,28	0,01	0	0	0	0	0	0	0	0,01	0	0,02	**2,3**
CG_ST(3)_C_F21_O	0,84	1,19	0,11	0,28	0,02	0,01	2,45	0,01	0	0	0	0	0	0	0	0,01	0	0,02	**2,48**
CG_ST(3)_C_F21_U	2,19	1,29	0,12	0,31	0,03	0,01	3,95	0,01	0	0	0	0	0	0	0	0,01	0	0,02	**3,98**
CG_ST(3)_M_F23_O	0,77	1,16	0,11	0,28	0,03	0,00	2,35	0,01	0	0	0	0	0	0	0	0,01	0	0,02	**2,37**
CG_ST(3)_M_F23_U	0,78	1,20	0,11	0,28	0,03	0,00	2,40	0,01	0	0	0	0	0	0	0	0,01	0	0,02	**2,43**
CG_ST(3)_C_F24_O	1,21	1,33	0,05	0,2	0,02	0,01	2,82	0,02	0,00	0,00	0,00	0,00	0,00	0,00	0,00	0,01	0	0,03	**2,86**
CG_ST(3)_C_F24_U	0,95	1,58	0,13	0,34	0,03	0	3,03	0,01	0,00	0,00	0,00	0,00	0,00	0,00	0,00	0,01	0	0,02	**3,06**

C.4 RARE EARTH ELEMENT, RARE EARTH OXIDE (LREO, HREO AND TREO) RESULTS FOR THE CG_F22 TAGUCHI SERIES

	Light Rare Earth Elements (LREEs)						Heavy Rare Earth Elements (HREEs)									
	mg/kg	mg/kg	mg/kg	mg/kg	mg/kg	mg/kg	mg/kg	mg/kg	mg/kg	mg/kg	mg/kg	mg/kg	mg/kg	mg/kg	mg/kg	mg/kg
Sample CG	**La**	**Ce**	**Pr**	**Nd**	**Sm**	**Eu**	**Gd**	**Tb**	**Dy**	**Ho**	**Er**	**Tm**	**Yb**	**Lu**	**Y**	**Sc**
CG_F22_1A_O	7710	10896	1000	2622	247	57,13	98,84	7,83	27,6	3,3	6,66	0,6	4,59	0,41	74,16	24,46
CG_F22_1A_U	4197	5787	546	1416	174	43,99	70,52	5,9	22,16	2,82	5,78	0,53	4,41	0,34	60,06	27,79
CG_F22_2A_O	3874	5077	476	1241	250	59,88	100,12	8,1	29,33	3,6	7,23	0,67	5,18	0,45	76,44	28,85
CG_F22_2A_U	3080	4027	378	997	224	54,67	90,17	7,62	28,46	3,62	7,39	0,72	5,5	0,47	75,09	32,54
CG_F22_3A_O	10747	7060	659	1731	449	102,08	176,18	13,86	48,42	5,94	11,58	1,08	7,96	0,73	125,69	37,38
CG_F22_3A_U	2679	3470	328	865	250	59,53	101,63	8,83	33,42	4,27	8,86	0,86	6,3	0,58	86,63	39,86
CG_F22_4A_O	4027	5118	485	1281	417	94,96	168,02	13,78	49,58	6,2	12,38	1,23	8,55	0,84	132,94	47,04
CG_F22_4A_U	2946	3792	359	944	274	62,64	111,37	9,43	35,35	4,51	9,43	0,93	6,56	0,62	92,62	40,87
CG_F22_5A_O	4027	5118	483	1273	367	82,64	144,87	11,89	42,77	5,32	10,66	1,05	7,27	0,71	109,12	40,93
CG_F22_5A_U	3236	3999	382	1004	388	89,55	156,44	13,12	48,7	6,18	12,35	1,21	8,54	0,83	122,26	48,83
CG_F22_6A_O	4104	5113	484	1271	480	110,25	190,13	15,4	55,59	6,88	13,81	1,36	9,4	0,92	140,29	53,14
CG_F22_6A_U	3018	3767	361	947	324	75,33	130,66	11,08	41,5	5,36	10,85	1,08	7,52	0,71	104,25	42,46
CG_F22_7A_O	3589	4398	415	1094	347	81,25	137,09	11,28	41,35	5,17	10,37	1,05	7,38	0,72	103,29	41,54
CG_F22_7A_U	3379	4189	401	1064	397	90,5	159,64	13,64	50,67	6,42	12,9	1,32	8,79	0,88	122,29	45,55
CG_F22_8A_O	4065	4979	474	1238	446	100,25	176,37	14,4	52,46	6,55	12,99	1,3	8,99	0,88	129,98	48,82
CG_F22_8A_U	3530	4660	446	1180	394	87,92	160,88	13,89	52,53	6,8	13,84	1,4	9,2	0,94	130,28	48,32

	Light Rare Earth Elements (LREE) Oxides						**TLREO**	**Heavy Rare Earth Elements (HREE) Oxides**										**THREO**	**TREO**
	%	**%**	**%**	**%**	**%**	**%**		**%**	**%**	**%**	**%**	**%**	**%**	**%**	**%**	**%**	**%**		
Sample CG	**La_2O_3**	**Ce_2O_3**	**Pr_2O_3**	**Nd_2O_3**	**Sm_2O_3**	**Eu_2O_3**	**%**	**Gd_2O_3**	**Tb_2O_3**	Dy_2O_3	**Ho_2O_3**	**Er_2O_3**	**Tm_2O_3**	**Yb_2O_3**	**Lu_2O_3**	**Y_2O_3**	**Sc_2O_3**	**%**	**%**
CG_F22_1A_O	0,9	1,28	0,12	0,31	0,03	0,01	2,65	0,01	0	0	0	0	0	0	0	0,01	0	0,02	**2,67**
CG_F22_1A_U	0,49	0,68	0,06	0,17	0,02	0,01	1,43	0,01	0	0	0	0	0	0	0	0,01	0	0,02	**1,45**
CG_F22_2A_O	0,45	0,59	0,06	0,14	0,03	0,01	1,28	0,01	0	0	0	0	0	0	0	0,01	0	0,02	**1,32**
CG_F22_2A_U	0,36	0,47	0,04	0,12	0,03	0,01	1,03	0,01	0	0	0	0	0	0	0	0,01	0	0,02	**1,06**
CG_F22_3A_O	1,26	0,83	0,08	0,2	0,05	0,02	2,44	0,02	0	0,01	0	0	0	0	0	0,02	0,01	0,06	**2,49**
CG_F22_3A_U	0,31	0,41	0,04	0,1	0,03	0,01	0,9	0,01	0	0	0	0	0	0	0	0,01	0,01	0,03	**0,93**
CG_F22_4A_O	0,47	0,6	0,06	0,15	0,05	0,01	1,34	0,02	0	0,01	0	0	0	0	0	0,02	0,01	0,06	**1,4**
CG_F22_4A_U	0,35	0,44	0,04	0,11	0,03	0,01	0,98	0,01	0	0	0	0	0	0	0	0,01	0,01	0,03	**1,02**
CG_F22_5A_O	0,47	0,6	0,06	0,15	0,04	0,01	1,33	0,02	0	0	0	0	0	0	0	0,01	0,01	0,04	**1,38**
CG_F22_5A_U	0,38	0,47	0,04	0,12	0,04	0,01	1,06	0,02	0	0,01	0	0	0	0	0	0,02	0,01	0,06	**1,12**
CG_F22_6A_O	0,48	0,6	0,06	0,15	0,06	0,02	1,37	0,02	0	0,01	0	0	0	0	0	0,02	0,01	0,06	**1,42**
CG_F22_6A_U	0,35	0,44	0,04	0,11	0,04	0,01	0,99	0,02	0	0	0	0	0	0	0	0,01	0,01	0,04	**1,04**
CG_F22_7A_O	0,42	0,52	0,05	0,13	0,04	0,01	1,17	0,02	0	0	0	0	0	0	0	0,01	0,01	0,04	**1,21**
CG_F22_7A_U	0,4	0,49	0,05	0,12	0,05	0,01	1,12	0,02	0	0,01	0	0	0	0	0	0,02	0,01	0,06	**1,17**
CG_F22_8A_O	0,48	0,58	0,06	0,14	0,05	0,02	1,33	0,02	0	0,01	0	0	0	0	0	0,02	0,01	0,06	**1,38**
CG_F22_8A_U	0,41	0,55	0,05	0,14	0,05	0,01	1,21	0,02	0	0,01	0	0	0	0	0	0,02	0,01	0,06	**1,26**

	Light Rare Earth Elements (LREEs)						Heavy Rare Earth Elements (HREEs)									
	mg/kg	mg/kg	mg/kg	mg/kg	mg/kg	mg/kg	mg/kg	mg/kg	mg/kg	mg/kg	mg/kg	mg/kg	mg/kg	mg/kg	mg/kg	mg/kg
Sample CG	**La**	**Ce**	**Pr**	**Nd**	**Sm**	**Eu**	**Gd**	**Tb**	**Dy**	**Ho**	**Er**	**Tm**	**Yb**	**Lu**	**Y**	**Sc**
CG_F22_1B_O	8359	11844	1086	2829	296	29,38	79,06	6,36	23,44	2,94	6	0,61	2,63	0,42	58,52	19,76
CG_F22_1B_U	6700	11017	941	2443	257	23,53	59,78	4,84	17,6	2,24	4,59	0,46	2,09	0,32	43,41	17,2
CG_F22_2B_O	7071	10986	1002	2577	268	25	60,95	4,93	17,9	2,26	4,56	0,48	2,2	0,33	44,69	18,12
CG_F22_2B_U	7895	12241	1123	2885	304	27	69,81	5,66	20,73	2,66	5,42	0,56	2,5	0,39	50,21	17,9
CG_F22_3B_O	7150	11632	1059	2735	289	26,54	67,93	5,54	20,16	2,6	5,22	0,55	2,41	0,37	50,78	19,76
CG_F22_3B_U	6223	9837	896	2334	248	25,06	70,82	5,89	21,92	2,87	5,93	0,62	2,41	0,41	53,48	21,05
CG_F22_4B_O	6211	9871	911	2348	247	23,38	61,97	5,07	19,13	2,5	5,18	0,54	2,33	0,37	47,59	19,01
CG_F22_4B_U	7138	11138	1004	2616	273	24,28	63,96	5,22	19,36	2,49	5,17	0,53	2,28	0,35	46,27	17,71
CG_F22_5B_O	7407	11761	1070	2735	286	25,24	64,56	5,14	18,58	2,36	4,72	0,49	2,18	0,34	44,29	16,82
CG_F22_5B_U	8337	13176	1194	3116	322	29,47	77,32	6,16	22,2	2,83	5,65	0,58	2,49	0,4	51,7	17,84
CG_F22_6B_O	6887	10964	1005	2589	271	22,92	58,08	4,7	17,16	2,18	4,42	0,46	2,05	0,31	0,01	0
CG_F22_6B_U	7531	11999	1089	2805	295	25,08	65,56	5,35	19,84	2,54	5,13	0,53	2,31	0,35	0,01	0

	Light Rare Earth Elements (LREE) Oxides						**TLREO**	**Heavy Rare Earth Elements (HREE) Oxides**										**THREO**	**TREO**
	%	**%**	**%**	**%**	**%**	**%**		**%**	**%**	**%**	**%**	**%**	**%**	**%**	**%**	**%**	**%**		
Sample CG	**La_2O_3**	**Ce_2O_3**	**Pr_2O_3**	**Nd_2O_3**	**Sm_2O_3**	**Eu_2O_3**	**%**	**Gd_2O_3**	**Tb_2O_3**	Dy_2O_3	**Ho_2O_3**	**Er_2O_3**	**Tm_2O_3**	**Yb_2O_3**	**Lu_2O_3**	**Y_2O_3**	**Sc_2O_3**	**%**	**%**
CG_F22_1B_O	0,98	1,39	0,13	0,33	0,03	0	2,86	0,01	0	0	0	0	0	0	0	0,01	0	0,02	**2,89**
CG_F22_1B_U	0,79	1,29	0,11	0,28	0,03	0	2,5	0,01	0	0	0	0	0	0	0	0,01	0	0,02	**2,52**
CG_F22_2B_O	0,83	1,29	0,12	0,3	0,03	0	2,57	0,01	0	0	0	0	0	0	0	0,01	0	0,02	**2,59**
CG_F22_2B_U	0,93	1,43	0,13	0,34	0,04	0	2,87	0,01	0	0	0	0	0	0	0	0,01	0	0,02	**2,89**
CG_F22_3B_O	0,84	1,36	0,12	0,32	0,03	0	2,67	0,01	0	0	0	0	0	0	0	0,01	0	0,02	**2,7**
CG_F22_3B_U	0,73	1,15	0,1	0,27	0,03	0	2,28	0,01	0	0	0	0	0	0	0	0,01	0	0,02	**2,31**
CG_F22_4B_O	0,73	1,16	0,11	0,27	0,03	0	2,3	0,01	0	0	0	0	0	0	0	0,01	0	0,02	**2,32**
CG_F22_4B_U	0,84	1,3	0,12	0,31	0,03	0	2,6	0,01	0	0	0	0	0	0	0	0,01	0	0,02	**2,62**
CG_F22_5B_O	0,87	1,38	0,13	0,32	0,03	0	2,73	0,01	0	0	0	0	0	0	0	0,01	0	0,02	**2,75**
CG_F22_5B_U	0,98	1,54	0,14	0,36	0,04	0	3,06	0,01	0	0	0	0	0	0	0	0,01	0	0,02	**3,09**
CG_F22_6B_O	0,81	1,28	0,12	0,3	0,03	0	2,54	0,01	0	0	0	0	0	0	0	0,01	0	0,02	**2,56**
CG_F22_6B_U	0,88	1,41	0,13	0,33	0,03	0	2,78	0,01	0	0	0	0	0	0	0	0,01	0	0,02	**2,8**

C.5 RARE EARTH ELEMENT, RARE EARTH OXIDE (LREO, HREO AND TREO) RESULTS FOR MAGNETIC PRE-CONCENTRATION AND SEQUENTIAL FLOTATION TESTS

	Light Rare Earth Elements (LREEs)						Heavy Rare Earth Elements (HREEs)									
	mg/kg	mg/kg	mg/kg	mg/kg	mg/kg	mg/kg	mg/kg	mg/kg	mg/kg	mg/kg	mg/kg	mg/kg	mg/kg	mg/kg	mg/kg	mg/kg
Sample CG	**La**	**Ce**	**Pr**	**Nd**	**Sm**	**Eu**	**Gd**	**Tb**	**Dy**	**Ho**	**Er**	**Tm**	**Yb**	**Lu**	**Y**	**Sc**
C4_F9A _O	7948	14229	1376	3481	338	51,4	95,8	7,1	24,3	3,06	6,21	0,67	4,37	0,52	75,3	36,1
C4_F9B_O	9893	18778	1763	4518	431	67,2	151,9	11,3	37,8	4,67	9,13	0,94	5,2	0,71	110,9	36,6
C4_F9B_U	5990	11847	1145	2908	281	36,3	78,8	5,9	20,7	2,65	5,46	0,6	3,39	0,47	61	34
C4_F12A_O	8305	17055	1450	3676	354	49,3	113,9	8,6	29,1	3,67	7,42	0,8	4,35	0,63	81,4	36,9
C4_F12B_O	13676	28812	2195	5531	508	41,7	96,6	6,6	21,2	2,41	4,15	0,37	2,02	0,25	55,9	13,8
C4_F12B_U	7168	13062	1278	3266	320	41,2	101,7	7,7	26,5	3,38	6,85	0,74	3,74	0,57	75,7	36,3
CG_NMAG_F25_O	9717	15927	1278	3314	351	34,3	83,17	6,72	23,84	3,02	6,01	0,61	2,83	0,42	64,08	20,26
CG_NMAG_F25_U	8616	12401	1147	2993	328	31,84	78,73	6,42	23,49	2,99	6	0,62	2,8	0,41	60,49	18,59
CG_F26A_O	8127	13131	1132	2901	308	29,92	73,68	5,9	21,35	2,69	5,42	0,57	2,54	0,38	55,44	19,88
CG_F26B_O	8754	14975	1218	3161	333	30,95	78,22	6,31	22,79	2,88	5,81	0,6	2,68	0,4	57,79	17,27
CG_FB26_U	5856	8958	821	2144	228	21,57	54,94	4,55	17,05	2,19	4,48	0,47	2,11	0,32	43,09	16,86

	Light Rare Earth Elements (LREE) Oxides						**TLREO**	**Heavy Rare Earth Elements (HREE) Oxides**										**THREO**	**TREO**
	%	**%**	**%**	**%**	**%**	**%**		**%**	**%**	**%**	**%**	**%**	**%**	**%**	**%**	**%**	**%**		
	La_2O_3	**Ce_2O_3**	**Pr_2O_3**	**Nd_2O_3**	**Sm_2O_3**	**Eu_2O_3**	**%**	**Gd_2O_3**	**Tb_2O_3**	Dy_2O_3	**Ho_2O_3**	**Er_2O_3**	**Tm_2O_3**	**Yb_2O_3**	**Lu_2O_3**	**Y_2O_3**	**Sc_2O_3**	**%**	**%**
C4_F9A _O	0,93	1,67	0,16	0,41	0,04	0,01	3,22	0,01	0	0	0	0	0	0	0	0,01	0,01	0,03	**3,24**
C4_F9B_O	1,16	2,2	0,21	0,53	0,05	0,01	4,16	0,02	0	0	0	0	0	0	0	0,01	0,01	0,04	**4,2**
C4_F9B_U	0,7	1,39	0,13	0,34	0,03	0,01	2,6	0,01	0	0	0	0	0	0	0	0,01	0,01	0,03	**2,63**
C4_F12A_O	0,97	2	0,17	0,43	0,04	0,01	3,62	0,01	0	0	0	0	0	0	0	0,01	0,01	0,03	**3,65**
C4_F12B_O	1,6	3,37	0,26	0,65	0,06	0,01	5,95	0,01	0	0	0	0	0	0	0	0,01	0	0,02	**5,97**
C4_F12B_U	0,84	1,53	0,15	0,38	0,04	0,01	2,95	0,01	0	0	0	0	0	0	0	0,01	0,01	0,03	**2,98**
CG_NMAG_F25_O	1,14	1,87	0,15	0,39	0,04	0,01	3,6	0,01	0,00	0,00	0,00	0,00	0,00	0,00	0,00	0,01	0,01	0,03	**3,61**
CG_NMAG_F25_U	1,01	1,45	0,13	0,35	0,04	0,01	2,99	0,01	0,00	0,00	0,00	0,00	0,00	0,00	0,00	0,01	0,01	0,03	**3,01**
CG_F26A_O	0,95	1,54	0,13	0,34	0,04	0	3	0,01	0,00	0,00	0,00	0,00	0,00	0,00	0,00	0,01	0,00	0,02	**3,03**
CG_F26B_O	1,03	1,75	0,14	0,37	0,04	0	3,33	0,01	0,00	0,00	0,00	0,00	0,00	0,00	0,00	0,01	0,00	0,02	**3,36**
CG_FB26_U	0,69	1,05	0,1	0,25	0,03	0	2,12	0,01	0,00	0,00	0,00	0,00	0,00	0,00	0,00	0,01	0,00	0,02	**2,13**

C.6 RARE EARTH ELEMENT, RARE EARTH OXIDE (LREO, HREO AND TREO) RESULTS FOR THE CG_F27 TAGUCHI SERIES

	Light Rare Earth Elements (LREEs)						Heavy Rare Earth Elements (HREEs)									
	mg/kg	mg/kg	mg/kg	mg/kg	mg/kg	mg/kg	mg/kg	mg/kg	mg/kg	mg/kg	mg/kg	mg/kg	mg/kg	mg/kg	mg/kg	mg/kg
Sample CG	**La**	**Ce**	**Pr**	**Nd**	**Sm**	**Eu**	**Gd**	**Tb**	**Dy**	**Ho**	**Er**	**Tm**	**Yb**	**Lu**	**Y**	**Sc**
CG_F27_1A_T_O	4287	4110	364	1018	71	165,2	321	24,9	84,6	9,8	17,7	1,6	8,8	1	274,2	47,8
CG_F27_1A_T_U	3993	5878	561	1461	155	48,6	97	8,4	32,2	4,5	9,1	1	5,2	0,7	117,9	57,6
CG_F27_1A_O	7685	11055	1051	2710	285	89,1	179	14,1	51,4	6,3	11,6	1,3	6,5	0,8	169,2	50,7
CG_F27_1A_U	4000	5930	560	1473	159	49,3	100	8,5	33	4,5	9,1	0,9	5	0,6	113,6	52,5
CG_F27_2A_O	8030	11487	1089	2828	297	94,6	194	15,6	53,8	6,5	12,4	1,2	6,5	0,8	52,5	52,5
CG_F27_2A_U	4326	6399	598	1571	166	53,5	118	9,9	37,2	4,9	10	1,1	5,4	0,7	126,9	53,9
CG_F27_3A_O	5775	8286	761	1987	209	72,4	166	13,2	47	6,1	11,9	1,2	6,2	0,9	156,8	62,3
CG_F27_3A_U	5366	7669	707	1857	192	65,6	143	11,3	40,7	5,1	10,3	1	5,6	0,8	132,3	57,1
CG_F27_4A_O	5769	8458	788	2058	207	77,1	169	13,4	49,1	6,2	12,1	1,3	6,6	0,9	157	54,7
CG_F27_4A_U	4674	6365	599	1536	152	66,3	145	11,2	39,9	5	9,7	1	5,5	0,7	130,1	56,2
CG_F27_5A_O	5904	8593	806	2093	224	77,5	175	13,8	48,9	6,3	12,4	1,3	6,5	0,9	159,8	53,1
CG_F27_5A_U	5317	7525	702	1819	186	71,1	158	12,4	43,7	5,5	11	1,1	5,9	0,8	140,5	61,1
CG_F27_6A_O	6733	9420	873	2271	239	95,6	216	17,2	60,8	7,8	16,1	1,6	8,1	1,1	205,7	72,6
CG_F27_6A_U	6141	9117	824	2120	213	81,8	179	14,2	49,9	6,4	12,8	1,4	7	0,9	169,9	72,3
CG_F27_7A_O	6144	9208	852	2220	230	92,5	205	16,4	58,5	7,6	15	1,6	8,2	1,1	195,8	70,1
CG_F27_7A_U	5515	7866	740	1925	204	85	193	15,2	52,8	7,1	13,8	1,8	7,4	1,3	180,4	75,2
CG_F27_8A_O	5551	7987	743	1926	208	94,2	208	16,6	59,1	7,5	14,6	1,5	7,9	1	198,3	69,6
CG_F27_8A_U	5291	7565	698	1834	188	80,8	177	14	49,7	6,4	12,8	1,3	6,9	0,9	167,6	66,6
CG_F27_2AR_O	5994	8798	817	2100	220	93	203	16,1	56,2	7,1	14,1	1,5	7,8	1	190,6	68,9
CG_F27_2AR_U	5685	8248	752	1974	202	85,8	190	14,9	52,2	6,5	13,3	1,5	7,1	1	177,6	72,4
CG_F27_8AR_O	5859	8820	820	2138	234	100,1	225	18	64,7	8,3	16,1	1,7	8,7	1,1	218,9	70,3
CG_F27_8AR_U	5053	7686	713	1860	201	82,3	181	14,7	54,6	6,9	14	1,4	7,5	0,9	181,2	68,6

	Light Rare Earth Elements (LREE) Oxides						**TLREO**	**Heavy Rare Earth Elements (HREE) Oxides**										**THREO**	**TREO**
	%	**%**	**%**	**%**	**%**	**%**		**%**	**%**	**%**	**%**	**%**	**%**	**%**	**%**	**%**	**%**		
Sample CG	**La_2O_3**	**Ce_2O_3**	**Pr_2O_3**	**Nd_2O_3**	**Sm_2O_3**	**Eu_2O_3**	**%**	**Gd_2O_3**	**Tb_2O_3**	Dy_2O_3	**Ho_2O_3**	**Er_2O_3**	**Tm_2O_3**	**Yb_2O_3**	**Lu_2O_3**	**Y_2O_3**	**Sc_2O_3**	**%**	**%**
CG_F27_1A_T_O	0,5	0,48	0,04	0,12	0,01	0,03	1,18	0,04	0	0,01	0	0	0	0	0	0,03	0,01	0,04	**1,28**
CG_F27_1A_T_U	0,47	0,69	0,07	0,17	0,02	0,01	1,43	0,01	0	0	0	0	0	0	0	0,01	0,01	0,02	**1,46**
CG_F27_1A_O	0,9	1,29	0,12	0,32	0,03	0,01	2,67	0,02	0	0,01	0	0	0	0	0	0,02	0,01	0,03	**2,74**
CG_F27_1A_U	0,47	0,69	0,07	0,17	0,02	0,01	1,43	0,01	0	0	0	0	0	0	0	0,01	0,01	0,02	**1,47**
CG_F27_2A_O	0,94	1,35	0,13	0,33	0,03	0,01	2,79	0,02	0	0,01	0	0	0	0	0	0,02	0,01	0,03	**2,86**
CG_F27_2A_U	0,51	0,75	0,07	0,18	0,02	0,01	1,54	0,01	0	0	0	0	0	0	0	0,02	0,01	0,03	**1,58**
CG_F27_3A_O	0,68	0,97	0,09	0,23	0,02	0,01	2,00	0,02	0	0,01	0	0	0	0	0	0,02	0,01	0,03	**2,06**
CG_F27_3A_U	0,63	0,9	0,08	0,22	0,02	0,01	1,86	0,02	0	0	0	0	0	0	0	0,02	0,01	0,03	**1,91**
CG_F27_4A_O	0,68	0,99	0,09	0,24	0,02	0,01	2,03	0,02	0	0,01	0	0	0	0	0	0,02	0,01	0,03	**2,09**
CG_F27_4A_U	0,55	0,75	0,07	0,18	0,02	0,01	1,58	0,02	0	0	0	0	0	0	0	0,02	0,01	0,03	**1,62**
CG_F27_5A_O	0,69	1,01	0,09	0,24	0,03	0,01	2,07	0,02	0	0,01	0	0	0	0	0	0,02	0,01	0,03	**2,13**
CG_F27_5A_U	0,62	0,88	0,08	0,21	0,02	0,01	1,82	0,02	0	0,01	0	0	0	0	0	0,02	0,01	0,03	**1,89**
CG_F27_6A_O	0,79	1,1	0,1	0,26	0,03	0,02	2,30	0,02	0	0,01	0	0	0	0	0	0,03	0,01	0,04	**2,38**
CG_F27_6A_U	0,72	1,07	0,1	0,25	0,02	0,01	2,17	0,02	0	0,01	0	0	0	0	0	0,02	0,01	0,03	**2,23**
CG_F27_7A_O	0,72	1,08	0,1	0,26	0,03	0,01	2,20	0,02	0	0,01	0	0	0	0	0	0,02	0,01	0,03	**2,27**
CG_F27_7A_U	0,65	0,92	0,09	0,22	0,02	0,01	1,91	0,02	0	0,01	0	0	0	0	0	0,02	0,01	0,03	**1,98**
CG_F27_8A_O	0,65	0,94	0,09	0,22	0,02	0,01	1,93	0,02	0	0,01	0	0	0	0	0	0,03	0,01	0,04	**2,01**
CG_F27_8A_U	0,62	0,89	0,08	0,21	0,02	0,01	1,83	0,02	0	0,01	0	0	0	0	0	0,02	0,01	0,03	**1,9**
CG_F27_2AR_O	0,7	1,03	0,1	0,24	0,03	0,01	2,11	0,02	0	0,01	0	0	0	0	0	0,02	0,01	0,03	**2,18**
CG_F27_2AR_U	0,67	0,97	0,09	0,23	0,02	0,01	1,99	0,02	0	0,01	0	0	0	0	0	0,02	0,01	0,03	**2,05**
CG_F27_8AR_O	0,69	1,03	0,1	0,25	0,03	0,02	2,12	0,03	0	0,01	0	0	0	0	0	0,03	0,01	0,04	**2,19**
CG_F27_8AR_U	0,59	0,9	0,08	0,22	0,02	0,01	1,82	0,02	0	0,01	0	0	0	0	0	0,02	0,01	0,03	**1,9**

	Light Rare Earth Elements (LREEs)						Heavy Rare Earth Elements (HREEs)									
	mg/kg	mg/kg	mg/kg	mg/kg	mg/kg	mg/kg	mg/kg	mg/kg	mg/kg	mg/kg	mg/kg	mg/kg	mg/kg	mg/kg	mg/kg	mg/kg
Sample CG	**La**	**Ce**	**Pr**	**Nd**	**Sm**	**Eu**	**Gd**	**Tb**	**Dy**	**Ho**	**Er**	**Tm**	**Yb**	**Lu**	**Y**	**Sc**
CG_F27_1B_O	4256	6338	597	1570	161	75,8	170	13,9	50,3	6,3	12,6	1,4	6,8	0,9	167,2	64,3
CG_F27_1B_U	4054	5991	560	1497	163	69,6	154	13	48,2	6,3	12,8	1,4	7	0,9	166,4	66,2
CG_F27_2B_O	5279	7484	702	1797	191	88,1	196	15	52,3	6,4	13,3	1,3	7,3	0,9	172,1	57,4
CG_F27_2B_U	4762	6824	636	1656	174	80,2	176	13,5	46,8	6	11,6	1,2	6,8	0,8	156,4	61,7
CG_F27_3B_O	4847	6790	634	1637	174	78,3	170	13,1	45,5	5,7	11,3	1,1	6,2	0,8	151,5	58,8
CG_F27_3B_U	4784	6977	647	1687	176	78,9	172	13,3	47,4	6	12,1	1,3	6,7	0,9	158,9	63,9
CG_F27_4B_O	2367	2541	232	630	52	98,6	223	17,4	61,5	7,7	15,3	1,6	7,9	1,2	216,1	84,9
CG_F27_4B_U	4359	6464	594	1562	159	85,6	190	14,8	52,5	6,8	13,6	1,4	7,5	1	181,6	80,4
CG_F27_5B_O	4256	5769	536	1393	135	110,8	251	19,3	67,5	8,5	16,8	1,7	8,9	1,1	227,7	80
CG_F27_5B_U	4600	6857	622	1645	165	84,6	187	14,9	51,5	6,7	13,4	1,4	7,4	0,9	177,2	78,6
CG_F27_6B_O	5740	8601	796	2072	226	109,3	246	19,3	67,5	8,4	17	1,7	8,9	1,2	222,5	72,8
CG_F27_6B_U	3627	4872	456	1185	122	84,9	187	14,6	51,6	6,6	13	1,4	7,2	0,9	171,6	70,1
CG_F27_7B_O	5392	7887	728	1908	193	94,9	208	16,4	57,2	7,3	14,6	1,6	7,9	1	189,1	68,1
CG_F27_7B_U	4894	7107	660	1710	181	84	187	14,2	49,8	6,3	12,5	1,4	6,8	0,9	170,6	71,4
CG_F27_8B_O	5119	7477	708	1868	199	74,6	165	13,4	48,7	6,2	12,6	1,3	6,8	0,9	163,2	62,6
CG_F27_8B_U	3505	5249	496	1308	140	71,5	160	13	47,1	6,1	12,4	1,3	6,5	0,9	157,2	60,7

	Light Rare Earth Elements (LREE) Oxides						**TLREO**	**Heavy Rare Earth Elements (HREE) Oxides**										**THREO**	**TREO**
	%	**%**	**%**	**%**	**%**	**%**		**%**	**%**	**%**	**%**	**%**	**%**	**%**	**%**	**%**	**%**		
Sample CG	**La_2O_3**	**Ce_2O_3**	**Pr_2O_3**	**Nd_2O_3**	**Sm_2O_3**	**Eu_2O_3**	**%**	**Gd_2O_3**	**Tb_2O_3**	Dy_2O_3	**Ho_2O_3**	**Er_2O_3**	**Tm_2O_3**	**Yb_2O_3**	**Lu_2O_3**	**Y_2O_3**	**Sc_2O_3**	**%**	**%**
CG_F27_1B_O	0,5	0,74	0,07	0,18	0,02	0,01	1,52	0,02	0	0,01	0	0	0	0	0	0,02	0,01	0,03	**1,59**
CG_F27_1B_U	0,48	0,7	0,07	0,17	0,02	0,01	1,45	0,02	0	0,01	0	0	0	0	0	0,02	0,01	0,03	**1,51**
CG_F27_2B_O	0,62	0,88	0,08	0,21	0,02	0,01	1,82	0,02	0	0,01	0	0	0	0	0	0,02	0,01	0,03	**1,89**
CG_F27_2B_U	0,56	0,8	0,07	0,19	0,02	0,01	1,65	0,02	0	0,01	0	0	0	0	0	0,02	0,01	0,03	**1,72**
CG_F27_3B_O	0,57	0,8	0,07	0,19	0,02	0,01	1,66	0,02	0	0,01	0	0	0	0	0	0,02	0,01	0,03	**1,72**
CG_F27_3B_U	0,56	0,82	0,08	0,2	0,02	0,01	1,69	0,02	0	0,01	0	0	0	0	0	0,02	0,01	0,03	**1,74**
CG_F27_4B_O	0,28	0,3	0,03	0,07	0,01	0,02	0,71	0,03	0	0,01	0	0	0	0	0	0,03	0,01	0,04	**0,78**
CG_F27_4B_U	0,51	0,76	0,07	0,18	0,02	0,01	1,55	0,02	0	0,01	0	0	0	0	0	0,02	0,01	0,03	**1,62**
CG_F27_5B_O	0,5	0,68	0,06	0,16	0,02	0,02	1,44	0,03	0	0,01	0	0	0	0	0	0,03	0,01	0,04	**1,52**
CG_F27_5B_U	0,54	0,8	0,07	0,19	0,02	0,01	1,63	0,02	0	0,01	0	0	0	0	0	0,02	0,01	0,03	**1,71**
CG_F27_6B_O	0,67	1,01	0,09	0,24	0,03	0,02	2,06	0,03	0	0,01	0	0	0	0	0	0,03	0,01	0,04	**2,14**
CG_F27_6B_U	0,43	0,57	0,05	0,14	0,01	0,01	1,21	0,02	0	0,01	0	0	0	0	0	0,02	0,01	0,03	**1,28**
CG_F27_7B_O	0,63	0,92	0,09	0,22	0,02	0,01	1,89	0,02	0	0,01	0	0	0	0	0	0,02	0,01	0,03	**1,97**
CG_F27_7B_U	0,57	0,83	0,08	0,2	0,02	0,01	1,71	0,02	0	0,01	0	0	0	0	0	0,02	0,01	0,03	**1,78**
CG_F27_8B_O	0,6	0,88	0,08	0,22	0,02	0,01	1,81	0,02	0	0,01	0	0	0	0	0	0,02	0,01	0,03	**1,87**
CG_F27_8B_U	0,41	0,61	0,06	0,15	0,02	0,01	1,26	0,02	0	0,01	0	0	0	0	0	0,02	0,01	0,03	**1,32**

D. SEM-EDS RESULTS FOR SELECTED FLOTATION PRODUCTS

D.1 CG_F22_1_O

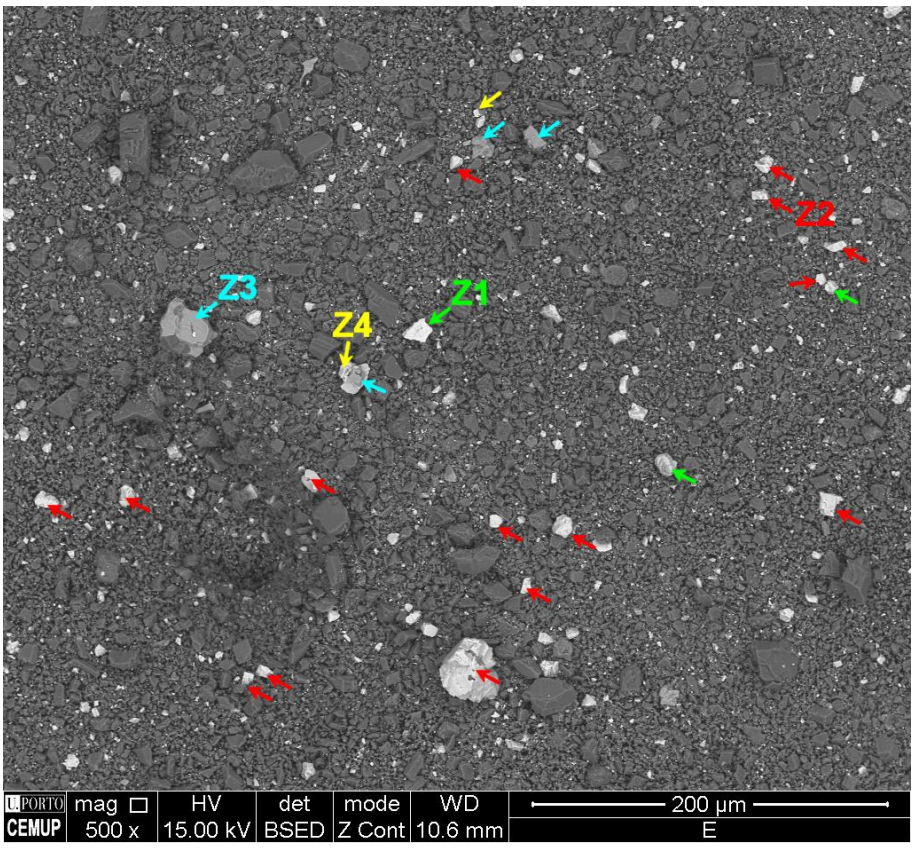

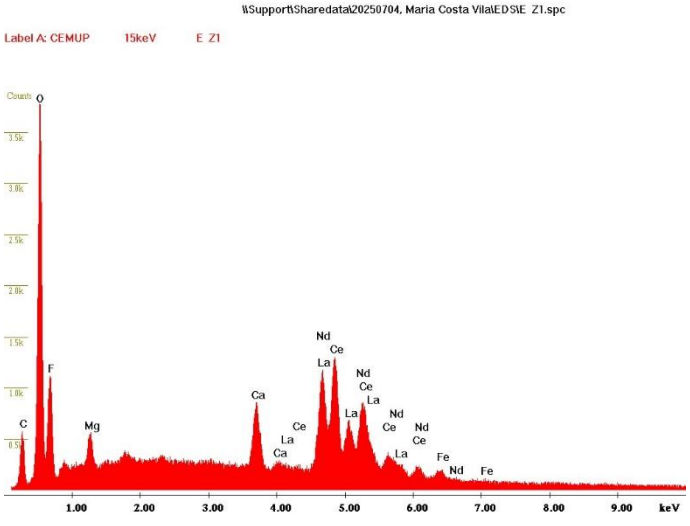

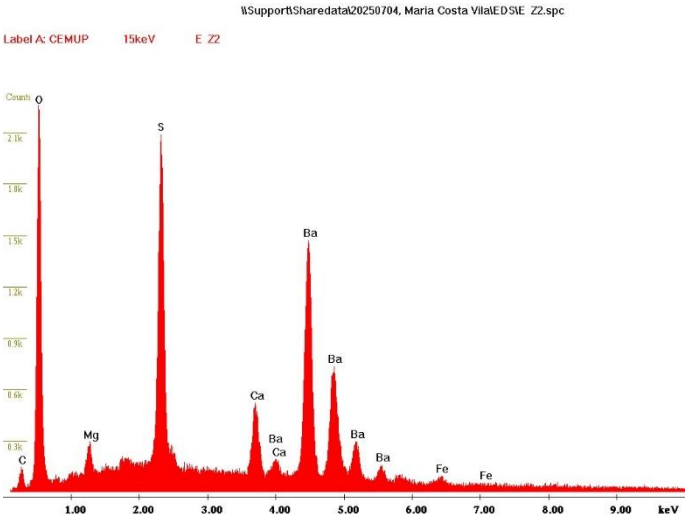

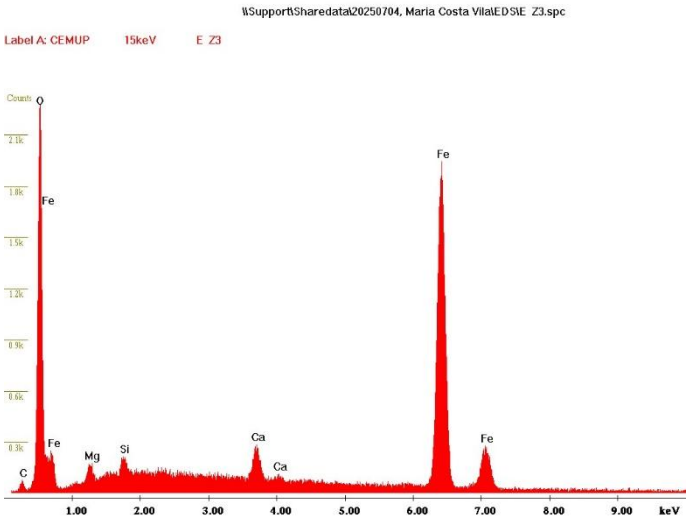

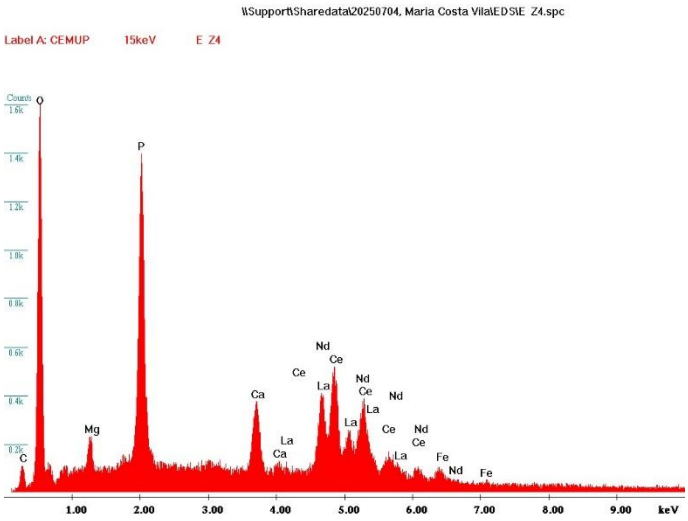

Zone	**Main elements detected**	**Mineral**	**Type**
Z1	C, O, F, Mg, Ca, La, Ce, Nd, Fe	Parisite	REE mineral
Z2	C, O, Mg, S, Ca, Ba, Fe	Barite	Gangue
Z3	C, O, Fe, Mg, Si, Ca, Fe	Magnetite	Iron oxide gangue
Z4	C, O, Mg, P, Ca, La, Ce, Nd, Fe	Monazite	REE mineral

D.2 CG_F22_2_O

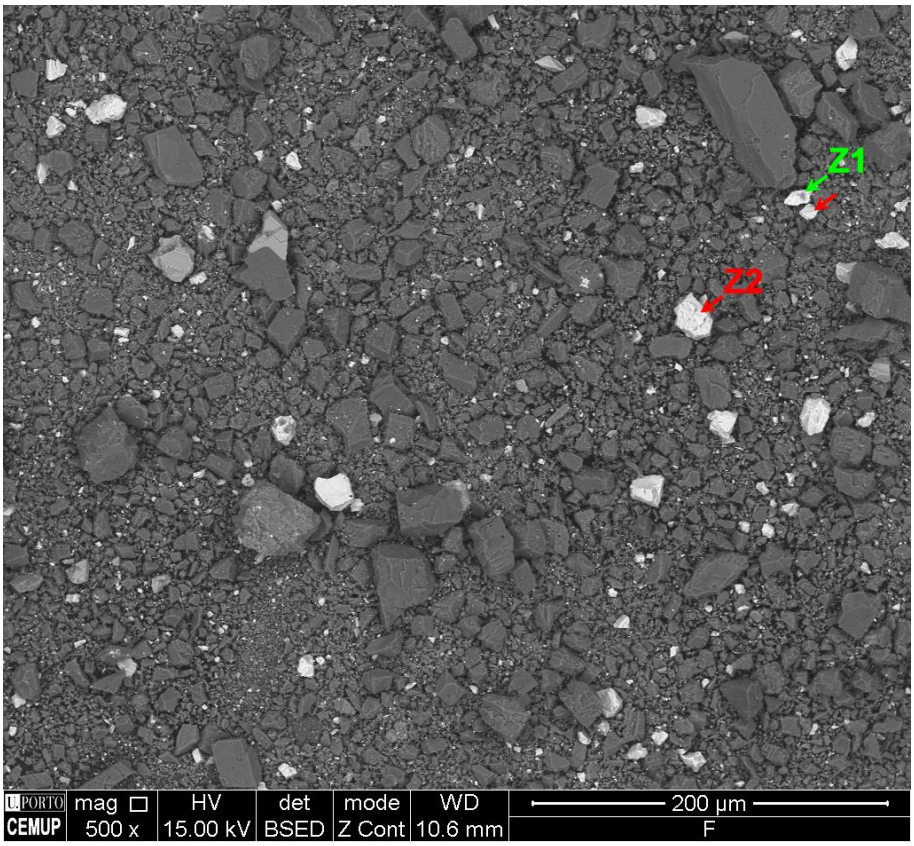
Z1
Z2
U.PORTO
CEMUP
mag
500 x
HV
15.00 kV
det
BSED
mode
Z Cont
WD
10.6 mm
200 µm
F

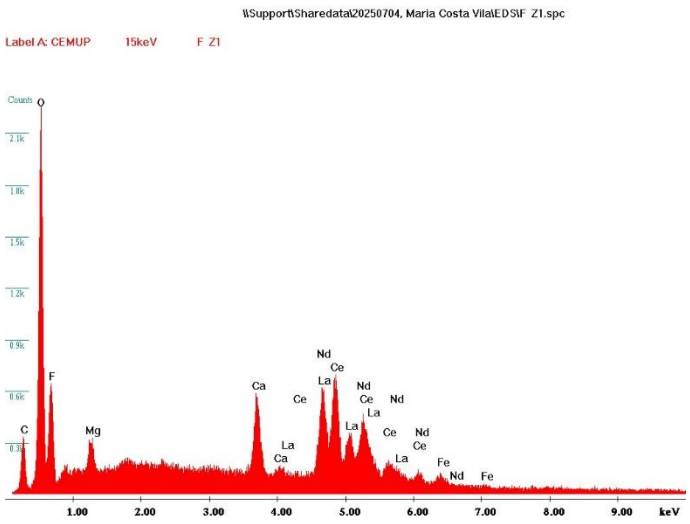
\\Support\Sharedata\20250704, Maria Costa Vila\EDS\F Z1.spc
Label A: CEMUP
15keV
F Z1
Counts
O
F
C
Mg
Ca
La
Ce
Nd
Fe
1.00
2.00
3.00
4.00
5.00
6.00
7.00
8.00
9.00
keV

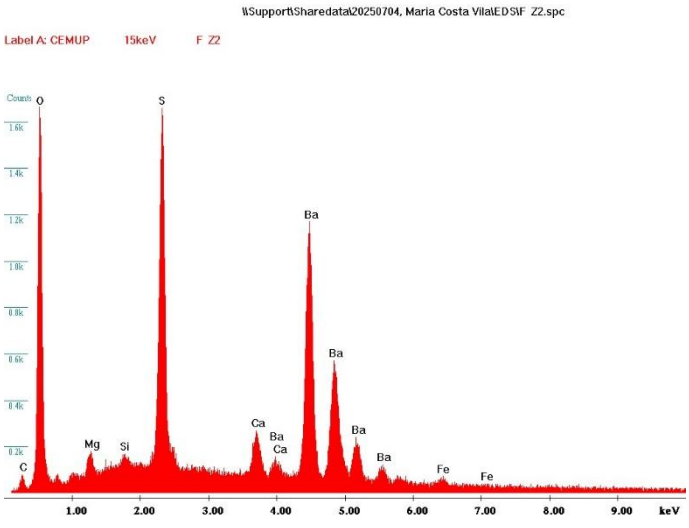
\\Support\Sharedata\20250704, Maria Costa Vila\EDS\F Z2.spc
Label A: CEMUP
15keV
F Z2
Counts
O
S
Ba
C
Mg
Si
Ca
Fe
1.00
2.00
3.00
4.00
5.00
6.00
7.00
8.00
9.00
keV

Zone	Main elements detected	Mineral	Mineral type
Z1	C, O, F, Mg, Ca, La, Ce, Nd, Fe	Parisite	REE-bearing mineral
Z2	C, O, Mg, Si, S, Ca, Ba, Fe	Barite	Gangue mineral

E. Numerical legend of global REE mines, deposits and occurrences

Nº	Deposit / occurrence location	Nº	Deposit / occurrence location	Nº	Deposit / occurrence location
1	Bokan Mountain, USA	**48**	Barra do Itapirapuã, Brazil	**95**	Tomtor, Russia
2	Alay, Canada	**49**	Poços de Caldas, Brazil	**96**	Seligdar, Russia
3	Thor Lake, Canada	**50**	Rio de Janeiro/Buena Mine, Brazil	**97**	Gornoe Ozero, Russia
4	Niskitatch, Canada	**51**	Bom Futuro, Brazil	**98**	Khamna, Russia
5	Hoidas Lake, Canada	**52**	Bahia, Brazil	**99**	Kutessay II, Kyrgyzstan
6	Rock Canyon Creek, Canada	**53**	Guaju Mine, Brazil	**100**	Mushgai Khudag, Mongolia
7	Elliot Lake, Canada	**54**	Penco Module/Biolantanidos, Chile	**101**	Lugin Gol, Mongolia
8	Kipawa/Zeus, Canada	**55**	Bou Naga, Mauritania	**102**	Wajiertage, China
9	Rex-Duquet/Rex South, Canada	**56**	Tamazeght complex, Morocco	**103**	Bayan Obo, China
10	Ashram/Eldor, Canada	**57**	Matamulas, Spain	**104**	Weishan, China
11	Saint-Honoré, Canada	**58**	Coola, Angola	**105**	Maoniuping/Dalucao, China
12	Fosse du Labrador, Canada	**59**	Longonjo, Angola	**106**	Miaoya, China
13	Strange Lake, Canada	**60**	Lofdal, Namibia	**107**	IADs, South China
14	Red Wine/Two Tom, Canada	**61**	Eteneno, Namibia	**108**	Sarnu, India
15	Kwyjibo, Canada	**62**	Steenkampskraal, South Africa	**109**	Amba Dongar, India
16	Foxtrot/Deep Fox, Canada	**63**	Zandkopsdrift, South Africa	**110**	Orissa, India
17	Henley Harbour, Canada	**64**	Karonge (Gakara), Burundi	**111**	Chavara, India
18	Karrat, Greenland	**65**	Mrima, Kenya	**112**	Manavalakurichi, India
19	Sarfartoq, Greenland	**66**	Nkombwa Hill, Zambia	**113**	IADs, Northern Myanmar
20	Qeqertassaq, Greenland	**67**	Wigu Hill, Tanzania	**114**	Thai Peninsula, Thailand
21	Tikiusaaq, Greenland	**68**	Kangankunde, Malawi	**115**	Perak, Malaysia
22	Kvanefjeld, Greenland	**69**	Songwe, Malawi	**116**	Then Chau deposit, Vietnam
23	Motzfeldt, Greenland	**70**	Ngualla, Mozambique	**117**	Muong Hum deposit, Vietnam
24	Snowbird, USA	**71**	Pilanesberg, South Africa	**118**	Nam Xe deposit, Vietnam

25	North Fork, USA	**72**	Naboomspruit, South Africa	**119**	Sin Quyen deposit, Vietnam
26	Lemhi Pass, USA	**73**	Phalaborwa complex, South Africa	**120**	Dong Pao deposit, Vietnam
27	Mountain Pass, USA	**74**	Richards Bay, South Africa	**121**	Gifford Creek/Yangibana, Australia
28	Bald Mountain, USA	**75**	Ambohimirahavavy, Madagascar	**122**	Gascoyne, Kingfisher, Mick Well, Arthur River, Mangaroon, Mt Clere
29	Bear Lodge, USA	**76**	Mandena, Madagascar	**123**	Cummins Range, Australia
30	Iron Hill, USA	**77**	Nile Delta and Rosetta, Egypt	**124**	John Gall, Australia
31	Wet Mountain, USA	**78**	Kizilcaören, Turkey	**125**	Brockman, Australia
32	Gallinas Mountain, USA	**79**	Aksu Diamas, Turkey	**126**	Boulder Ridge, Australia
33	Pajarito Mountain, USA	**80**	Ditrau, Romania	**127**	Browns Range, Australia
34	La Paz, USA	**81**	Fen, Norway	**128**	Eneabba, Australia
35	Jemi, Mexico	**82**	Norra Kärr, Sweden	**129**	Nolans, Australia
36	Elk Creek, USA	**83**	Olserum, Sweden	**130**	Brighton, Australia
37	Pea Ridge, USA	**84**	Bastnäs, Sweden	**131**	Jangardup, Australia
38	Hicks Dome, USA	**85**	Korsnäs, Finland	**132**	Circle Valley, Cascade, Mt Ridley, Lort River
39	Green Cove Springs, USA	**86**	Kiruna, Sweden	**133**	Lake Labyrinth Shear Zone, Comet.
40	Carolina Placers, USA	**87**	Khibiny complex, Russia	**134**	Mount Weld, Australia
41	Sierra de Tamaulipas, Mexico	**88**	Lovozero complex, Russia	**135**	Olympic Dam, Australia
42	Morro dos Seis Lagos, Brazil	**89**	Monazite inventory in the former USSR	**136**	WIM 150, Australia
43	Pitinga, Brazil	**90**	Yaregskoe, Russia	**137**	Narraburra, Australia
44	Chiriguelo, Brazil	**91**	Uranium Deposit, Mongolia	**138**	Dubbo Zirconia, Australia
45	Catalão I/II, Brazil	**92**	Zashikhinskoye, Russia	**139**	Fraser Island, Australia
46	Araxá, Brazil	**93**	Beloziminskoe, Russia	**140**	North Stradbroke Island, Australia
47	Serra Verde, Brazil	**94**	Chuktukon, Russia		